



**DEVELOPMENT OF INJECTABLE HYDROGELS LOADED  
WITH SMALL INTERFERING RNA (siRNA)  
NANOPARTICLES FOR BREAST  
CANCER TREATMENT**

**TANAWAT BUNTUM**

**DOCTOR OF PHILOSOPHY  
IN  
APPLIED CHEMISTRY**

**SCHOOL OF SCIENCE  
MAE FAH LUANG UNIVERSITY**

**2024**

**©COPYRIGHT BY MAE FAH LUANG UNIVERSITY**

**DEVELOPMENT OF INJECTABLE HYDROGELS LOADED  
WITH SMALL INTERFERING RNA (siRNA)  
NANOPARTICLES FOR BREAST  
CANCER TREATMENT**

**TANAWAT BUNTUM**

**THIS DISSERTATION IS A PARTIAL FULFILLMENT OF  
THE REQUIREMENTS FOR THE DEGREE OF  
DOCTOR OF PHILOSOPHY  
IN  
APPLIED CHEMISTRY**

**SCHOOL OF SCIENCE  
MAE FAH LUANG UNIVERSITY**

**2024**

**©COPYRIGHT BY MAE FAH LUANG UNIVERSITY**



**DISSERTATION APPROVAL  
MAE FAH LUANG UNIVERSITY  
FOR**

**DOCTOR OF PHILOSOPHY IN APPLIED CHEMISTRY**

**Dissertation Title:** Development of Injectable Hydrogels Loaded with Small Interfering RNA (siRNA) Nanoparticles for Breast Cancer Treatment


**Author:** Tanawat Buntum

**Examination Committee:**

Uracha Ruktanonchai, Ph. D.	Chairperson
Associate Professor Orawan Suwantong, Ph. D.	Member
Professor Hasan Uludag, Ph. D.	Member
Assistant Professor Plaipol Dedvisitsakul, Ph. D.	Member
Assistant Professor Nanthanit Jaruseranee, Ph. D.	Member

**Advisors:**

  
.....Advisor  
(Associate Professor Orawan Suwantong, Ph. D.)

  
.....Co-Advisor  
(Professor Hasan Uludag, Ph. D.)

**Dean:**

  
.....  
(Professor Surat Laphookhieo, Ph. D.)

## ACKNOWLEDGEMENTS

Completing this dissertation marks a key milestone in my academic journey, and I am deeply grateful for the invaluable support I received. I would like to express my sincere gratitude to my advisor, Assoc. Prof. Dr. Orawan Suwantong, from School of Science, Mae Fah Luang University, for her unwavering support, kind assistance, insightful advice, and consistent encouragement throughout my Ph. D. study. I sincerely thank my co-advisor, Prof. Dr. Hasan Uludag, from the University of Alberta, Canada, for his helpful guidance and support with my experiments. Furthermore, I am profoundly grateful to Dr. Uracha Ruktanonchai, Asst. Prof. Dr. Plaipol Dedvisitsakul, Dr. Mattaka Khongkow, and Asst. Prof. Dr. Nanthanit Jaruseranee for their constructive comments and suggestions throughout my Ph. D. studies.

This Ph.D. study received support from the National Research Council of Thailand (NRCT) and Mae Fah Luang University. I also extend my gratitude to the Toray Science Foundation, Japan (TSF), for the partial funding through Science and Technology Research Grants. We sincerely thank the National Nanotechnology Center (NANOTEC), the National Science and Technology Development Agency (NSTDA), the Oral Biology Laboratory and Research Center (Santi Bhirom Bhakdi) at the School of Dentistry, Cell culture room at the School of Medicine, the Scientific and Technological Instruments Center (STIC), Mae Fah Luang University, and the Department of Chemical & Materials Engineering, University of Alberta, for laboratory facilities. We also thank the Cancer and Immunology Research Unit, School of Medicine, Mae Fah Luang University, for providing Hoechst 333258. Furthermore, I would like to acknowledge Mae Fah Luang University for the Postgraduate scholarship (grant no. 023) for tuition fees and the Graduate Research Grant financially for supporting this research. The School of Science, Mae Fah Luang University, Outbound Research Exchange for Excellence Research Collaboration Programme. In addition, I am grateful to the Queen Sirikit Sericulture Center in Chiang Mai, Thailand, for supplying the silk cocoons (Nang Lai Saraburi).

Finally, I want to express my sincere gratitude to my fellow laboratory members in Room 204 of the S2 Building, as well as the dedicated individuals at the National

Nanotechnology Center, Chulabhorn Research Institute, and those in Rooms 7-128 and 7-132 of the Department of Chemical and Materials Engineering at the University of Alberta. Their support, kindness, and the enjoyable times we shared over the past few years are deeply appreciated. I am also profoundly grateful to my wonderful family for their unwavering love, patience, and encouragement throughout this journey. Furthermore, I extend my thanks to my Thai friends in Alberta for their friendship and support during my time there.

Tanawat Buntum



<b>Dissertation Title</b>	Development of Injectable Hydrogels Loaded with Small Interfering RNA (siRNA) Nanoparticles for Breast Cancer Treatment
<b>Author</b>	Tanawat Buntum
<b>Degree</b>	Doctoral of Philosophy (Applied Chemistry)
<b>Advisor</b>	Associate Professor Orawan Suwantong, Ph. D.
<b>Co-Advisor</b>	Professor Hasan Uludag, Ph. D.

## ABSTRACT

Breast cancer remains one of the most prevalent and serious global health challenges, with new diagnoses projected to exceed 3 million annually by 2040. Despite the widespread use of conventional treatments like surgery, chemotherapy, and radiation, these methods often lead to significant side effects and do not consistently prevent recurrence. Gene therapy, particularly using small interfering RNA (siRNA), offers a promising alternative due to its ability to specifically silence cancer-related genes while minimizing adverse effects. Furthermore, integrating gene therapy with conventional treatments could improve outcomes, reduce recurrence rates, and protect healthy tissues. This study investigated the use of siRNA nanoparticles loaded into injectable quaternized chitosan (QCS)/oxidized pectin (OxPec) hydrogels and injectable thermosensitive chitosan (CS)/silk sericin (SS) hydrogels as delivery platforms to enhance siRNA nanoparticle stability and facilitate targeted release in breast cancer treatment.

The first study focused on optimizing siRNA nanoparticle preparation using varying ratios of Trans-Booster, Prime-Fect, and siRNA. The optimal formulation (siRNA:Trans-Booster:Prime-Fect of 1:1:10) yielded stable, uniformly sized nanoparticles (~230 nm) with a moderately negative zeta potential (-6.8 to -10.2 mV). These nanoparticles demonstrated efficient cellular uptake (>98%) and significantly silenced survivin expression, resulting in reduced viability of breast cancer cells.

The second study explored injectable self-healing hydrogels composed of QCS and OxPec as a delivery platform for the optimized siRNA nanoparticles. Hydrogel

formulations were fabricated by varying QCS and OxPec concentrations. The siRNA nanoparticles formulated via electrostatic interactions using Trans-Booster and Prime-Fect were incorporated into the injectable self-healing QCS/OxPec hydrogels. The resulting siRNA nanoparticle-loaded QCS/OxPec hydrogels exhibited favorable gelation times (13-18 min) and self-healing properties (3-10 min). Importantly, media extracted from these hydrogels showed significant cytotoxicity against breast cancer cells and high cellular uptake of the nanoparticles, highlighting their potential for localized delivery.

The third study developed injectable thermosensitive hydrogels from CS and SS for localized survivin siRNA nanoparticle delivery. Optimal conditions for hydrogel preparation were determined by varying  $\beta$ -glycerophosphate concentrations. The siRNA nanoparticles incorporated into these injectable thermosensitive CS/SS hydrogels maintained a uniform spherical morphology (~182 nm). These hydrogels demonstrated a gelation time of 20–29 min and exhibited time-dependent swelling and degradation, which was accelerated in the presence of lysozyme. While varying  $\beta$ -glycerophosphate concentrations (0.8-1.0 mL) did not affect mechanical strength, the inclusion of siRNA nanoparticles slightly reduced it. Media extracted from hydrogels loaded with survivin siRNA nanoparticles significantly inhibited the growth of MDA-MB-231 and MDA-MB-436 cells after 72 h, outperforming both untreated and control siRNA groups. Additionally, high cellular uptake was observed in both cell lines. Overall, this study successfully developed and characterized the siRNA nanoparticles-loaded hydrogel systems, each demonstrating promising properties for localized and effective siRNA delivery in breast cancer therapy.

**Keywords:** siRNA Nanoparticles, Injectable Hydrogel, Self-healing, Thermoresponsive Polymers, Biopolymers, Breast Cancer Cells

## TABLE OF CONTENTS

<b>CHAPTER</b>	<b>Page</b>
<b>1 INTRODUCTION</b>	<b>1</b>
1.1 Background and Significance of the Research Problem	1
1.2 Research Objectives	4
1.3 Scope of Research	4
<b>2 LITERATURE REVIEWS</b>	<b>6</b>
2.1 Cancer	6
2.2 Breast Cancer	7
2.3 Small Interfering RNA (siRNA)	11
2.4 Hydrogel	16
<b>3 MATERIALS</b>	<b>27</b>
<b>4 PREPARATION AND CHARACTERIZATION OF SMALL INTERFERING RNA NANOPARTICLES FOR TARGETED DELIVERY TO BREAST CANCER CELLS</b>	<b>30</b>
4.1 Methodology	30
4.2 Results and Discussion	35
<b>5 INJECTABLE SELF-HEALING QUATERNIZED CHITOSAN/OXIDIZED PECTIN HYDROGELS LOADED WITH siRNA NANOPARTICLES FOR BREAST CANCER TREATMENT</b>	<b>43</b>
5.1 Methodology	43
5.2 Results and Discussion	53
<b>6 INJECTABLE THERMOSENSITIVE CHITOSAN/SILK SERICIN HYDROGELS LOADED WITH siRNA NANOPARTICLES FOR BREAST CANCER TREATMENT</b>	<b>75</b>
6.1 Methodology	75
6.2 Results and Discussion	87
<b>7 CONCLUSION</b>	<b>112</b>



## TABLE OF CONTENTS

CHAPTER	Page
REFERENCES	115
APPENDIX	130
CURRICULUM VITAE	134



## LIST OF TABLES

<b>Table</b>	<b>Page</b>
4.1 Compositions of siRNA Nanoparticles	31
4.2 Compositions, Size, PDI, and Zeta Potential of siRNA Nanoparticles	36
4.3 Cellular Uptake of FAM-siSVV Nanoparticles after Transfection for 72 h was Captured by Fluorescence Microscopy (Magnification of 40×)	42
5.1 Compositions of Injectable Self-Healing Hydrogels	46
5.2 Gelation Time, Self-healing Time, and Gel Fraction of Injectable Self-healing Hydrogels (n=3)	59
5.3 Morphology of HDFa Cells Cultured with Extraction Media of Injectable Self-Healing Hydrogels Loaded with siRNA Nanoparticles	70
5.4 Cellular Uptake of FAM-siSVV Nanoparticles Loaded-Injectable Self-Healing Hydrogels After Transfection of 72 h was Captured by Fluorescence Microscopy (Magnification 20×)	74
6.1 Preparation Parameters and Gelation Time of the Injectable Thermosensitive Hydrogels Loaded with siRNA Nanoparticles	78
6.2 Compositions of the Injectable Thermosensitive Hydrogels Loaded with CsiRNA Nanoparticles and siRNA Nanoparticles	83
6.3 Preparation Parameters and Gelation Time of the Injectable Thermosensitive Hydrogels Loaded with siRNA Nanoparticles	91
6.4 Morphology of HDFa Cells Cultured with Extraction Media of Hydrogels Loaded with siRNA Nanoparticles	106
6.5 Cellular Uptake of FAM-siRNA Nanoparticles and FAM-siRNA Nanoparticles Loaded in the Hydrogels after Transfection of 72 h was Captured by Fluorescence Microscope. (Magnification 20×)	111

## LIST OF FIGURES

Figure	Page
2.1 Normal Breast Tissue	7
2.2 Gene Silencing Mechanisms of siRNA	12
2.3 A Phase Diagram Showing the UCST and LCST Points for a Thermoresponsive Polymer	23
4.1 Selected TEM Images of siRNA Nanoparticles at siRNA:Trans-Booster:Prime-Fect Weight Ratio of 1:1:10 (A) CsiRNA Nanoparticles and (B) siSVV Nanoparticles	37
4.2 The <i>In Vitro</i> Cytotoxicity of siRNA Nanoparticles Cultured with MDA-MB-231 and MDA-MB-436 Cells (n = 4). (siRNA Nanoparticles at siRNA:Trans-Booster:Prime-Fect Weight Ratio of 1:1:10). * $p < 0.05$ Compared with the Non-treat and # $p < 0.05$ Compared Between CsiRNA Nanoparticles and siSVV Nanoparticles	38
4.3 Relative Fold Change of CsiRNA Nanoparticles and siSVV Nanoparticles Cultured with MDA-MB-231 and MDA-MB-436 Cells by RT-qPCR after Transfection for 72 h (n = 2). * $p < 0.05$ Compared with the Non-Treat and # $p < 0.05$ Compared between CsiRNA Nanoparticles and siSVV Nanoparticles	41
4.4 Cell Uptake of siRNA Nanoparticles. (A) Percentage of siSVV Positive Cell Population and (B) Mean Fluorescence Intensity of siSVV Nanoparticles after 72 h Treatment	42
5.1 FTIR Spectra of CS, QCS, Pec, and OxPec	54
5.2 The Cytotoxicity of OxPec and QCS Cultured with (A) HDFa, (B) MDA-MB-231, and (C) MDA-MB-436 Cells (n = 3). * $p < 0.05$ Compared with the Control	56
5.3 (A) Gel Formation and (B) Self-healing Behavior of the Hydrogels Loaded with siRNA Nanoparticles at 37 °C	57

## LIST OF FIGURES

Figure	Page
5.4 Selected TEM Image of siSVV Nanoparticles Loaded in the Hydrogel, with a Magnification of 10,000× at 80 kV	58
5.5 (A) Water Swelling and (B) Weight Loss of the Hydrogels at 37°C (n =3) * <i>p</i> < 0.05 Compared with the Values at 30 min at Any Given Material Type	60
5.6 Released Study of siRNA Nanoparticles-Loaded Self-Healing Hydrogels	62
5.7 Rheological Analysis of (A) 15H, (B) 15HS, (C) 17.5H, and (D) 17.5HS. Storage Modulus G' (●) and Loss Modulus G'' (○) Strain Sweep at 37 °C and Frequency 10 rad/s	64
5.8 Rheological Analysis (A) 15H, (B) 15HS, (C) 17.5H, and (D) 17.5HS. Storage Modulus G' (●) and Loss Modulus G'' (○) Time Sweep at 37 °C, Frequency 10rad/s, and Strain 1%	65
5.9 Continuous Step Strain Analysis of (A) 15H, (B) 15HS, (C) 17.5H, and (D) 17.5HS. Storage Modulus G' (●) and Loss Modulus G'' (○) at Low Strain of 1% and High Strain of 3000% with 50 s of Intervals	66
5.10 Indirect Cytotoxicity of Extraction Media from Hydrogels Cultured with (A) MDA-MB-231 and (B) MDA-MB-436 Cells for 72 h (n = 3). * <i>p</i> < 0.05 Compared with the Non-treat at Any Given Concentration. # <i>p</i> < 0.05 Compared Between 15HC and 15HS and Compared between 17.5HC and 17.5HS at Any Given Concentration	68
5.11 Biocompatibility of Hydrogels (n=3). * <i>p</i> < 0.05 Compared with the Non-Treated Group at Each Time Point	69
5.12 Relative Fold Change of Hydrogels Loaded with siRNA Nanoparticles Cultured with MDA-MB-231 and MDA-MB-436 Cells by RT-qPCR After Transfection for 72 h. * <i>p</i> < 0.05 Compared with the Non-Treated Group	71

## LIST OF FIGURES

Figure	Page
5.13 Cell Uptake of siRNA Nanoparticles Loaded in Hydrogels (A) Percentage of FAM-Labeled siRNA Positive Cell Population and (B) Mean Fluorescence Intensity of FAM-labeled siRNA Nanoparticles after 72 h Treatment. * $p < 0.05$ Compared with the Non-Treated Group at Each Time Point	73
6.1 The Indirect Cytotoxicity of Raw Materials Cultured with (A) HDFa, (B) MDA-MB-231, and (C) MDA-MB-436 Cells for 24 h	88
6.2 Photographs of Injectable Thermosensitive Hydrogel Loaded with siRNA Nanoparticles at 37 °C	89
6.3 ATR-FTIR Spectra of CS, SS, $\beta$ -GP, and 1.0HS	93
6.4 TEM Images of siRNA Nanoparticles Loaded in the Hydrogel at 15.0k Magnification 15.0k and at 80.0 kV	94
6.5 (A) Water Swelling, (B) Weight Loss in PBS, and (C) Weight Loss in PBS containing Lysozyme of the Injectable Thermosensitive Hydrogels. * $p < 0.05$ Compared with The Values at 24 h. # $p < 0.05$ Compared 0.8H with 0.8HS and 1.0H with 1.0HS at Each Time Point	96
6.6 Released Study of siRNA Nanoparticles-Loaded Thermosensitive Hydrogels	98
6.7 Typical Temperature Dependence of (○) $G'$ and (●) $G''$ Values of (A) 0.8H, (B) 0.8HS, (C) 1.0H, and (D) 1.0HS	100
6.8 Rheology Curves of (○) $G'$ and (●) $G''$ Values of (A) 0.8H, (B) 0.8HS, (C) 1.0H, and (D) 1.0HS	101
6.9 Solution Viscosity of (A) 0.8H, (B) 0.8HS, (C) 1.0H, and (D) 1.0HS as a Function of Temperature	102

## LIST OF FIGURES

Figure	Page
<p>6.10 Indirect Cytotoxicity of Extraction Media from Hydrogels Cultured with (A) MDA-MB-231 and (B) MDA-MB-436 Cells for 72 h (n = 3).  <math>*p &lt; 0.05</math> Compared with the Non-Treatment at Each Concentration.  <math>^{\#}p &lt; 0.05</math> Compared 0.8HC with 0.8HS and 1.0HC with 1.0HS at Each Concentration</p>	104
<p>6.11 Biocompatibility of Thermosensitive Hydrogels (n=3). <math>*p &lt; 0.05</math> Compared with the Non-Treated Group at Each Time Point</p>	105
<p>6.12 Relative Fold Change of CsiRNA and siSVV Nanoparticles Loaded in Hydrogel Cultured with MDA-MB-231 and MDA-MB-436 Cells by RT-qPCR After Transfection for 72 h</p>	108
<p>6.13 Cell Uptake of siRNA Nanoparticles Loaded in Hydrogel. (A) Percentage of FAM-Labeled siRNA Positive Cell Population and (B) Mean Fluorescence Intensity of FAM-Labeled siRNA Nanoparticles Ffter 72 h Treatment</p>	109

## ABBREVIATIONS AND SYMBOLS

°C	Degree Celsius
μg/mL	Microgram per Milliliter
<sup>1</sup> H NMR	Proton Nuclear Magnetic Resonance
a.u.	Arbitrary Units
AGO2	Endonuclease Argonaute 2
AMF	Actual Macromer Fraction
ANOVA	Analysis of Variance
ATR	Attenuated Total Reflectance
cDNA	Complementary Deoxyribonucleic Acid
CO <sub>2</sub>	Carbon Dioxide
Conc.	Concentration
CS	Chitosan
CsiRNA	Control Small Interfering Ribonucleic Acid
CST	Critical Solution Temperature
D <sub>2</sub> O	Deuterium Oxide
DA	Degree of Acetylation
DMEM	Dulbecco's Modified Eagle Medium
DMSO	Dimethyl Sulfoxide
DOX	Doxorubicin
DS	Degree of Substitution
dsRNA	Double-stranded Ribonucleic Acid
ECM	Extracellular Matrix
FAM	Fluorescein Amidites
FAM-survivin	6-Carboxyfluorescein Survivin siRNA
FBS	Fetal Bovine Serum
FE-SEM	Field Emission Scanning Electron Microscope
FTIR	Fourier Transform Infrared Spectroscopy
g	Gram

## ABBREVIATIONS AND SYMBOLS

G'	Storage Modulus
G''	Loss Modulus
G/C	Guanine/Cytosine
GTMAC	Glycidyl Trimethylammonium Chloride
h	Hour
HBSS	Hank's Balanced Salt Solution
HDFa	Human Dermal Fibroblasts Adult
HR+	Hormone Receptor-Positive
kDa	Kilodalton
kV	Kilovolt
LCST	Low Critical Solution Temperature
M	Molar
md,i	Initial Dry Mass
md,w	Final Dry Mass
mg/mL	Milligram per Milliliter
min	Minute
mL	Milliliter
mL:mL	Milliliter per Milliliter
mRNA	Messenger Ribonucleic Acid
MTT	3-(4,5-Dimethylthiazol-2-yl)-2,5-Diphenyltetrazolium Bromide
mV	Millivolt
Mw,i	Initial Wet Mass
Mw,t	Swollen Mass
Na <sub>2</sub> CO <sub>3</sub>	Anhydrous Sodium Carbonate
nM	Nanomolar
nm	Nanometer
NMR	Nuclear Magnetic Resonance



## ABBREVIATIONS AND SYMBOLS

OxPec	Oxidized Pectin
PBS	Phosphate Buffered Saline
PDI	Polydispersity Index
Pec	Pectin
PEI	Polyethyleneimine
PO <sub>4</sub> <sup>3-</sup>	Phosphate Ions
ppm	Parts per Million
QCS	Quaternized Chitosan
rad/s	Radians Per Second
rcf	Relative Centrifugal Force
RISC	Ribonucleic Acid Interference
RNAi	Ribonucleic Acid Interference
RNase	Ribonuclease
rpm	Revolutions per Minute
RT-qPCR	Real-Time Reverse Transcription Quantitative PCR
s	Second
SD	Standard Deviation
SF	Silk Fibroin
siRNA	Small Interfering Ribonucleic Acid
siSVV	Survivin
SS	Silk Sericin
SS	Silk Sericin
SVV	Primers for Human-Survivin
TEM	Transmission Electron Microscopy
UCST	Upper Critical Solution Temperature
w/v	Weight/Volume
WHO	World Health Organization

## ABBREVIATIONS AND SYMBOLS

wt%	Weight Percent
$\beta$ -GP	Beta-glycerol phosphate
$\lambda_{em}$	Emission Wavelength
$\lambda_{ex}$	Excitation Wavelength



## CHAPTER 1

### INTRODUCTION

#### 1.1 Background and Significance of the Research Problem

Cancer is a group of diseases characterized by the uncontrolled growth and spread of abnormal cells, which can begin in virtually any tissue of the human body. If not detected and treated early, cancer can invade surrounding tissues and metastasize to distant organs through the lymphatic system or bloodstream. Among various cancer types, breast cancer remains a major global health concern. In 2023, it was the most commonly diagnosed cancer worldwide, with approximately 297,790 new cases and 43,170 deaths reported (Siegel et al., 2023). The most common symptoms and signs of breast cancer are nipple turning inward, nipple discharge, breast swelling, skin change on the breast or nipple, change in breast size, and nipple pain. Nipple inversion or retraction can suggest underlying tissue changes. Similarly, discharge, particularly if bloody or spontaneous (occurring without squeezing), may indicate abnormal cell growth. Swelling and skin alterations like redness, dimpling (resembling an orange peel), or flaking could point to inflammation or the presence of a tumor. Furthermore, a noticeable change in breast size or persistent nipple pain, especially if localized to one side, should not be overlooked, as these may suggest deeper tissue involvement (Cancer Facts & Figures, 2023). The most common risk factors for breast cancer are genetic abnormality, short lactation period, drinking alcohol, increasing age, overweight or obese, family history of breast cancer, exposure to female hormones, and radiation exposure (World Health Organization, 2021; NHS: Breast Cancer in Women, 2019; Breast cancer: American Cancer Society, 2023).

Breast cancer affects both women and, less commonly, men, and its risk factors include genetics, hormonal influences, lifestyle, and environmental exposures. According to the World Health Organization (WHO), the global incidence of breast cancer is projected to rise significantly, with new cases expected to exceed 3 million annually by 2040, highlighting the urgent need for more effective prevention, early

detection, and treatment strategies. Breast cancer treatment can be separated into 2 types, which are local treatments and systemic treatments. Local treatments are surgery and radiation to treat or remove the tumor without affecting the rest of the body. Systemic treatments include chemotherapy, hormone therapy, targeted drug therapy, gene therapy, and immunotherapy. The advantage of systemic treatment is drugs can reach cancer cells almost anywhere in the body (American Cancer Society: Treating Breast Cancer, 2023; Almurshidi Medical Agency, 2020). Gene therapy was used in breast cancer treatment due to low side effects, non-cytotoxicity, and high potential treatment for breast cancer. Small interfering ribonucleic acid (siRNA) therapy is the inhibition of the expression of selected genes by siRNA in cells. siRNA is a class of double-stranded ribonucleic acid (dsRNA) non-coding RNA molecules, typically 21-23 nucleotides long in length with hydroxylated 3' and phosphorylated 5' ends by the endonuclease dicer (Singh et al., 2018). siRNA can interact with the specific mRNA to silence the expression or inhibit the translation of the protein in the cell. This process known as ribonucleic acid interference (RNAi), involves the incorporation of siRNA into the ribonucleic acid-induced silencing complex (RISC), which then guides the siRNA to bind to its complementary mRNA sequence. Once bound, the RISC complex cleaves the target mRNA, leading to its degradation and preventing the production of the corresponding protein. This mechanism allows siRNA to selectively downregulate disease-related genes, making it a powerful tool for gene therapy and targeted treatments, particularly in cancer and genetic disorders (McManus et al., 2002; Wilson & Doudna, 2013). However, siRNA can be degraded by biological liquids before it reaches the target site. Thus, the development of gene carriers for siRNA is significant in increasing the efficiency of siRNA for cancer treatment (Pecot et al., 2011). By utilizing carriers such as hydrogels, siRNA can be better protected and delivered more effectively to the desired location, thereby enhancing its therapeutic potential in cancer treatment.

Injectable hydrogel is considered the most promising carrier for siRNA nanoparticles delivery by extruding the liquid form of the solution into the body and instantly converting into a solid hydrogel (Mathew et al., 2018). The injectable hydrogel can be crosslinked through mechanisms such as thermal transitions, Schiff's base reactions, or electrostatic interaction (Ahsan et al., 2020; Pankongadisak & Suwantong,

2018; Mo et al., 2021; Liang et al., 2019; Mahanta & Maiti, 2019). The injectable hydrogel serves as a vehicle to protect various biomolecules at specific sites, including siRNA (Wang et al., 2018; Kim et al., 2012). In addition, it is used as a carrier to avoid surgical implantation with reduced infection risk, control drug release rate, improve therapeutic concentrations, and improve therapeutic efficacy and sustained delivery (Li et al., 2020; Sun et al., 2020). Furthermore, when used in conjunction with surgery, these carriers can enhance the precision of drug delivery to the breast cancer site, reducing the need for invasive procedures while still ensuring that the therapeutic agents reach the targeted area effectively. By controlling the release rate and sustaining the drug's presence at the treatment site, this approach can complement surgical interventions by providing continuous treatment and minimizing the risk of recurrence, ultimately improving patient outcomes. Biopolymers such as chitosan, silk sericin, and pectin exhibit biocompatibility, biodegradability, non-toxicity, and the ability to absorb bioactive molecules (Park et al., 2017), making them suitable candidates for the development of injectable hydrogels for siRNA nanoparticle delivery. Therefore, these injectable hydrogels can be applied to deliver siRNA nanoparticles in breast cancer treatment.

The aim of this study was to develop injectable self-healing hydrogels and injectable thermosensitive hydrogels containing siRNA nanoparticles for the treatment of breast cancer. siRNA nanoparticles were fabricated through electrostatic interactions between siRNA, Trans-Booster, and Prime-Fect or modified polyethyleneimine. This process formed nanoparticles that protect the siRNA from enzymatic degradation and enhance cellular uptake. The resulting siRNA nanoparticles were characterized for size, polydispersity index, zeta potential, morphology, *in vitro* cytotoxicity, gene silencing efficiency, and cellular uptake. Furthermore, injectable self-healing quaternized chitosan (QCS)/oxidized pectin (OxPec) hydrogels containing these siRNA nanoparticles were characterized for morphology, chemical structure, gelation time, self-healing time, gel fraction, rheological properties, water swelling, weight loss, biocompatibility, *in vitro* cytotoxicity, cell morphology, gene silencing, and cellular uptake. Injectable thermosensitive chitosan (CS)/silk sericin (SS) hydrogels containing siRNA nanoparticles were characterized for gelation time, gel fraction, morphology, chemical structure, water swelling, weight loss behavior, *in vitro* degradation,

rheological behaviors, biocompatibility, cell morphology, *in vitro* cytotoxicity, gene silencing, and cellular uptake.

## 1.2 Research Objectives

1.2.1. To prepare and investigate siRNA nanoparticles formulated with Prime-Fect as a transfection reagent and Trans-Booster as an additive, aiming to enhance siRNA nanoparticles delivery efficiency.

1.2.2 To investigate the potential use of injectable self-healing QCS/OxPec hydrogels and injectable thermosensitive CS/SS hydrogels loaded with siRNA nanoparticles for breast cancer treatment.

## 1.3 Scope of Research

The fabrication and evaluation of siRNA nanoparticles-loaded hydrogel systems involve several key experimental steps.

First, optimal conditions for siRNA nanoparticle preparation were determined by varying the amount of Trans-Booster as an additive, specifically using siRNA:Trans-Booster:Prime-Fect ratios of 1:0:10 and 1:1:10 (w/w). This variation aimed to evaluate the influence of Trans-Booster on the nanoparticles' physicochemical characteristics. Subsequently, the formulated siRNA nanoparticles were thoroughly characterized for particle size, polydispersity index, zeta potential, morphology, cytotoxicity, gene silencing efficiency, and cellular uptake.

To develop injectable self-healing hydrogels, the concentrations of QCS (15% w/v) and OxPec (15% and 17.5% w/v) were varied to optimize the conditions, while maintaining a fixed QCS to OxPec volume ratio of 0.8:0.2 mL. The optimized siRNA nanoparticle formulation was then incorporated into these injectable self-healing hydrogels. Following this, the hydrogels were characterized for their chemical structure, gelation time, self-healing ability, water swelling, weight loss, release profiles, rheological properties, biocompatibility, *in vitro* cytotoxicity, cell morphology, gene silencing, and cellular uptake.

For the injectable thermosensitive hydrogels, the concentrations of CS and SS were fixed at 3% and 7% w/v, respectively. The volume ratios between CS and 50% w/v  $\beta$ -GP were varied at 1:0.2, 1:0.5, 1:0.8, and 1:1 mL/mL. The optimized condition for preparing these injectable thermosensitive hydrogels was then used to incorporate the siRNA nanoparticles. These thermosensitive CS/SS hydrogels were subsequently characterized for their gelation time, chemical structure, water swelling, weight loss, release profiles, rheological properties, biocompatibility, *in vitro* cytotoxicity, cell morphology, gene silencing, and cellular uptake.



## CHAPTER 2

### LITERATURE REVIEWS

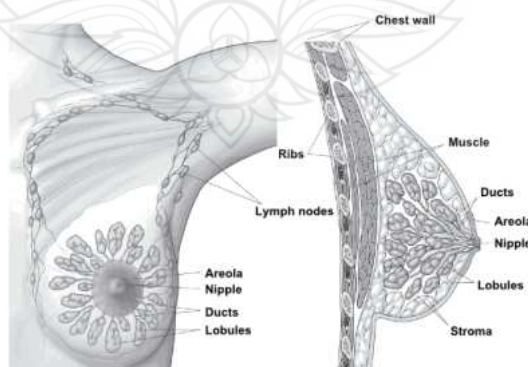
#### 2.1 Cancer

Cancer is a group of diseases in the body's cells that can start anywhere in the human body, grow uncontrollably, and spread to other body parts. This process is known as metastasis. Generally, human cells grow and multiply to form new cells instead of old or damaged cells, called the cell division process. If this process breaks down and abnormal cells grow, tumor cells can be cancerous (Li et al., 2025; Fares et al., 2020). Unlike normal cells, these malignant cells characteristically disregard regulatory signals that govern cellular proliferation and apoptosis. Moreover, they can infiltrate adjacent tissues and stimulate angiogenesis, the formation of new blood vessels necessary to support their rapid growth. Ultimately, these cells may detach from the primary tumor and spread through the circulatory or lymphatic systems, leading to the development of secondary tumors in distant sites, a process known as metastasis (Labi & Erlacher, 2015; Otrrock et al., 2007). Cancer is a leading cause of death worldwide, accounting for nearly 10 million deaths in 2020 (World Health Organization: Cancer, 2022). The newest cases of cancer in 2020 were breast (2.26 million cases), lung (2.21 million cases), colon and rectum (1.93 million cases), prostate (1.41 million cases), skin (non-melanoma) (1.20 million cases), and stomach (1.09 million cases). World Health Organization reported 685,000 deaths in 2020 from breast cancer and predicts that in 2040 breast cancer globally will increase to more than 3 million new cases per year (World Health Organization: Cancer Today, 2023; World Health Organization: Breast Cancer, 2022; Arnold et al., 2022).



## 2.2 Breast Cancer

Breast cancer can develop in various parts of the breast, including the lobules, ducts, nipple, fatty tissue, connective tissue, blood vessels, and lymph vessels (as illustrated in Figure 2.1). While breast cancer presents with several potential symptoms, the initial sign is often a palpable lump or an area of thickened breast tissue. Other symptoms may include an inverted nipple, nipple discharge, breast swelling, changes in the skin of the breast or nipple, alterations in breast size, nipple pain, and a rash on or around the nipple. It's important to note that these symptoms can differ significantly among individuals, and not everyone with breast cancer will experience all of them. Notably, early-stage breast cancer may be asymptomatic and is frequently detected through routine screenings like mammography. Consequently, early detection and timely medical evaluation are critical for improved treatment outcomes and increased survival rates. Breast cancer can metastasize to other parts of the body via the bloodstream and lymphatic system, as depicted in Figure 2.1. The lymphatic system, a component of the body's immune system, comprises lymph nodes, vessels, and fluid that help filter harmful substances and combat infections. When cancer cells enter the lymphatic vessels, they can travel to nearby lymph nodes and potentially spread to distant organs such as the lungs, liver, bones, or brain. The presence of cancer cells in lymph nodes often suggests that the disease has begun to metastasize, which can impact treatment strategies and prognosis (American Cancer Society: Breast Cancer Basics, 2019).



Source Kumar et al. (2024)

**Figure 2.1** Normal Breast Tissue

### **2.2.1 Causes of Breast Cancer**

A combination of factors, including age, genetics, lifestyle, and hormone exposure influences the risk of developing breast cancer. A woman's age is a significant factor, with the likelihood of developing breast cancer increasing as she gets older. Most cases are diagnosed after the age of 50. Genetic mutations also play a crucial role, particularly for women who inherit abnormal genes like BRCA1 and BRCA2. Reproductive history can also impact risk. Women who began menstruating before age 12 or reached menopause after age 55 have a longer lifetime exposure to hormones, which may elevate their risk. Lifestyle choices are another contributing element. A lack of physical activity is associated with a higher chance of developing breast cancer. Additionally, being overweight or obese after menopause can increase risk. Alcohol consumption can also affect hormone levels and contribute to an elevated risk. A family history of breast or ovarian cancer, especially among close relatives, can significantly increase an individual's risk. Furthermore, certain medical exposures are linked to an increased risk. Taking hormone therapy for more than five years has been associated with a greater chance of breast cancer. Women who received radiation treatment to the chest or breasts before the age of 30 may also face a higher risk later in life. All these conditions can influence the likelihood of developing breast cancer and are important considerations for prevention and early detection strategies (Hulk & Stark, 1995; Kori, 2018; MacMahon et al., 1973).

### **2.2.2 Breast Cancer Treatment**

Breast cancer treatment can be separated into two types: local treatments and systemic treatments.

#### **2.2.2.1 Local Treatments**

Some localized medical procedures, such as surgery and radiation, target the tumor and do not affect the rest of the body. Surgery for breast cancer involves surgically removing tumors or reconstructing the breast after tumor removal. Surgical procedures include lumpectomy, mastectomy (simple or total, partial, and nipple-sparing), breast reconstruction surgery, and lymphadenectomy. The potential side effects of breast cancer surgery include seroma or hematoma formation, lymphedema, pain, infection, and cosmetic issues. While surgery is a crucial component of breast cancer treatment, it can lead to complications such as seroma (fluid accumulation),

hematoma (blood accumulation), lymphedema (swelling), pain, an increased risk of infection, and cosmetic concerns like scarring or changes in breast appearance. Despite these potential side effects, surgery plays a critical role in treating breast cancer and is often tailored to the patient's specific condition and preferences (Sharma et al., 2010; Golar et al., 2024; Tosello et al., 2018; Collins et al., 2011). Radiotherapy uses high-energy X-rays directed at the target area to destroy cancer cells, shrink tumors, and help prevent breast cancer recurrence after surgery. The side effects of radiation therapy can include skin color changes, soreness, blisters, skin peeling, blurry vision, cough, breathing difficulties, difficulty swallowing, and headache. These side effects generally result from the radiation's impact on healthy tissues surrounding the treatment area. Moreover, these side effects typically subside after the completion of treatment, although some may persist or require additional care. The severity of side effects varies depending on the treatment area, radiation dose, and the patient's individual response, and they are usually managed with medications or supportive care (Rutqvist et al., 2003; Cutuli et al., 2022).

#### 2.2.2.2 Systemic Treatments

Systemic treatments for breast cancer encompass a range of approaches, including chemotherapy, hormone therapy, targeted drug therapy, gene therapy, and immunotherapy. A key benefit of systemic treatments is their ability to reach cancer cells virtually anywhere in the body through the bloodstream. Chemotherapy functions by eliminating or reducing the size of cancer cells throughout the body and is typically administered intravenously every one to three weeks, spanning a total duration of twelve to twenty-four weeks. In some instances, chemotherapy is combined with other therapeutic modalities such as hormone therapy, biologically targeted therapy, or immunotherapy in the management of breast cancer. Potential side effects of chemotherapy include fatigue, hair loss, increased susceptibility to bruising or bleeding, risk of infection, anemia, nausea, vomiting, changes in appetite, and constipation. Hormone therapy, usually administered orally in tablet form, is used to treat hormone receptor-positive (HR+) breast cancer in women by blocking the supply of hormones that fuel tumor growth and spread. This type of therapy often requires a prolonged course of treatment, typically lasting five to ten years. Common side effects associated with hormone therapy include hot flashes, vaginal dryness, night sweats, bone pain, and

headaches. Targeted drug therapy, also known as molecularly targeted therapy, focuses specifically on breast cancer cells, with these drugs acting by targeting particular characteristics of the cancer. Targeted drug therapy aims to inhibit or eliminate cancer by interfering with the signals that promote cancer cell growth. Unlike chemotherapy, which can harm healthy cells and lead to side effects such as hair loss and reduced blood cell counts, targeted therapy is designed to primarily affect cancer cells. However, targeted drugs can have their side effects, including heart problems, diarrhea, and shortness of breath. Immunotherapy functions by enabling the body's immune system to identify and attack cancerous or abnormal cells, thereby hindering or slowing cancer progression. Similar to targeted therapy, immunotherapy is not typically harmful to normal cells. Nevertheless, its effectiveness in treating cancer can be limited because cancer cells have mechanisms to evade or suppress the immune system. Potential side effects of immunotherapy include flu-like symptoms, skin rash, and fatigue (American Cancer Society: Treating Breast Cancer, 2023; Almurshidi Medical Agency, 2020; Health Central: Breast Cancer, 2021; Conquer: Breast Cancer Treatments, 2020; Novartis Gene Therapies: Gene Therapy, 2022; Dastjerd et al., 2022). Gene therapy, an innovative treatment approach, introduces genetic material via a vector into target cells or surrounding tissues. This process aims to suppress gene function or impede cancer development. A particularly promising avenue within gene therapy involves utilizing nanoparticles to deliver small interfering RNA (siRNA). This method allows for the specific silencing of genes associated with cancer. These siRNA molecules function by binding to and breaking down messenger RNA (mRNA), which carries the instructions for producing proteins in tumor growth or survival. Nanoparticles are valuable delivery tools as they shield siRNA from degradation within the body, enhance its stability, and improve targeted delivery to tumors, thereby reducing impact on healthy tissues. This technique offers a highly precise way to deactivate specific genes, contributing to cancer progression (Mirzaei et al., 2023; Nicolescu et al., 2023; Mirza et al., 2021).

Breast surgery, chemotherapy, and radiation therapy are used extensively for breast cancer treatment. However, many side effects are associated with this technique, which is a major challenge for cancer treatment. To solve this problem, gene therapies have become more attractive in breast cancer treatment, resulting in high potential treatment and low side effects. While traditional treatments demonstrate

efficacy in numerous instances, they frequently impose considerable physical and emotional distress, encompassing issues like exhaustion, pain, hair loss, lymphedema, and lasting tissue damage. Gene therapy offers a more targeted approach by modifying or silencing specific genes involved in cancer development, thereby reducing harm to healthy cells. One of the most promising strategies is using small interfering RNA nanoparticles, which allow precise gene silencing with minimal toxicity. In clinical settings, gene therapy may not entirely supplant traditional modalities but holds promise as a complementary approach to enhance the effectiveness of surgery, chemotherapy, or radiation and lessen associated side effects. This combined strategy facilitates more individualized and thorough care, particularly for individuals with aggressive or treatment-resistant breast cancer.

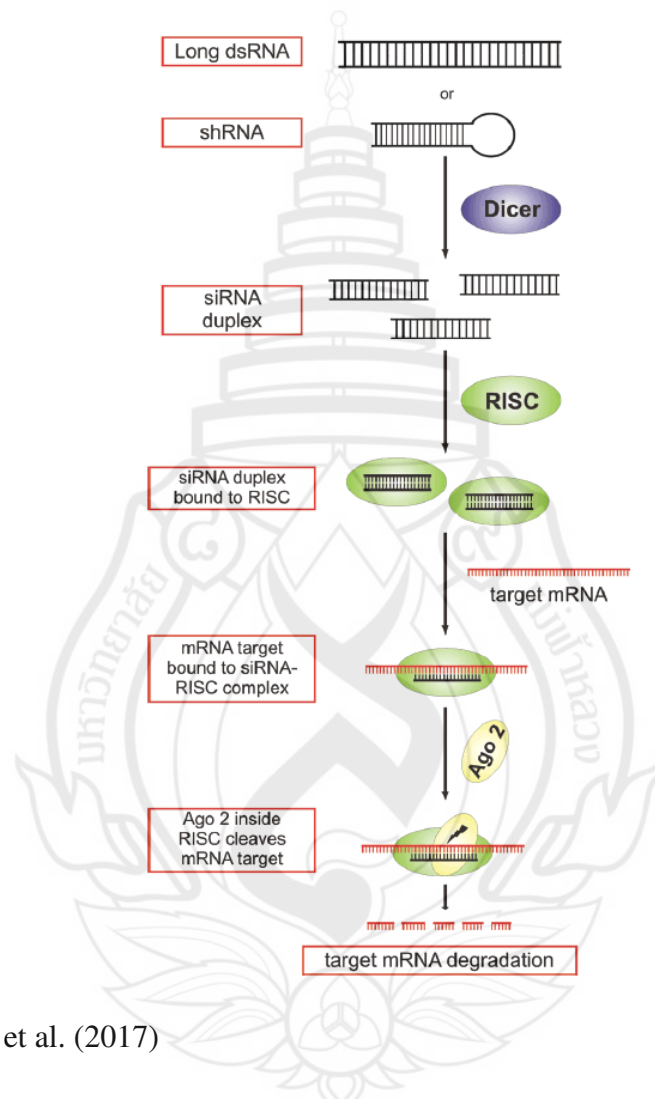
## **2.3 Small Interfering RNA (siRNA)**

siRNA is a class of double-stranded RNA (dsRNA) non-coding RNA molecules, typically 21-23 nucleotides long in length with hydroxylated 3' and phosphorylated 5' ends by the endonuclease dicer (Singh et al., 2018). siRNA has more attention in medical applications because of its role in gene silencing. Indeed, the therapeutic potential of siRNAs has been demonstrated in treating many diseases, including cancers (Taberner et al., 2013) and infections (Chandra et al., 2012). In siRNA-based therapeutic methods, a synthetic siRNA is introduced into the target cells to cause RNA interference (RNAi), which suppresses the expression of a particular messenger RNA (mRNA) and results in a gene-silencing effect (Lam et al., 2015).

### **2.3.1 Gene Silencing Mechanism of siRNA**

A normal biological process called RNA interference (RNAi) inhibits the expression of genes by encouraging mRNA breakdown. It plays an important role in gene regulation and is innate against invading viruses (Agrawal et al., 2003). Typically, a specialist ribonuclease (RNase) III-like enzyme called Dicer breaks down the dsRNA into a smaller dsRNA molecule in the cytoplasm. This short dsRNA molecule is known as siRNA. siRNA interacts and activates the RISC. The endonuclease argonaute 2 (AGO2) component of the RISC cleaves the passenger strand (sense strand) of siRNA,

while the guide strand (antisense strand) remains associated with the RISC. The active RISC is then directed by the guide strand to its target mRNA for AGO2 to cleave. Specific genes are silenced by siRNA because the guide strand only binds to the mRNA of the target cell (Agrawal et al., 2003; Pecot et al., 2011; Lam et al., 2015), as shown in Figure 2.2.



Source Brea et al. (2017)

**Figure 2.2** Gene Silencing Mechanisms of siRNA Demonstrate That the Sense Strand is Removed, Leaving Only the Antisense Strand to Bind the Target mRNA

### 2.3.2 siRNA as Therapeutic Agents

The specific gene silencing of siRNAs is important for target identification and validation in drug discovery and development (Perwitasari et al., 2013; Drosopoulos & Linardopoulos, 2019). The siRNA's total guanine/cytosine (G/C) composition

influences the siRNA activity (Reynolds et al., 2004). G/C content impacts both target site accessibility and the overall thermodynamic stability of the duplex. siRNAs with very high G/C content seem to be less useful (Wang et al., 2009). This is because a high G/C content increases the stability of the siRNA duplex, making it more difficult to unwind and thus reducing its ability to bind to the target mRNA effectively. The higher stability might also interfere with the siRNA's ability to be processed by the RISC, a crucial step for gene silencing. Furthermore, siRNAs with excessive G/C content might lead to off-target effects or induce immune responses, hindering their therapeutic potential. For these reasons, siRNAs with moderate G/C content are typically preferred, as they balance stability and efficient gene silencing while minimizing adverse effects (Reynolds et al., 2004; Ui-Tei et al., 2004). Some studies suggest that the optimal G/C content of siRNA was around 30–50%, while others showed that siRNAs with G/C contents of about 60% were highly efficient (Kurreck, 2006; Tafer et al., 2008). These findings highlight that the relationship between G/C content and siRNA efficacy is not linear, and the optimal percentage can vary depending on the specific target and application. siRNAs with a 30-50% G/C content tend to balance stability and flexibility well. This allows them to efficiently interact with the target mRNA and be processed by the RISC for gene silencing. On the other hand, siRNAs with around 60% G/C content are sometimes more effective because the increased stability helps them bind more securely to their target sites, improving their ability to silence genes. On the other hand, increased guanine and cytosine (G/C) content may also confer greater resistance to degradation on siRNAs, potentially improving their suitability for therapeutic applications where prolonged activity is desired. While siRNAs within a broad range of G/C content can demonstrate efficacy, fine-tuning this ratio is critical for achieving the best possible outcomes in siRNA-based therapies. The specific sequence, the target tissue, and the intended therapeutic goal frequently dictate the optimal composition. Ultimately, despite the need for caution regarding very high G/C content in siRNAs, elevated levels can offer advantages in certain circumstances. These findings do not conflict; instead, they emphasize that the ideal G/C content for siRNAs is determined by the specific design and its intended use in therapy. In essence, siRNAs with G/C content ranging from moderate to high can be effective, but a careful balance is necessary to maximize their efficacy and minimize potential negative consequences

such as reduced target binding or unintended off-target effects (Chan et al., 2009; Lam et al., 2015; Safari et al., 2017).

### **2.3.3 Survivin siRNA**

Survivin siRNA is a small interfering RNA molecule specifically designed to silence the survivin gene, which is known to inhibit apoptosis and support uncontrolled cell division in many types of cancer. By targeting and degrading the mRNA of survivin, this siRNA can effectively reduce the expression of the survivin protein, thereby promoting cancer cell death and enhancing the effectiveness of other treatments such as chemotherapy and radiation (Mobahat et al., 2014; Khan et al., 2019; Vaidya et al., 2023). Suppressing survivin also helps overcome resistance to conventional therapies, as many cancer cells rely on its presence to survive treatment-induced stress. However, one of the significant challenges in using siRNA as a therapeutic agent is its poor stability in the bloodstream and limited ability to enter cells on its own. siRNA molecules are easily degraded by enzymes in the blood and have difficulty crossing the cell membrane due to their negative charge and relatively large size. Moreover, even when taken up by cells, siRNA can become trapped in endosomes, preventing it from reaching the cytoplasm where gene silencing occurs. Therefore, efficient delivery systems are essential to protect siRNA from degradation, facilitate cellular uptake, and ensure its release into the cytoplasm for maximum therapeutic effect.

Researchers have developed survivin siRNA-based nanoparticles to overcome these limitations by directly formulating the siRNA into nanoparticle structures using positively charged polymers, such as polyethyleneimine. These polymers interact with the negatively charged siRNA through electrostatic binding, condensing the siRNA into stable nanoparticle complexes. This formulation protects the siRNA from enzymatic degradation in the bloodstream and facilitates cellular uptake by improving membrane interaction and internalization. Trans-Booster can be incorporated as an additive into the nanoparticle system to further enhance transfection efficiency. These components facilitate the escape of nanoparticles from endosomes and their release of siRNA into the cytoplasm, where gene silencing occurs. This strategy of creating survivin siRNA nanoparticles represents a promising and efficient delivery platform with a high potential for targeted breast cancer therapy and improved treatment outcomes.



### 2.3.4 Polyethyleneimine (PEI)

PEI is a cationic polymer widely used in gene delivery due to its strong positive charge, which allows it to efficiently bind to negatively charged nucleic acids such as siRNA through electrostatic interactions. One of the main advantages of PEI is its high transfection efficiency, as it can condense siRNA into compact nanoparticles and promote cellular uptake through endocytosis. Additionally, PEI possesses a “proton sponge effect,” which helps disrupt endosomal membranes and release the siRNA into the cytoplasm, enhancing gene silencing efficiency. However, PEI has notable drawbacks, including cytotoxicity, especially at high molecular weights or concentrations, which can limit its clinical application. To address this, researchers often modify PEI or use lower molecular weight forms to balance efficacy and biocompatibility. In the context of siRNA particle formation, PEI's ability to generate stable nanoparticles, protect against enzymatic degradation, and enhance intracellular delivery renders it a crucial component in the development of siRNA-based treatments (Yin et al., 2014; Hanzlíková et al., 2011; Wu et al., 2017; Kichler et al., 2001). PEI is the most widely investigated polymer for *in vivo* siRNA delivery (Neuberg et al., 2014; Chiou et al., 2012; Höbel & Aigner, 2013; Urban-Klein et al., 2005). Li et al. developed a nanocarrier based on PEI, folic acid, and cyclodextrin for the siRNA delivery system for tumor-targeted delivery. The siRNA delivery system shows low cytotoxicity and high siRNA delivery activity. Moreover, the copolymer/siRNA can efficiently target tumors and inhibit tumor growth by silencing the VEGF gene *in vivo*. The siRNA-loaded nanocomplexes showed uniform size distribution, high cellular uptake, and significant gene suppression for enhancing the effect of anticancer drugs (Li et al., 2015). Santadkha et al. improved the delivery of myeloid cell leukemia-1 and survivin siRNA combination through anionic of siRNA and cationic of PEI for treating breast cancers. PEI was used as a transfection reagent. The siRNA and PEI complexes showed the highest inhibition of cell viability and effectiveness of siRNA delivery. Moreover, the cellular uptake showed the fluorescein amidites (FAM)-positive population was 80% on day 1 for all formulations with the PEI (Santadkha et al., 2022).

## 2.4 Hydrogel

Hydrogel is a three-dimensional network of hydrophilic polymer chains formed chemical or physical crosslinking using covalent bonds, hydrogen bonds, and Van der Waals interactions. Biopolymer hydrogels, such as proteins and polysaccharides are suitable for biomedical applications because of their biocompatibility, biodegradability, and non-toxicity. Moreover, they can absorb large amounts of water or biological fluids and inject them into the target site (Van-Vlierbergh et al., 2011). This unique ability to retain water makes hydrogels structurally similar to natural tissue, which enhances their performance as drug delivery carriers or tissue engineering scaffolds. Their high-water content also allows for the sustained and controlled release of therapeutic agents, such as siRNA or chemotherapeutic drugs, improving treatment efficiency and reducing side effects. Moreover, their tunable mechanical properties and biocompatibility enable hydrogels to closely mimic the extracellular matrix (ECM), providing a supportive environment for cell growth, differentiation, and tissue regeneration. Hydrogels can be engineered to vary in stiffness, porosity, and degradation rate, allowing precise customization for specific tissue types such as soft tissue. This adaptability enhances cell-material interactions and supports the integration of the hydrogel with surrounding tissues. Hydrogels can encapsulate living cells, proteins, or genetic material, preserving their biological function while allowing gradual release in response to environmental cues such as pH, temperature, or enzymatic activity. In particular, hydrogels have emerged as effective platforms for the localized and sustained delivery of siRNA nanoparticles. siRNA is highly susceptible to degradation by nucleases in the biological environment and has limited cellular uptake. To address these challenges, siRNA is often complexed into nanoparticles using carriers such as lipids, polymers, or inorganic materials, which protect it from degradation and enhance intracellular delivery. When embedded within a hydrogel matrix, these siRNA nanoparticles can be shielded from harsh extracellular conditions while being released gradually at the target site. This improves the bioavailability and therapeutic efficacy of siRNA and allows for spatial and temporal control over gene silencing. As a result, hydrogel-based systems for siRNA nanoparticle delivery hold promise for treating various diseases, including

cancer, inflammatory disorders, and genetic conditions. To further enhance the targeted delivery and clinical applicability of siRNA nanoparticles-loaded hydrogels, injectable formulations have emerged as a particularly promising strategy.

Injectable hydrogels can conform to irregularly shaped defects or tumor sites, enabling minimally invasive administration. The most promising carrier for siRNA delivery is the injectable hydrogel (Nguyen & Lee, 2010). The injectable hydrogel is a subclass prepared by extruding various hydrogel components through a syringe to a specific site. This injectable hydrogel is injected in a liquid form into the body and instantly converted into a solid hydrogel *in situ* via physical or chemical crosslinking without the aid of a potentially toxic or denaturalizing crosslinking agent (Mathew et al., 2018). The injectable hydrogels can access the target site in difficult-to-reach areas. The injectable hydrogel has been developed to deliver therapeutic agents such as drugs, cells, and genes to treat inflammatory, infectious diseases, and cancers (Cao et al., 2015). Wang et al. developed an injectable polymer assembly from PEI and polyethylene glycol to promote local and sustained siRNA delivery. The polyplexes of guest-host-modified polymers assembled with siRNAs improved transfection and decreased cytotoxicity compared to PEI (Wang et al., 2017). Basu et al. studied the self-healing deoxyribonucleic acid-based hydrogel crosslinked with oxidized alginate via the formation of reversible imine linkages for controlled drug delivery to restore damaged tissue functionality. The results showed that this hydrogel had sustained-release properties for minimally invasive therapeutic approaches (Basu et al., 2020).

#### **2.4.1 Injectable Self-healing Hydrogels**

Injectable self-healing hydrogels are advanced materials that transition from a liquid to a gel state once injected into the body, forming a solid structure at the target site. Self-healing hydrogel dressings represent a significant innovation in modern biomedical applications, particularly for controlled and localized drug delivery (Chen et al., 2018; Chen et al., 2022). These hydrogels exhibit an exceptional capacity to restore their structural integrity following physical damage or deformation, making them highly effective in maintaining sustained therapeutic delivery within dynamic physiological environments. Constructed from biocompatible polymeric materials, self-healing hydrogels establish a dynamic network that can reassemble itself after mechanical stress, thereby enhancing their reliability and functionality in drug delivery

systems (Sharma et al., 2018; Han et al., 2019). This transition happens quickly when the liquid solution is extruded through a syringe and undergoes gelation, making them ideal for localized delivery of therapeutic agents like siRNA nanoparticles (Mathew et al., 2018). These hydrogels are particularly effective in siRNA therapy because they allow targeted treatment directly at the site of interest, bypassing the challenges associated with systemic administration, which may lead to uneven distribution of siRNA. The self-healing properties of these hydrogels refer to spontaneous chemical reactions where the hydrogels can re-form themselves after being damaged or cut, allowing them to restore their original structure and functionality. This ability is typically enabled through crosslinking mechanisms such as the Schiff base reaction, where amino groups react with aldehyde or ketone groups to form imine bonds, contributing to the self-healing characteristics (Devi et al., 2021; Yu et al., 2023).

#### 2.4.1.1 Dynamic Covalent Bonds

Dynamic covalent bonds are increasingly utilized in developing biomedical materials because of their ability to undergo reversible chemical reactions (Bertsch et al., 2022). This reversible nature allows materials to adapt to environmental changes, repair themselves, or reconfigure their structure in response to external stimuli. These characteristics are particularly important for designing effective self-healing systems, with imine bonds (Schiff base) commonly employed due to their ability to reversibly form and cleave under mild conditions (Liu et al., 2018). Schiff base chemistry, involving the reaction of an amine with an aldehyde or ketone to form an imine bond, offers distinct advantages for biomedical applications, particularly in drug delivery. Its reversible and pH-responsive nature allows for developing smart drug delivery systems that can respond to changes in the physiological environment. For instance, imine bonds can remain stable at neutral pH but cleave in acidic conditions, enabling targeted release of therapeutic agents in areas such as tumor tissues or intracellular compartments where the pH is lower than normal. Drug delivery systems based on Schiff base linkages can be engineered to provide controlled release profiles, enhancing the efficiency of drug administration while minimizing systemic side effects. Additionally, the dynamic behavior of these bonds allows the carrier system to self-heal or reassemble, which can extend its functional lifespan and responsiveness. These features make Schiff base chemistry a promising platform for designing intelligent drug carriers with

environmental adaptability and high biocompatibility. Zhang et al. developed a multifunctional hydrogel dressing using Schiff base chemistry and thiol-alkynone cross-linking. The amino groups from chitosan reacted with the aldehyde groups of oxidized alginates to form dynamic imine bonds. The resulting hydrogel exhibited good mechanical strength, self-healing capability, and antibacterial activity, highlighting its potential for wound care applications (Zhang et al., 2022). Chen et al. developed an injectable, self-healing hydrogel for enhanced wound healing. Oxidized konjac glucomannan provided aldehyde groups that reacted with chitosan's amino groups to form imine bonds via Schiff base chemistry. The resulting hydrogel demonstrated excellent injectability, self-healing ability, and significantly accelerated the healing of full-thickness skin wounds (Chen et al., 2018). Sun et al. developed self-healing hydrogels with stimuli responsiveness using poly(N-isopropylacrylamide) copolymers and oxidized sodium alginate, forming self-healing and pH-sensitive hydrogels through acylhydrazone bonds (imine bond). These hydrogels exhibit reversible sol-gel transitions and tunable phase transition temperatures between 30 °C and 40 °C, adjustable by varying the aldehyde-hydrazone ratio. The self-healing ability was confirmed by rheological recovery tests, and the hydrogels can be reshaped repeatedly in response to pH changes. The gelation time is 10-20 min, with healing occurring over 24 h at 37 °C (Sun et al., 2019).

#### 2.4.1.2 Quaternized Chitosan (QCS)

The application of CS as a carrier for siRNA nanoparticles faces significant limitations due to its poor solubility at physiological pH, particularly around neutral pH (pH ~7.4). This low solubility occurs because the amino groups on CS become protonated and positively charged, primarily in acidic environments. Consequently, under neutral conditions, the charge density is reduced, resulting in a decreased interaction with negatively charged siRNA. This can compromise the efficiency of gene loading, cellular uptake, and delivery, thereby limiting its therapeutic potential (Croisier & Jérôme, 2013; Jayakumar et al., 2011). To address this drawback, chemical modification of CS has been widely explored. The quaternization reaction between the amino groups of CS and epoxy groups of glycidyl trimethylammonium chloride (GTMAC) was employed, producing quaternary ammonium groups to the polymer chain (Zhao et al., 2015; Sajjan et al., 2015; Ruihua et al., 2012). The resulting QCS

exhibits improved aqueous solubility, enhanced electrostatic interaction with siRNA, and better stability of nanoparticles. These enhancements make QCS a promising non-viral vector for gene delivery, particularly in systemic applications with critical stability and bioavailability. Moreover, the improved physicochemical properties of QCS allow for better control over nanoparticle size, surface charge, and release behavior, essential in designing efficient and targeted siRNA nanoparticle delivery systems. Additionally, QCS can react with OxPec to form a self-healing hydrogel. This hydrogel system not only improves the mechanical properties of the matrix, allowing it to recover its structure after deformation, but also provides a more controlled and sustained release of therapeutic agents. The self-healing characteristic ensures the hydrogel remains intact at the application site, even under mechanical stress, making it particularly useful for localized treatments.

#### 2.4.1.3 Oxidized Pectin (OxPec)

Pectin (Pec) is an anionic polysaccharide found in 30% of the cell walls of higher plants. It is a heterogeneous polymer, consisting of homogalacturonan regions interrupted by ramified regions (Harholt et al., 2010; Moreira et al., 2014). Pec has been used in biomedical applications because of its hydrophilicity, biocompatibility, low toxicity, and biodegradability (Li et al., 2021). Pec has the carboxylate and methylated ester groups, giving it water solubility. Pectin (Pec) can be modified through sodium periodate oxidation to enhance its functional properties by introducing aldehyde groups, producing OxPec (Gupta et al., 2013). Sodium periodate oxidizes the hydroxyl groups at the carbon-2 and carbon-3 positions of the glucuronic acid residues in the pectin backbone, which cleaves the carbon-carbon bond between these positions. This oxidative cleavage results in the opening of the sugar ring and the generation of two aldehyde groups per modified unit of pectin (Fan et al., 2012; Chen et al., 2015; Freitas et al., 2021). In addition, introducing these reactive aldehyde functionalities significantly enhances the chemical reactivity of Pec, enabling it to form dynamic covalent bonds such as Schiff bases when combined with the amino group of polymers like CS. This modification alters both the structural and chemical properties of Pec and crucially enables hydrogel formation, leading to the development of self-healing, injectable, and biocompatible materials suitable for biomedical applications (Chen et al., 2015; Chanmontri et al., 2023).

Numerous researchers have studied injectable self-healing hydrogels for biomedical applications. Ren et al. prepared injectable hydrogels based on QCS, gelatin, and dopamine as localized release systems. The results showed that the dopamine was sustained without a burst release for over 12 days. Moreover, these injectable hydrogels exhibited good degradability and no toxicity to L929 cells (Ren et al., 2017). Chanmontri et al. developed an injectable self-healing hydrogel using QCS and OxPec for wound dressing applications. The hydrogel formed rapidly (<1 min) through Schiff's base and ionic interactions, showing good mechanical properties, self-healing ability, and suitable adhesiveness. Overall, the hydrogel is a promising biocompatible material for wound management (Chanmontri et al., 2023). An et al. developed the injectable and self-healing hydrogel from pectin and acylhydrazide functionalized poly(N-isopropylacrylamide-stat-acylhydrazide) for enhanced synergistic anticancer therapy. The results showed that the hydrogel formed gel in around 1 min without any stimulus. Moreover, the self-healing hydrogels are injectable, biodegradable, and self-healing for localized anticancer therapy (An et al. 2021). Based on the aforementioned research, this combination of QCS and OxPec offers an innovative, biocompatible, and stable system, enhancing the potential for efficient delivery to targeted sites such as breast cancer cells.

#### **2.4.2 Injectable Thermosensitive Hydrogels**

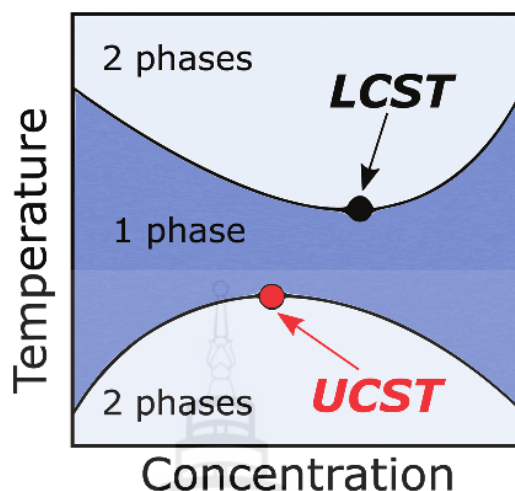
Injectable thermosensitive hydrogels are an innovative class of materials that undergo a phase transition in response to temperature changes, making them highly suitable for localized drug delivery, especially in cancer therapy. These hydrogels are designed to be injected in a liquid form, and once inside the body, they quickly transform into a gel at body temperature. This temperature-sensitive behavior allows for controlled and sustained drug release directly at the cancer site, improving the efficacy of treatments and minimizing systemic side effects (Shaker et al., 2016; Ahsan et al., 2020; Mohammed et al., 2020). Typically, these hydrogels are composed of thermosensitive polymers, which are often derived from natural sources. These polymers contain both hydrophobic (water-repelling) and hydrophilic (water-attracting) components, and temperature variations alter the balance between these components and water molecules in the polymer. As a result, the hydrogel's solubility

changes, causing it to transition from a liquid state to a gel (Bajpai et al., 2008; Huang et al., 2019). In addition, the injectability of these hydrogels provides the advantage of minimally invasive administration, enabling them to be delivered directly to difficult-to-reach cancer sites. Once injected, the hydrogel forms a stable, localized depot that ensures prolonged drug release, which is particularly beneficial for therapies such as siRNA delivery, where controlled release is critical for effective gene silencing (Mathew et al., 2018).

#### **2.4.2.1 Critical Solution Temperature**

The critical solution temperature (CST) is the temperature at which a polymer solution undergoes a distinct phase transition, changing from a single homogeneous phase to two separate phases. This transition is crucial in thermoresponsive polymers, which are materials that can reversibly change their physical properties, such as solubility and structure, in response to temperature variations. At lower temperatures, these polymers generally remain dissolved in a solvent, while at higher temperatures, they either phase separate, precipitate, or form gels due to changes in their solubility (Musarurwa et al., 2022; Hasnain et al., 2019; Gandhi et al., 2015). Thermoresponsive polymers are classified based on the nature of their CST behavior into two main categories: low critical solution temperature (LCST) and upper critical solution temperature (UCST). Polymers exhibiting LCST behavior are soluble below their LCST. However, as the temperature rises above this threshold, their solubility decreases, resulting in phase separation or gelation. Conversely, UCST-type polymers are insoluble at lower temperatures and become soluble only when the temperature exceeds their UCST. The lower critical solution temperature (LCST) and upper critical solution temperature (UCST), illustrated in Figure 2.3, represent the critical points below and above which a polymer and solvent become miscible (Le et al., 2022; Marsili et al., 2021; Bordat et al., 2019).





**Source** Niskanen and Tenhum (2017)

**Figure 2.3** A Phase Diagram Showing the UCST and LCST Points for a Thermoresponsive Polymer

#### 2.4.2.2 Chitosan

Chitosan (CS) is a cationic polysaccharide derived from chitin through a chemical process known as deacetylation, in which acetyl groups are removed from the chitin structure. Chitin is a natural polymer commonly found in the exoskeletons of crustaceans and insects. The molecular structure of CS consists of repeating units of D-glucosamine and N-acetyl-D-glucosamine, linked together by  $\beta$ -1,4 glycosidic bonds (Nguyen et al., 2013). Due to the presence of free amino groups, CS carries a positive charge in acidic environments, contributing to its unique biological properties, including biocompatibility and biodegradability (Baldrick, 2010; Ma et al., 2014). The characteristics of CS make it a valuable material for biomedical and pharmaceutical applications. Building on these favorable biological properties, CS has attracted considerable attention as a key component in developing thermosensitive hydrogels, particularly for biomedical applications such as drug delivery systems. CS is a natural biopolymer derived from chitin that typically exhibits LCST behavior. This means it is soluble in aqueous solutions at lower temperatures but undergoes a phase transition, such as gelation or precipitation, as the temperature increases beyond a specific point. The LCST of CS can be influenced by several factors, including its degree of deacetylation (which affects its molecular structure), its concentration in solution, the

ionic strength of the solvent, and the presence of specific additives like salts. These factors alter the polymer's hydration and interaction with water molecules, influencing the temperature at which phase separation occurs. Understanding and controlling the LCST of CS is crucial for its applications in areas like drug delivery, tissue engineering, and biomedical applications, where temperature-triggered responses are needed. Upon injection, the formulation remains in a liquid state at room temperature, allowing for easy administration, and subsequently forms a gel at body temperature, enabling prolonged retention at the cancer site. This localized gel matrix protects siRNA nanoparticles from enzymatic degradation in the extracellular environment and facilitates sustained release, improving cellular uptake and gene silencing efficiency in target cancer cells. Furthermore, the mild gelation conditions preserve the structural integrity and biological activity of siRNA, making this delivery platform a promising approach for enhancing the therapeutic efficacy and specificity of RNA interference-based treatments in breast cancer (Rahmanian-Devin et al., 2021; Rezakhani et al., 2021; Karimi et al., 2022).

#### 2.4.2.3 Beta-glycerol Phosphate

Beta-glycerol phosphate ( $\beta$ -GP) is an organic phosphate compound commonly used in biomedical research. It acts as a buffering and crosslinking agent and is primarily known for its role in forming thermosensitive hydrogels when combined with CS, a natural biopolymer. One of the main advantages of  $\beta$ -GP is its ability to induce temperature-responsive gelation. When mixed with CS, the solution remains liquid at room temperature but turns into a gel at body temperature (around 37°C). This property makes the CS/ $\beta$ -GP system particularly useful for injectable hydrogel formulations, as the material can be easily administered in liquid form and then solidified in situ after injection. In addition to its thermosensitive behavior,  $\beta$ -GP is also biocompatible and supports cell viability, making it a suitable candidate for applications in tissue engineering, drug delivery, and wound healing. Furthermore, it contributes to the mechanical stability of the hydrogel and enhances its potential as a scaffold for cell growth (Ahmadi & de Bruijn, 2008; Rahmanian-Devin et al., 2021; Qin et al., 2018; Yang et al., 2020). Additionally,  $\beta$ -GP can play a significant role in modifying the thermoresponsive properties of polymers, particularly in regulating their gelation behavior or phase transitions. When combined with thermoresponsive

polymers like CS,  $\beta$ -GP can influence the sol-gel transition by altering the polymer's solubility at different temperatures.  $\beta$ -GP may interact with the polymer matrix, potentially lowering or raising the LCST of chitosan or other similar polymers, thus allowing for more precise control over their thermo-responsive behaviors. This makes  $\beta$ -GP a useful agent in fine-tuning the phase transition temperatures for various biomedical and drug delivery applications, where temperature-controlled responses are critical.

#### 2.4.2.4 Silk Sericin

Silk is a natural polymer from protein produced by spiders, insects, and silkworms. Silk consists of two major components: fibroin (72–81 wt%) and sericin (19–28 wt%). Silk sericin (SS) is a biocompatible protein exhibiting low immunogenicity, biodegradability, and excellent biocompatibility. Moreover, it has antioxidant and anti-coagulation activities and can promote cell growth and differentiation. Due to these beneficial properties, SS has gained attention as a functional biomaterial in drug delivery systems. Its ability to interact with various therapeutic agents enables controlled and sustained drug release, while its natural origin and biocompatibility reduce the risk of adverse immune responses. Additionally, SS can be incorporated into different delivery systems, such as nanoparticles, films, or hydrogels, to enhance drug stability, improve bioavailability, and support targeted delivery to specific tissues or cells (Zhang et al., 2006; Wenk et al., 2011; Meechaisue et al., 2007; Nguyen et al., 2019; Koh et al., 2015).

The potential of injectable, temperature-responsive hydrogels in biomedical applications has been explored by many researchers.. Ma et al. developed a thermosensitive CS hydrogel as siRNA reservoir and vector for periodontitis. The thermosensitive CS hydrogel was formed from a solution (pH 7.2, at 4°C) into a hydrogel at 37°C within 8 min. The degradation rate of CS hydrogel was 50%, over 20 days. The *in vitro* release of siRNA from the hydrogel was 50% and 17% over 14 days, with or without lysozyme digestion, respectively (Ma et al., 2014). Ahsan et al. developed a thermosensitive CS-based injectable hydrogel for sustained delivery of disulfiram to cancer cells. The hydrogel rapidly transitioned from sol to gel at body temperature, with gelation occurring within 3 min. It showed high encapsulation efficiency (93%) and sustained drug release. Cellular uptake of disulfiram was

enhanced compared to the free drug, indicating improved delivery potential (Ahsan et al., 2020). Han et al. developed the CS hydrogel for localized gene silencing. The CS hydrogel displayed a liquid-solid phase transition in a temperature-dependent manner and formed an endothermic hydrogel in tumor tissue after intra-tumoral injection. The liquid phase at room temperature changed to the solid phase after injection into the tumor. Moreover, the release of siRNA occurred within 12 h, followed by a slower release over time (Han et al., 2011). Pankongadisak and Suwantong developed thermosensitive CS/SS hydrogels loaded with longan seed extract for bone tissue engineering.  $\beta$ -GP was used as a catalyst for achieving a sol-to-gel transition in chitosan solutions at 37 °C. The combination of CS and SS could form a sol at room temperature (25 °C) and be transformed rapidly into a gel state at physiological temperature (37 °C). Moreover, the incorporation of SS into hydrogel resulted in a shorter gelation time of 5-7 min (Pankongadisak & Suwantong, 2018). In 2019, Pankongadisak and Suwantong developed the injectable thermogelling hydrogels based on CS and silk fibroin (SF), loaded with longan seed water extract for bone tissue engineering. The gelation process, triggered by the interaction between the amino groups of CS and the phosphate groups of  $\beta$ -GP, resulted in a gelation time of 10 min for CS hydrogels and 4-7 min for CS/SF hydrogels. The incorporation of SF reduced gelation time and improved the porous structure and degradability of hydrogels. Biocompatibility tests showed the hydrogels were non-toxic, with enhanced cell attachment and proliferation of MC3T3-E1 cells on CS/SF hydrogels loaded with water extract of longan seed (Pankongadisak & Suwantong, 2019). Bahmanpour et al. prepared the thermosensitive hydrogel from CS, QCS, and gelatin as a carrier for intranasal insulin administration. The hydrogels showed a low gelation time, uniform pore structure, and a desirable swelling rate. The release of insulin from thermosensitive hydrogel occurred 16% at 24 h (Bahmanpour et al., 2021).

## CHAPTER 3

### MATERIALS

**Table 3.1** Materials

Chemical / Reagent Name	Supplier
Trans-Booster (Mw of 1.2 kDa)	RJH Bioscience Inc. (Edmonton, Alberta, Canada)
Prime-Fect	RJH Bioscience Inc. (Edmonton, Alberta, Canada)
Dulbecco's Modified Eagle Medium (DMEM)	Gibco (USA)
Fetal Bovine Serum (FBS)	Gibco (USA)
Antibiotic-antimycotic	Gibco (USA)
Hank's Balanced Salt Solution (HBSS)	Gibco (USA)
Phosphate buffered saline (PBS) pH 7.4	Gibco (USA)
3-(4,5-Dimethylthiazol-2-yl)-2,5-diphenyltetrazolium bromide (MTT)	Sigma-Aldrich (USA)
Dimethyl sulfoxide (DMSO)	Sigma-Aldrich (USA)
Pectin (Pec) from citrus peel	Sigma-Aldrich (USA)
Doxorubicin	Sigma-Aldrich (USA)
Glycidyl trimethylammonium chloride (GTMAC)	Sigma-Aldrich (USA)
Beta-Glycerophosphate ( $\beta$ -GP)	Sigma-Aldrich (USA)

**Table 3.1** (continued)

<b>Chemical / Reagent Name</b>	<b>Supplier</b>
6-Caboxyfluorescein survivin siRNA (FAM-survivin) (forward: 5'-56-FAM-AGACAGAAUAGAGUGAUAGGAAGCG-3'; reverse: 5'-CGCUUCCUAUCACUCUAUUCUGUCU-3')	IDT Technologies (USA)
Primers for Human-survivin (SVV; forward: 5'-TGAGAACGAGCCAGACTTGG-3'; reverse: 5'-ATGTTCTCTATGGGGTCGT-3')	IDT Technologies (USA)
SensiFAST™ SYBR Hi-ROX kit	Bioline (CA)
SensiFast™ cDNA synthesis kit	Bioline (CA)
Sodium periodate	Loba Chemie Pvt. Ltd (India)
Survivin siRNA (siSVV) Cat. No. HSC.RNAIN001012271.12.1	IDT Technologies (USA)
Negative control scrambled siRNA (CsiRNA; Cat No.308480258)	IDT Technologies (USA)
6-carboxyfluorescein negative control siRNA (FAM-CsiRNA) (forward: 5'-56-FAM-GCGUAUUAUACGCGAUUAACG-3'; reverse: 5'-CGUUAUUCGCGUAUAAUACGC-3')	IDT Technologies (USA)
Lysozyme	Himedia (India)
Paraformaldehyde	Himedia (India)
Ethanol	RCI LabScan Limited (Bangkok, Thailand).
Anhydrous sodium carbonate (Na <sub>2</sub> CO <sub>3</sub> )	Ajax Chemicals (Australia)
TRIzol™ reagent	Invitrogen™, Thermo Fisher Scientific (USA)

**Table 3.1** (continued)

<b>Chemical / Reagent Name</b>	<b>Supplier</b>
1X Trypsin-EDTA (0.5%), without phenol red	Gibco, Thermo Fisher Scientific, Massachusetts (USA)
Phenol red	(Gibco, Thermo Fisher Scientific, Massachusetts, USA)
Dialysis bag (SnakeSkin™ Dialysis Tubing, MWCO: 3500)	Thermo Scientific™, Thermo Fisher Scientific, USA
Chitosan (CS) low molecular weight with a molecular weight of 20-30 kDa and a degree of deacetylation of 86%	Bio 21 Co., Ltd. (Thailand)
CS medium molecular weight with molecular weight = 25-500 kDa and degree of deacetylation = 91.46%	Bio 21 Co., Ltd (Thailand)
Raw silk cocoons	Queen Sirikit Sericulture Center (Chiang Mai, Thailand).

## **CHAPTER 4**

# **PREPARATION AND CHARACTERIZATION OF SMALL INTERFERING RNA NANOPARTICLES FOR TARGETED DELIVERY TO BREAST CANCER CELLS**

### **4.1 Methodology**

#### **4.1.1 Preparation of Small Interfering RNA (siRNA) Nanoparticles**

The siRNA nanoparticles were prepared using a modified method according to Santadkha et al. (Santadkha et al., 2022). Table 4.1 presents an overview of the siRNA nanoparticles formulations. First, the Trans-Booster as an additive was incorporated into the siRNA solution, which had been dissolved in DMEM, using a 1:1 weight-to-weight (w/w) ratio of siRNA to Trans-Booster. This resulted in a final siRNA concentration of 80 nM in DMEM. The 1:1 ratio was selected based on prior findings demonstrating that it achieved the highest level of cellular uptake. Subsequently, the Prime-Fect was introduced at a 1:10 (w/w) ratio relative to the siRNA. The resulting mixture was then incubated at room temperature for 30 min to ensure efficient complex formation.



**Table 4.1** Compositions of siRNA Nanoparticles

siRNA	siRNA Conc. (nM)	siRNA/Trans- s-Booster /Prime-Fect	DME M ( $\mu$ L)	siRNA (0.14 $\mu$ g/ $\mu$ L)	Trans- Booster (0.14 $\mu$ g/ $\mu$ L)	Prime Fect (1 $\mu$ g/ $\mu$ L)	Transfect ion volume ( $\mu$ L)
CsiRNA	80	1:1:10	8.7	1.3	1.3	3.7	15
siSVV	80	1:1:10	8.7	1.3	1.3	3.7	15
CsiRNA	80	1:0:10	11.8	1.3	0	1.8	15
siSVV	80	1:0:10	11.8	1.3	0	1.8	15

#### 4.1.2 Size, Polydispersity, and Zeta-Potential of siRNA Nanoparticles

The hydrodynamic diameter (Z-average), polydispersity index (PDI), and zeta-potential of the siRNA nanoparticles were assessed using a Zetasizer Nano ZS (Malvern, UK), which is an advanced instrument designed to measure these critical parameters. The Z-average refers to the mean size of the nanoparticles in solution, while the PDI indicates the distribution of particle sizes within the sample, with a lower PDI value suggesting a more uniform nanoparticle population. The zeta-potential measurement provides insight into the surface charge of the nanoparticles, which is essential for understanding their suspension stability and potential interactions with biological systems. To prepare 80 nM of siRNA nanoparticles, siRNA, along with an additive and Prime-Fect transfection reagent as a 1:1:10 w/w, were formulated in 20  $\mu$ L of Milli-Q water, a highly purified form of water with minimal ions and impurities. The mixture was gently flushed with an autopipette to ensure complete dissolution and homogeneity of the components. After the formulation was prepared, the mixture solution was incubated at room temperature for 30 min to allow proper nanoparticle formation and stabilization. Before performing each measurement, the siRNA nanoparticles were diluted to a final volume of 1.0 mL with Milli-Q water to ensure the sample concentration was appropriate for the analysis. This dilution step helps avoid interference from overly concentrated samples that affect the accuracy of the measurements. The data from the Zetasizer Nano ZS provided key information on the size, distribution, and surface charge of the siRNA nanoparticles, which are crucial parameters for evaluating their effectiveness as a drug delivery system.

### **4.1.3 Morphology of siRNA Nanoparticles**

Morphology of the siRNA nanoparticles was observed using Hitachi HT7800 series transmission electron microscopy (TEM). The siRNA nanoparticles were prepared on a carbon-coated grid by adding a droplet of the suspension of siRNA nanoparticles. The siRNA nanoparticles suspension was then dried on the grid for 5 min. After that, the samples were negatively stained using an UranylLess (Electron Microscopy Sciences, USA) solution for 30 s. After that, the samples were observed by TEM with an accelerating voltage of 100 kV.

### **4.1.4 *In Vitro* Cytotoxicity Test of siRNA Nanoparticles**

The MDA-MB-231 (Passage 14<sup>th</sup>) and MDA-MB-436 (Passage 14<sup>th</sup>) cells at a density of 12,000 cells/well in a volume of 100  $\mu$ L were cultured in a 96-well cell culture plate containing DMEM, 10% FBS, 1% antibiotic and antimycotic formulation and incubated in 5% CO<sub>2</sub> atmosphere at 37 °C for 24 h. After that, 15  $\mu$ L of CsiRNA nanoparticles or siSVV nanoparticles was added into the wells, resulting in a final siRNA nanoparticle concentration of 80 nM. The cells were treated with CsiRNA and siRNA nanoparticles for 72 h. After treatment, the cell viability was determined by MTT assay. The MTT solution was added to the cells and incubated in 5% CO<sub>2</sub> at 37 °C for 3 h. After incubation, the medium was removed, and the formazan crystals formed were dissolved using DMSO. The absorbance of the solution was measured by a microplate reader (Molecular Devices Spectramax 250, California, USA) at a wavelength of 570 nm. The viability of cultured cells in the fresh DMEM was used as a non-treatment. The CsiRNA nanoparticles were used as the negative controls.

### **4.1.5 Reverse Transcription Quantitative PCR (RT-qPCR) for Gene Silencing**

First, 300  $\mu$ L of MDA-MB-231 (passage 15<sup>th</sup>) or MDA-MB-436 cells (passage 15<sup>th</sup>) at  $5 \times 10^4$  cells/wells were seeded in a 48-well cell culture plate and incubated in 5% CO<sub>2</sub> at 37 °C for 24 h. The cells were treated with 50  $\mu$ L of CsiRNA or siSVV nanoparticles in culture medium for 72 h. The transfection was terminated, and the gene expression was measured by RT-qPCR after transfection for 72 h. Before disrupting cells, the cells were washed with 200  $\mu$ L of HBSS 1 time, and then 200  $\mu$ L of TRIzol<sup>TM</sup> reagent solution was added to isolate the total RNA. The cell lysates were incubated at room temperature for 15 min and transferred into a 1.5 mL microcentrifuge tube,

followed by the addition of 300  $\mu$ L of chloroform, and centrifuged at 6500 rpm for 10 min. The upper phase solution (clear solution) was transferred to a new 1.5 mL centrifuge tube and mixed with 500  $\mu$ L of 2-propanol. The mixture solution was centrifuged at 12.2 rcf at 4 °C for 10 min. The supernatant was discarded from the tube and air dried for 45 min. After that, 500  $\mu$ L of 75% w/v of ethanol was added and kept at -20 °C for overnight. Next, the solution was centrifuged at 12.2 rcf at 4 °C for 5 min. The supernatant was then discarded, and the pellet was air-dried for 60 min. Following this, 15  $\mu$ L of RNase-free water was added, and the mixture was vortexed at medium speed at room temperature for 10 s. Finally, the solution was incubated in a water bath at 60 °C for 10 min. Then, 1  $\mu$ g of extracted RNA was converted into cDNA using the SensiFAST™ cDNA Synthesis kit for RT-qPCR per the manufacturer's instructions (Meridian Bioscience, USA) by the reaction mixtures containing 15  $\mu$ L of RNA, 4  $\mu$ L of TransAmp buffer, 1  $\mu$ L of Reverse Transcriptase. For RT-qPCR analysis, human Beta-actin and siSVV were used as an endogenous housekeeping gene.

#### **4.1.6 Cellular Uptake Study by Flow Cytometry**

To quantify siRNA nanoparticles uptake, MDA-MB-231 and MDA-MB-436 cells were seeded ( $8 \times 10^5$  cells/well) in 24-well plates for 24 h. MDA-MB-231 and MDA-MB-436 cells were cultured in each extraction media solution for 24, 48, and 72 h. Following each time point, the culture medium was removed, and the cells were soaked in 500  $\mu$ L of HBSS for 20 min. Next, the cells were trypsinized with 200  $\mu$ L of 1X Trypsin-EDTA (0.5% v/v), without phenol red and then incubated in a hot air oven at 37 °C for 15 min. After incubation, the cells were collected and transferred to 1.5 mL centrifuge tubes and centrifuges 3,000 rpm for 10 min. Then, the supernatant was removed and fixed with 200  $\mu$ L of 3.7% v/v formaldehyde. The solution was transferred to the flow cytometer tube, and 200  $\mu$ L of HBSS was added. The high-parameter flow cytometer LSRFortessa™ (BD Biosciences, Franklin Lakes, New Jersey) was used to quantify the mean fluorescence in cells and the FAM-positive cell population. In addition, the mean fluorescence intensity of the recovered cell population and the percentage of cells exhibiting FAM fluorescence were determined by gating a representative portion of nontreated cells to account for autofluorescence, typically set at 1 % of the total population. This approach ensures accurate analysis of the fluorescence signals by excluding background interference.

#### **4.1.7 Fluorescence Microscopy Analysis**

A fluorescence microscopy analysis was performed on MDA-MB-231 and MDA-MB-436 cells transfected with FAM-siRNA nanoparticles after incubation for 72 h. The cells were washed thoroughly with 500  $\mu$ L of PBS to remove excess reagents or unbound nanoparticles. After that, the cells were fixed using 250  $\mu$ L of 4% w/v paraformaldehyde solution at 37 °C for 10 min. This fixation step is essential for preserving the cellular structure and immobilizing the nanoparticles within the cells. After fixation, the cellular uptake of FAM-siSVV nanoparticles was observed under the ECLIPSE Ti2 inverted microscope (Nikon Instruments Inc., Japan) with high-resolution fluorescence imaging.

#### **4.1.8 Statistical Analysis**

All experiments were expressed as triplicates and the mean  $\pm$  standard deviation (SD). Data analysis was performed using a one-way analysis of variance (ANOVA) with Tukey's post hoc in SPSS (IBM SPSS, USA) and the student's t-test when comparing two groups. The statistical significance was considered for a *p*-value of 0.05.

## 4.2 Results and Discussion

### 4.2.1 Size, Polydispersity, and Zeta-Potential

The siRNA nanoparticles were prepared and adapted from the previous method (Santadkha et al., 2022). Santadkha et al. studied the formulations of siRNA nanoparticles using commercial transfection reagent and Trans-Booster to improve gene silencing and delivery efficiency. The results showed that increasing the Prime-Fect:siRNA ratio (5:1 and 10:1) resulted in smaller siRNA nanoparticles. The size of siRNA nanoparticles at siRNA:Trans-Booster:Prime-Fect ratio of 1:1:10 was 225 nm. From Table 4.2, the size of CsiRNA nanoparticles and siSVV nanoparticles of siRNA:Trans-Booster:Prime-Fect weight ratio of 1:1:10 was  $247 \pm 2$  and  $230 \pm 2$  nm, respectively. While, CsiRNA nanoparticles and siSVV nanoparticles of siRNA:Trans-Booster:Prime-Fect weight ratio of 1:0:10 were  $823 \pm 33$  and  $499 \pm 8$  nm, respectively. Therefore, adding anionic Trans-Booster caused the particle size assembled with the cationic charges of Prime-Fect to decrease, possibly leading to more effective delivery of siRNA nanoparticles. The PDI, which refers to a measure of particle size distribution, was below 0.2, which is acceptable as a relatively uniform distribution (Danaei et al., 2018). Thus, the PDI of siRNA nanoparticles of siRNA:Trans-Booster:Prime-Fect weight ratio of 1:1:10 showed excellent size distribution (see Table 4.2). CsiRNA nanoparticles had a PDI of  $0.038 \pm 0.003$ , indicating a highly monodisperse population, while siSVV nanoparticles had a PDI of  $0.139 \pm 0.015$ , which is still within the acceptable range for uniform nanoscale formulations. These values confirmed that both nanoparticle formulations, particularly siSVV, possess a narrow size distribution, which is an essential parameter in developing siRNA delivery systems. A low PDI ensures consistent cellular uptake, predictable biodistribution, and reproducible biological responses. Therefore, achieving acceptable PDI values at this stage suggests that the siRNA nanoparticles are suitably formulated, providing a strong basis for further investigation in gene delivery applications. The zeta potential is a measurement of the particle surface charge, indicating the stability and electrostatic repulsion among particles. The zeta potential value of more than +30 mV is considered to maintain sufficient repulsive force for attaining good physical stability in a formulation. On the

other hand, a small zeta potential value close to zero can lead to the aggregation of the particles (Gumustas et al., 2017; Ding et al., 2018). The zeta potential of the CsiRNA nanoparticles and siSVV nanoparticles at siRNA:Trans-Booster:Prime-Fect weight ratio of 1:1:10 was  $-6.8 \pm 0.4$  and  $-10.2 \pm 0.6$  mV, respectively. While, the CsiRNA nanoparticles and siSVV nanoparticles of siRNA:Trans-Booster:Prime-Fect weight ratio of 1:0:10 were  $-8.9 \pm 0.2$  and  $-11.5 \pm 0.4$  nm, respectively. However, the negative charge below  $\pm 10$  mV showed decreased cytotoxicity and protected the siRNA from enzymatic degradation.

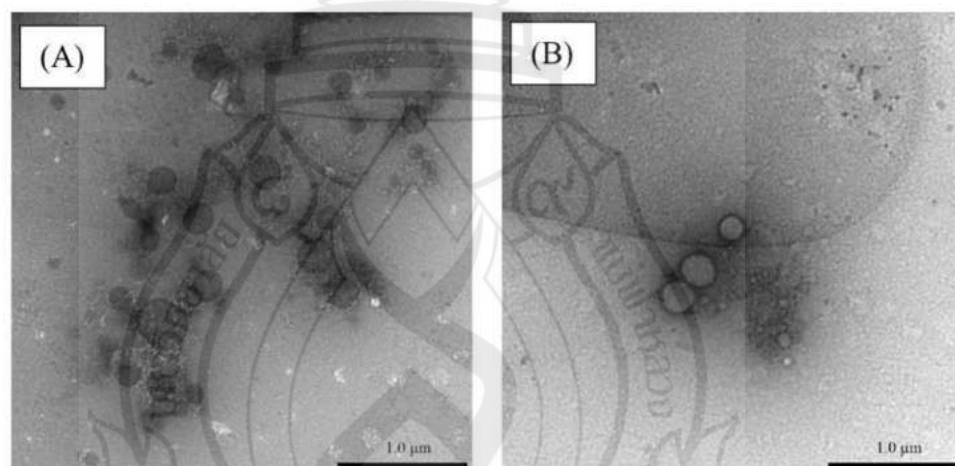
**Table 4.2** Compositions, Size, PDI, and Zeta Potential of siRNA Nanoparticles

siRNA	siRNA Conc. (nM)	siRNA/Trans-Booster /Prime-Fect ratio	Size (nm)	PDI	Zeta potential (mV)
CsiRNA	80	1:1:10	$247 \pm 2$	$0.038 \pm 0.003$	$-6.8 \pm 0.4$
siSVV	80	1:1:10	$230 \pm 2$	$0.139 \pm 0.015$	$-10.2 \pm 0.6$
CsiRNA	80	1:0:10	$823 \pm 33$	$0.620 \pm 0.010$	$-8.9 \pm 0.2$
siSVV	80	1:0:10	$499 \pm 8$	$0.435 \pm 0.010$	$-11.5 \pm 0.4$

#### 4.2.2 Morphology of siRNA Nanoparticles

The morphology of these siRNA nanoparticles showed uniform and spherical particles without agglomeration. Meanwhile, the siRNA nanoparticles at siRNA:Trans-Booster:Prime-Fect ratios of 1:0:10 and 1:0:5 (i.e., without Trans-Booster) showed more heterogeneous complex structures and aggregated particles. The TEM images of siRNA nanoparticles are shown in Figure 4.1. It confirmed that siRNA nanoparticles with a spherical shape were successfully formed. This was in line with Santadkha et al. observations, which showed that the siRNA:Trans-Booster:Prime-Fect weight ratio of 1:1:10 showed uniform particles and spherical shape without agglomerated particles (Santadkha et al., 2022). The uniform size and spherical shape of the nanoparticles are critical for their efficient delivery and cellular uptake, as they can facilitate better dispersion in aqueous environments and prevent potential issues such as particle clumping, which could hinder the efficacy of siRNA delivery. Moreover, the spherical morphology ensures that the nanoparticles remain stable during their transport to target

cells and can efficiently enter cells via endocytosis. These structural characteristics suggest that the siRNA nanoparticles are well-suited for gene silencing applications, offering a promising approach for targeted siRNA delivery in breast cancer therapy. Additionally, the consistent size of the nanoparticles, as confirmed by TEM analysis, likely contributes to more predictable and reliable therapeutic effects. This is because uniform size helps reduce variability in their performance during treatment. This uniformity is particularly crucial for cellular uptake, as similarly sized nanoparticles are more likely to be internalized by cells through the same endocytic pathways, leading to more consistent intracellular delivery and therapeutic action. Ultimately, this ensures the nanoparticles behave consistently, improving the overall effectiveness and repeatability of therapeutic outcomes. (Owens & Peppas, 2006).

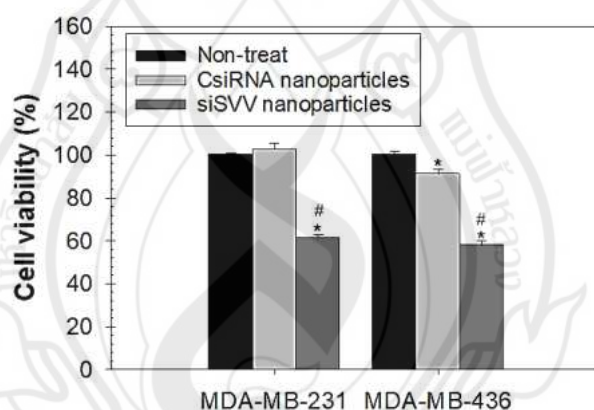


**Figure 4.1** Selected TEM Images of siRNA Nanoparticles at siRNA:Trans-Booster:Prime-Fect Weight Ratio of 1:1:10 (A) CsiRNA Nanoparticles and (B) siSVV Nanoparticles

#### 4.2.3 *In Vitro* Cytotoxicity of siRNA Nanoparticles

The cytotoxicity of the CsiRNA nanoparticles and siSVV nanoparticles (siRNA concentration at 80 nM, siRNA:additive:Prime-Fect weight ratio of 1:1:10) was investigated in breast cancer cells, including MDA-MB-231 and MDA-MB-436 cells, after 72 h treatment, as shown in Figure 4.2. The viability of cells cultured with the culture medium (non-treatment) was used as a control. The CsiRNA nanoparticles served as the negative controls. The results showed that the viability of MDA-MB-231

cells treated with CsiRNA nanoparticles, and siSVV nanoparticles was  $102.47 \pm 2.92\%$ , and  $61.41 \pm 1.35\%$ . While the viability of MDA-MB-436 cells treated with CsiRNA nanoparticles, and siSVV nanoparticles was  $91.02 \pm 2.45\%$  and  $57.80 \pm 2.39\%$ , respectively. The relative cell viability treated with CsiRNA nanoparticles was negligibly decreased, compared to the non-treated cells. These results confirmed that CsiRNA nanoparticles (negative control) are less effective at inhibiting cell growth of MDA-MB-231 and MDA-MB-436 cells. The efficacy of siSVV nanoparticles for inhibiting cell growth significantly decreased to  $\sim 60\%$  compared to non-treated cells. Thus, siSVV nanoparticles could inhibit the growth of MDA-MB-231 and MDA-MB-436 cells after treatment for 72 h. These results can confirm that siSVV nanoparticles treated with the breast cancer cells appeared to be more sensitive to the therapy, while CsiRNA nanoparticles did not respond to the specific cell killing due to the non-specific effect of CsiRNA.

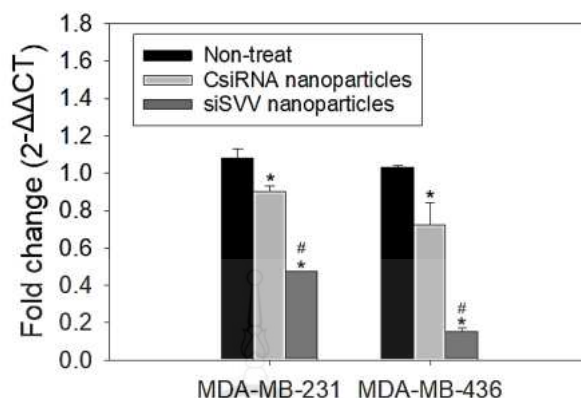


**Figure 4.2** The *In Vitro* Cytotoxicity of siRNA Nanoparticles Cultured with MDA-MB-231 and MDA-MB-436 Cells ( $n = 4$ ). (siRNA Nanoparticles at siRNA:Trans-Booster:Prime-Fect Weight Ratio of 1:1:10). \* $p < 0.05$  Compared with the Non-treat and # $p < 0.05$  Compared Between CsiRNA Nanoparticles and siSVV Nanoparticles



#### 4.2.4 RT-qPCR for Gene Silencing of siRNA Nanoparticles

To evaluate the effect of siRNA nanoparticle treatments on gene expression, MDA-MB-231 and MDA-MB-436 cells were treated with 80 nM CsiRNA nanoparticles and siSVV nanoparticles for 72 h (Figure 4.3). CsiRNA nanoparticles led to a slight increase in SVV expression (0.90- and 0.72-fold) compared to non-treatment (1.08- and 1.03-fold, respectively) in both cells, suggesting a lack of suppression. Conversely, siSVV nanoparticles decreased SVV expression (0.47- and 0.15-fold) compared to CsiRNA nanoparticles (0.90- and 0.72-fold) in both cells, reflecting siSVV suppression. The notably reduced SVV expression in MDA-MB-231 and MDA-MB-436 cells demonstrated the successful delivery and silencing of the target gene by siSVV nanoparticles. These results were consistent with findings from Santadkha et al. They found that siRNA nanoparticles from siRNA:Trans-Booster:Prime-Fect weight ratio of 1:1:10 were highly effective in achieving gene silencing after 72 h of treatment (Santadkha et al., 2022). The siSVV nanoparticles efficiently delivered siRNA into the cells, facilitating its incorporation into the RNA-induced silencing complex and effectively silencing the target gene. These results highlight the potential of siSVV nanoparticles to precisely target and silence the SVV gene in both breast cancer cell lines, confirming their ability to induce gene silencing with minimal off-target effects. The siSVV nanoparticles hold promise as a therapeutic strategy for breast cancer treatment, offering a more targeted and effective alternative to traditional therapies. However, future research should focus on optimizing siSVV nanoparticle formulations and evaluating their *in vivo* performance to further enhance their therapeutic efficacy.

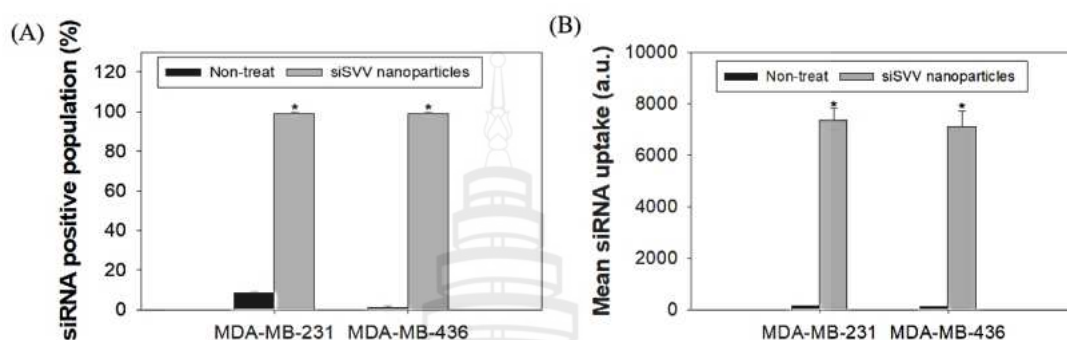


**Figure 4.3** Relative Fold Change of CsiRNA Nanoparticles and siSVV Nanoparticles Cultured with MDA-MB-231 and MDA-MB-436 Cells by RT-qPCR After Transfection for 72 h (n = 2). \* $p < 0.05$  Compared with the Non-Treat and # $p < 0.05$  Compared between CsiRNA Nanoparticles and siSVV Nanoparticles

#### 4.2.5 Cellular Uptake Study by Flow Cytometry

Cellular uptake assessed by flow cytometry involves incubating cells with a FAM-siSVV nanoparticle, followed by measuring fluorescence intensity to quantify the amount of uptake. The siRNA positive population (%) represents the percentage of cells that have internalized FAM-siSVV nanoparticles, as determined by fluorescence signals. This value represents the proportion of cells that successfully internalized siRNA. Concurrently, the mean siRNA uptake (a.u.) indicates the average quantity of siRNA per cell, determined by fluorescence intensity. The cellular uptake efficiency of siRNA nanoparticles was evaluated using flow cytometry after a 72 h incubation period, as shown in Figure 4.4. In the non-treated groups, the siRNA-positive cell population was relatively low, with  $8.27 \pm 0.67\%$  in MDA-MB-231 cells and  $1.10 \pm 0.50\%$  in MDA-MB-436 cells. In contrast, treatment with siSVV nanoparticles resulted in an increase in the siRNA-positive population, reaching  $98.70 \pm 0.55\%$  in MDA-MB-231 cells and  $98.70 \pm 0.50\%$  in MDA-MB-436 cells. For MDA-MB-231 cells, the mean siRNA uptake increased from  $153.00 \pm 2.00$  a.u. in the non-treated group to  $7347.67 \pm 474.95$  a.u. in the siSVV nanoparticles group. Similarly, in MDA-MB-436 cells, the uptake increased significantly from  $105.00 \pm 14.73$  a.u. to  $7098.67 \pm 620.61$  a.u. These

findings collectively demonstrate the high efficiency of siRNA delivery and intracellular accumulation facilitated by the nanoparticle system in both breast cancer cell lines.


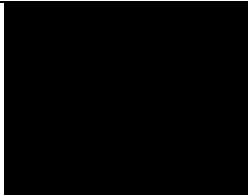


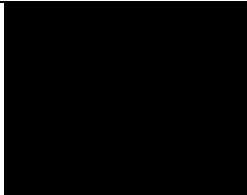

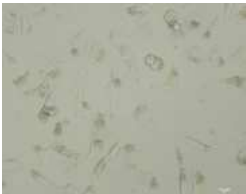
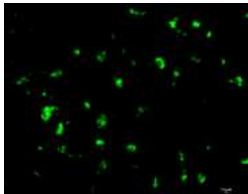

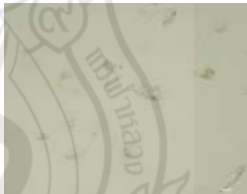
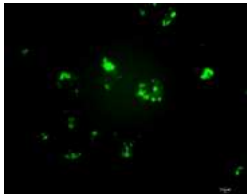
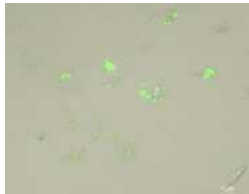

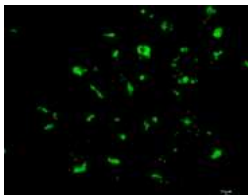
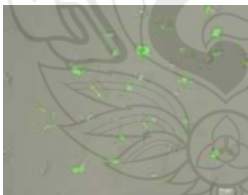
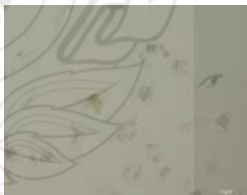
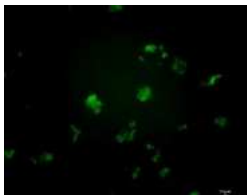



**Figure 4.4** Cell Uptake of siRNA Nanoparticles. (A) Percentage of siSVV Positive Cell Population and (B) Mean Fluorescence Intensity of siSVV Nanoparticles After 72 h Treatment

#### 4.2.6 Fluorescence Microscopy Analysis

The MDA-MB-231 and MDA-MB-436 cells transfected with FAM-siRNA nanoparticles after 72 h were investigated using a fluorescent microscope to confirm the cellular uptake. The results showed that the green signal of FAM-siRNA was noticeably detected (Table 4.3). In addition, the merged images of FAM-CsiRNA nanoparticles and FAM-siSVV nanoparticles in MDA-MB-231 and MDA-MB-436 cells confirmed the successful internalization of siRNA nanoparticles into the cell membrane. Prime-Fect formed complexes with siRNA to create siRNA nanoparticles that protect siRNA from degradation by RNase in the extracellular environment, contributing to the inherently low pharmacokinetic profile. Moreover, the siRNA nanoparticles demonstrated high efficiency in delivering siRNA into cells and facilitating its incorporation into the RNA-induced silencing complex, a result attributed to the cationic nature of Prime-Fect, which enhances binding with siRNA compared to naked siRNA (Santadkha et al., 2022).

**Table 4.3** Cellular Uptake of FAM-siSVV Nanoparticles After Transfection for 72 h was Captured by Fluorescence Microscopy  
(Magnification of 40×)

Condition	MDA-MB-231			MDA-MB-436		
	Brightfield	FAM	Merged	Brightfield	FAM	Merged
Non-treat						
FAM-CsiRNA						
FAM-siSVV						

## **CHAPTER 5**

### **INJECTABLE SELF-HEALING QUATERNIZED CHITOSAN/OXIDIZED PECTIN HYDROGELS LOADED WITH siRNA NANOPARTICLES FOR BREAST CANCER TREATMENT**

#### **5.1 Methodology**

##### **5.1.1 Synthesis and Characterization of QCS and OxPec**

First, CS solution was prepared by dissolving 5.0 g of CS in 350 mL of 1% v/v glacial acetic acid. Then, 50 mL of GTMAC was added to the CS solution under continuous stirring. The mixture solution was then refluxed at 60 °C for 6 h. After that, the mixture solution was dialyzed with deionized water using a dialysis membrane (Molecular weight cut-off 3,500) for 3 days. Finally, QCS was lyophilized using the freeze-drying method for 24 h.

First, 2.0 g of Pec was dissolved overnight in 100 mL of 20%v/v ethanol to obtain the homogeneous pectin solution. Then, 3.0 mL of 0.5 M sodium periodate solution was added to the Pec solution under magnetic stirring at room temperature for 2 h in the dark. After this, 300 mL of absolute ethanol was added, and the solution was stirred for 30 min to obtain OxPec solution. The OxPec solution was filtered using filter paper (Whatman No.1) and dried in a hot air oven at 40 °C for 24 h. Finally, OxPec was obtained and stored in a desiccator before use.

##### **5.1.2 Fourier Transform Infrared Spectroscopy (FTIR) Analysis**

The functional groups of CS, QCS, Pec, and OxPec were characterized using the ATR mode of the FTIR spectrophotometer. All spectra of the samples were observed in the range of 4000-400  $\text{cm}^{-1}$  at a resolution of 4  $\text{cm}^{-1}$  in a transmittance mode.

### 5.1.3 Nuclear Magnetic Resonance (NMR) spectroscopy

The  $^1\text{H}$  NMR spectra of CS and QCS were examined using NMR Bruker Biospin (Bruker, Germany) spectroscopy. The samples were dissolved in acetic acid- $d_4$  for CS and  $\text{D}_2\text{O}$  for QCS, with a concentration of 10 mg/mL for each sample. The degree of acetylation (DA) of CS was determined using the following equation:

$$DA (\%) = \frac{\frac{\int CH_3}{3}}{\frac{\int H(C2-C6)}{6}} \times 100$$

where  $\int H(C2-C6)$  denotes the integration of protons located on carbon atoms C2 to C6 in both monomer units. Similarly,  $\int CH_3$  reflects the integration of the three methyl protons in the N-acetyl-D-glucosamine unit of CS.

The integrals of the peak corresponding to the methylene and methyl protons of the N-acetyl-D-glucosamine unit of chitosan were utilized to measure the degree of substitution (DS) of QCS, as demonstrated by the following equation:

$$DS (\%) = \frac{\frac{\int CH_2}{2}}{\frac{\int CH_3}{3}} \times DA (\%)$$

### 5.1.4 Indirect Cytotoxicity of QCS and OxPec

The cytotoxicity evaluation of QCS and OxPec was adapted from the ISO 10993-5 standard test method. The cells (i.e., MDA-MB-231, MDA-MB-436, and HDFa) were seeded in a 96-well tissue culture plate and incubated at 37 °C for 24 h. OxPec was dissolved in warm deionized water at 40 °C under magnetic stirring to obtain a homogeneous solution. QCS solution was prepared by dissolving QCS in deionized water under magnetic stirring to obtain a clear homogenous solution. Each raw material was diluted with the cell culture medium to produce various concentration solutions, including 5, 2.5, 1.25, 0.625, 0.313, 0.156, 0.078, 0.039, and 0.02 mg/mL. The cells were then replaced with raw materials solution and cultured for 24 h. After treatment, the cell viability was determined by MTT assay. MTT solution was added to

the cells and incubated in 5% CO<sub>2</sub> at 37 °C for 3 h. After incubation, the medium was removed and the formazan crystals formed were dissolved with DMSO. The absorbance of the solution was measured by a microplate reader (BioTek Synergy H1, USA) at the wavelength of 570 nm. The viability of cells cultured by the fresh DMEM was used as a control.

#### **5.1.5 Preparation of Injectable Self-Healing Hydrogels Loaded with siRNA Nanoparticles**

First, 15% w/v QCS solution was prepared by dissolving QCS in deionized water under magnetic stirring to obtain a clear homogeneous solution. OxPec solutions (15 and 17.5% w/v) were prepared by dissolving OxPec in warm deionized water at 40 °C under magnetic stirring to obtain a homogeneous solution. After that, the OxPec solution was added to the QCS solution in a volume ratio of 0.8:0.2 and stirred with a spatula. Then, the mixture solution was incubated at 37 °C to give the injectable self-healing QCS/OxPec hydrogels.

To prepare injectable self-healing QCS/OxPec hydrogels loaded with siRNA nanoparticles, 100 µL of siRNA nanoparticles was added to the QCS solution (15% w/v) and stirred with a spatula for 10 s to obtain a homogeneous solution. Then, the QCS solution containing siRNA nanoparticles was mixed with the OxPec solution (15% and 17.5%w/v) at a volume ratio of 0.8:0.2. After that, the mixture solution was stirred using a spatula for 10 s and incubated at 37 °C to obtain the injectable self-healing QCS/OxPec hydrogels loaded with siRNA nanoparticles. The compositions of the injectable self-healing QCS/OxPec hydrogels loaded with siRNA nanoparticles are shown in Table 5.1.

**Table 5.1** Compositions of Injectable Self-Healing Hydrogels

Samples	Concentration (% w/v)		Ratio of QCS:OxPec (mL:mL)	Nanoparticles ( $\mu$ L)	
	QCS	OxPec		CsiRNA	siSVV
15H	15	15	0.8:0.2	0	0
15HC	15	15	0.8:0.2	100	0
15HS	15	15	0.8:0.2	0	100
17.5H	15	17.5	0.8:0.2	0	0
17.5HC	15	17.5	0.8:0.2	100	0
17.5HS	15	17.5	0.8:0.2	0	100

### 5.1.6 Morphology of siRNA Nanoparticles Loaded in Injectable Self-Healing Hydrogels

The morphology of the siRNA nanoparticles loaded in the injectable self-healing hydrogels was observed by TEM. The siRNA nanoparticles in the QCS solution were prepared over a carbon-coated grid by adding a droplet of the suspension of 20  $\mu$ L of siRNA nanoparticles in 0.2 mL of 15% w/v QCS solution for 5 min and blotting it out using filter paper. Then, the samples were negatively stained using UranylLess solution for 3 min. After that, the samples were observed by HT7800 TEM (Hitachi, Japan) with an accelerating voltage of 80 kV.

### 5.1.7 Gelation Time and Gel Fraction

The gelation time of the injectable self-healing hydrogels was observed using the inverting method. For the injectable self-healing hydrogels, 0.8 mL of QCS solution (15% w/v) and 0.2 mL of OxPec solution (15% w/v and 17.5% w/v) were added to the vial and stirred with a spatula for 10 s to obtain a homogeneous solution. For the injectable self-healing hydrogels loaded with siRNA nanoparticles, 0.8 mL of QCS solution (15% w/v), 0.1 mL of siRNA nanoparticles solution, and 0.2 mL of OxPec solution (15% w/v and 17.5% w/v) were added to the vial and stirred with a spatula for 10 s to obtain a homogeneous solution. After that, the mixture solution was incubated in a water bath at 37 °C. The formation of gel was observed every 1 min. The gelation time was recorded by inverting the vial upside down until the gels did not flow over 30 s.

The gel fraction was performed to determine the sol and gel proportion of hydrogel. First, the hydrogels were stored in the refrigerator at -20 °C overnight. The



hydrogels were then lyophilized by the freeze-drying method for 2 days to obtain the initial dry mass ( $m_{d,i}$ ). The dried samples were immersed in deionized water at 37 °C for 3 h. After 3 h, the swollen hydrogels were removed, wiped thoroughly with Kimtech tissue paper (Kimwipes®), and then freeze-dried to obtain the final dry mass ( $m_{d,w}$ ). The measurements of each sample were calculated as shown in equation (5.1):

$$\text{Gel fraction (\%)} = \frac{m_{d,w}}{m_{d,i}} \times 100 \quad (5.1)$$

### 5.1.8 Water Swelling and Weight Loss Study

The water swelling and weight loss of hydrogels were measured via the immersion method. The investigation was conducted following the published method (Martens et al., 2002). The freshly prepared hydrogel samples were weighed and recorded as initial wet mass ( $M_{w,i}$ ). The hydrogels were immersed in 2 mL of phosphate buffer solution (pH 7.4) at 37 °C for 30, 60, 120, 180, 240, and 1440 min. After immersion, the hydrogels were collected and weighed as swollen mass ( $M_{w,t}$ ). Then, the swollen hydrogels were dried using freeze-dryer and weighed as  $M_d$ . To evaluate the weight loss of hydrogels, the actual macromer fraction (AMF) was calculated using equation (5.2). The initial weight of the hydrogels in dry state ( $M_{d,i}$ ) was calculated using equation (5.3). The water swelling and weight loss of the hydrogels were calculated using equations (5.4) and (5.5), respectively.

$$\text{Actual macromer fraction (AMF)} = \frac{M_{d,i}}{M_{w,i}} \quad (5.2)$$

$$M_{d,i} = M_{w,i} \times \text{AMF} \quad (5.3)$$

$$\text{Water swelling (\%)} = \frac{M_{w,t} - M_{w,i}}{M_{w,i}} \times 100 \quad (5.4)$$

$$\text{Weight loss (\%)} = \frac{M_{d,i} - M_d}{M_{d,i}} \times 100 \quad (5.5)$$

### 5.1.9 Released Profile

The actual amount of siRNA nanoparticles loaded into the hydrogels was quantified prior to evaluating their release behavior. In this study, 100 mg of siRNA nanoparticles-loaded hydrogel was used for each sample. Each hydrogel sample was completely dissolved in 1.0 mL of PBS (pH 7.4) at 37 °C. Subsequently, 0.1 mL of the dissolved solution was analyzed using a fluorescence microplate reader. Subsequently, 0.1 mL of the sample solution was analyzed by a fluorescence microplate reader (Thermo Ascent;  $\lambda_{\text{ex}}$  485 nm,  $\lambda_{\text{em}}$  527 nm) to determine the amount of siRNA nanoparticles.

To investigate the release profile of siRNA nanoparticles, 100 mg of each hydrogel sample was placed into a 24-well transwell insert (Corning Incorporated Costar®, USA). The inserts were then transferred into individual wells of a 24-well plate containing 1.0 mL of PBS (pH 7.4) and incubated at 37 °C for 24, 48, 72, 96 h. After incubation, 0.1 mL of the sample solution was collected and analyzed at  $\lambda_{\text{ex}}$  485 nm and  $\lambda_{\text{em}}$  527 nm using the fluorescence microplate reader.

### 5.1.10 Rheological Analysis

The rheology of the hydrogel samples was observed by ARES-G2 rheometer (TA Instruments Ltd., USA) equipped with a parallel geometry with a diameter of 25 mm. The gap was set to 1 mm. First, the sample solution (1 mL) was placed on the top of the rheometer and equilibrated at 20 °C for 4 min. During the gelation process, the rheological properties were measured at the temperature range of 20 to 50 °C with a heating rate of 2 °C/min and a frequency of 3 Hz. The elastic (storage) modulus ( $G'$ ) and the viscous (loss) modulus ( $G''$ ) were recorded as a function of temperature. To evaluate the self-healing properties of the hydrogels, the continuous step strain measurement was performed from a strain of 1% and 3000% with time intervals of 50 s and fixed frequency at 10 rad/s. During these steps, the hydrogels were kept for 30 s to stabilize the gel recovery before switching %strain.

#### 5.1.11 *In Vitro* Cytotoxicity Evaluation

The *in vitro* cytotoxicity evaluation of the injectable self-healing hydrogels loaded with siRNA nanoparticles was adapted from the ISO 10993-5 standard test method. 100  $\mu$ L of MDA-MB-231 (passage 14<sup>th</sup>) or MDA-MB-436 (passage 14<sup>th</sup>) cells at 12,000 cells/well were seeded in a 96-well tissue culture plate and incubated at 37 °C for 24 h. Before testing, the hydrogel samples were sterilized under UV light for 30 min, then immersed in the culture media to prepare the extraction medium solutions. The cells were then replaced with an extraction medium and cultured for 24 and 72 h. After treatment, the cell viability was determined by MTT assay. MTT solution was added to the cells and incubated in 5% CO<sub>2</sub> at 37 °C for 2 h. After incubation, the medium was removed, and the formed formazan crystals were dissolved with DMSO. The absorbance of the solution was measured by a microplate reader (Molecular Devices Spectramax 250) at a wavelength of 570 nm. The viability of cells cultured in fresh DMEM was used as a control.

#### 5.1.12 Biocompatibility Evaluation and Cell Morphology of Hydrogels

The biocompatibility evaluation of hydrogels was performed using HDFa cells. Initially, HDFa cells were seeded at a density of 8,000 cells/well in 96-well tissue culture polystyrene plates (TCPS; SPL Life Science, Korea) and allowed to grow for 24 h. Before testing, the hydrogel samples were sterilized under UV light for 30 min, then immersed in the culture media to prepare the extraction medium solutions. After 24 h of cell culture, the cell culture media was removed, and 100  $\mu$ L of each extraction media solution was added to the wells. HDFa cells were then cultured with each sample solution for 24, 48, and 72 h. At each time point, cell viability was assessed using the MTT assay.

The morphology of cells cultured with hydrogels was observed using FE-SEM. HDFa cells were seeded at a density of 25,000 cells/well onto cover glasses in the 24-well plates and cultured for 24 h to allow cell attachment. Before testing, each hydrogel sample was sterilized under UV light for 30 min, then immersed in the cell culture media to prepare the extraction media solutions at 0.5 mg/mL. Each sample solution was then added to each well in the 24-well plates. After 24, 48, and 72 h, the culture medium in each well was removed, and the cells were washed with 500  $\mu$ L of phosphate-buffered saline (pH 7.4). The cells cultured with the sample solutions were fixed with

250  $\mu\text{L}$  of 3% v/v glutaraldehyde for 30 min. Following fixation, the cells were dehydrated in 250  $\mu\text{L}$  of ethanol solutions with increasing concentrations (30%, 50%, 70%, 90%, and 100% v/v) for 2 min each. The cells were then immersed in 500  $\mu\text{L}$  of 100% hexamethyldisilazane for 5 min and allowed to air dry in a desiccator at room temperature for 24 h. Finally, the cells were coated with gold before being observed under the FE-SEM.

#### **5.1.13 Reverse Transcription Quantitative PCR (RT-qPCR) for Gene Silencing**

First, 500  $\mu\text{L}$  of MDA-MB-231 or MDA-MB-436 cells, at a density of  $3.2 \times 10^5$  cells/well, were seeded in 12-well cell culture plates and incubated at 37 °C in 5% CO<sub>2</sub> for 24 h. Before testing, the 15HS and 17.5HS were sterilized by UV light for 30 min, and then immersed in cell culture media to prepare 10 mg/mL solutions for each sample. Following the incubation, 500  $\mu\text{L}$  of each sample solution was added to the cells. After 72 h of transfection, gene expression was analyzed by RT-qPCR. Before cell disruption, the cells were washed twice with 500  $\mu\text{L}$  of HBSS. Subsequently, 200  $\mu\text{L}$  of TRIzol™ reagent was added to the wells to isolate total RNA. The lysates were incubated at room temperature for 15 min, transferred to 1.5 mL microcentrifuge tubes, and mixed with 300  $\mu\text{L}$  of chloroform. The mixture was then centrifuged at 6,500 rpm for 10 min. The upper phase (clear solution) was collected and transferred to a fresh 1.5 mL tube, where 500  $\mu\text{L}$  of 2-propanol was added. This solution was centrifuged at 12.2 rcf at 4 °C for 10 min, and the supernatant was discarded. The RNA pellet was air-dried for 45 min. Next, 500  $\mu\text{L}$  of 75% ethanol was added, and the solution was stored at -20 °C overnight. Next, the mixture was centrifuged at 12.2 rcf at 4 °C for 5 min. After discarding the supernatant, the pellet was air-dried for 60 min, and then resuspended in 15  $\mu\text{L}$  of RNase-free water. The solution was vortexed at medium speed for 10 sec at room temperature, and the RNA was placed in a water bath at 60 °C for 10 min. To synthesize cDNA, 1  $\mu\text{g}$  of the extracted RNA was used in a reaction mixture containing 15  $\mu\text{L}$  of RNA, 4  $\mu\text{L}$  of TransAmp buffer, and 1  $\mu\text{L}$  of reverse transcriptase, according to the manufacturer's instructions (SensiFAST™ cDNA Synthesis kit, Meridian Bioscience, USA). For RT-qPCR, human Beta-actin and siSVV were used as endogenous housekeeping genes.

#### 5.1.14 Cellular Uptake Study by Flow Cytometry

To quantify cellular uptake of siRNA nanopartilces-loaded hydrogels, MDA-MB-231 and MDA-MB-436 cells were seeded ( $8 \times 10^5$  cells/well) in the 24-well plates for 24 h. Before testing, the 15HS and 17.5HS were sterilized by UV light for 30 min, and then immersed in the cell culture media to prepare 10 mg/mL for each sample. MDA-MB-231 and MDA-MB-436 cells were cultured with each extraction media solution for 24, 48, and 72 h. After each time point (24, 48, and 72 h), the culture medium was removed from each well, and the cells were washed three times in 500  $\mu$ L of HBSS for 20 min to remove the dissolved hydrogel coating. Next, the cells were trypsinized with 200  $\mu$ L of 1X Trypsin-EDTA (0.5%), without phenol red (Gibco, Thermo Fisher Scientific, Massachusetts, USA), and then incubated in a hot air oven at 37 °C for 15 min. After incubation, the cells were collected and transferred to 1.5 mL centrifuge tubes and centrifuged at 3,000 rpm for 10 min. Then, the supernatant was removed and fixed with 200  $\mu$ L of 3.7% v/v formaldehyde. The solution was transferred to the flow cytometer tube, and 200  $\mu$ L of HBSS was added. The high-parameter flow cytometer LSRFortessa™ (BD Biosciences, Franklin Lakes, New Jersey) was used to quantify the mean fluorescence in cells and the FAM-positive cell population. In addition, the mean fluorescence intensity of the recovered cell population and the percentage of cells exhibiting FAM fluorescence were determined by gating a representative portion of nontreated cells to account for autofluorescence, typically set at 1 % of the total population. This approach ensures accurate analysis of the fluorescence signals by excluding background interference.

#### 5.1.15 Fluorescence Microscopy Analysis

A fluorescence microscopy analysis of MDA-MB-231 and MDA-MB-436 cells transfected with FAM-siSVV nanoparticles released from the hydrogels was performed after 72 h of cell uptake. The hydrogel samples were immersed in the cell culture medium for 24 h to produce an extraction medium at 0.5 mg/mL. The cells were then replaced with an extraction medium and cultured for 72 h. The cells were washed with 500  $\mu$ L of PBS and fixed with 250  $\mu$ L of 4%w/v of paraformaldehyde at 37 °C for 10 min. Fluorescence images of cells were performed using the ECLIPSE Ti2 inverted microscope (Nikon Instruments Inc., Japan).

#### 5.1.16 Statistical Analysis

All experiments were expressed as triplicates and the mean  $\pm$  standard deviation (SD). Data analysis was performed using a one-way analysis of variance (ANOVA) with Tukey's post hoc in SPSS (IBM SPSS, USA) and the student's t-test when comparing two groups. The statistical significance was considered for a *p*-value of 0.05.

## 5.2 Results and Discussion

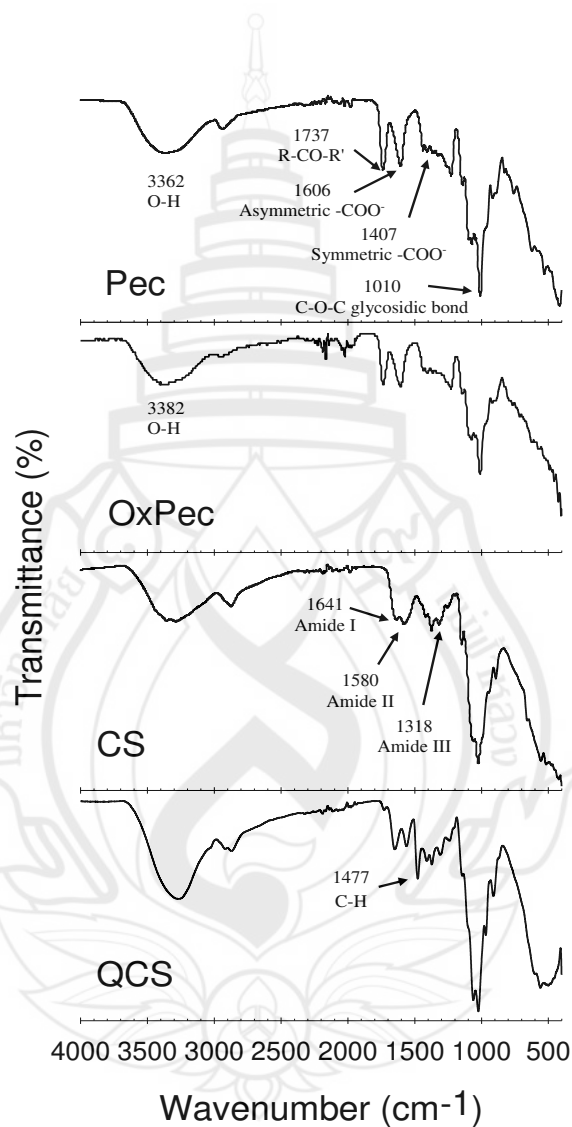
### 5.2.1 Characterization of QCS and OxPec

This work examined the development of injectable self-healing hydrogels based on QCS and OxPec. The QCS was synthesized by reacting low molecular weight CS with GTMAC, while OxPec was synthesized using the periodate oxidation of Pec, following the method described by Chanmontri et al. (Chanmontri et al., 2023). The CS spectrum consists of a peak at 1.9 ppm, corresponding to methyl protons of the N-acetylglucosamine unit and a peak at 3.1 ppm, corresponding to the proton on C2 of the glucosamine unit. The resonances observed in the 3.5-4 ppm range correspond to the protons located on carbon atoms C3 to C6, as well as the proton on carbon atom C2, for the N-acetylglucosamine unit. While, the resonance at 4.8 ppm is specifically caused by the proton on carbon atom C1. The  $^1\text{H}$  NMR data indicated a degree of acetylation (DA%) of 14%. The spectrum of QCS was consistent with the findings reported in the previous work (Chanmontri et al., 2023). The peaks at 2.6 ppm, 4.4 ppm, and 3.1 ppm correspond to the methylene, methine, and methyl protons, respectively, of the quaternary ammonium groups. The degree of substitution (DS%) in QCS was determined using  $^1\text{H}$  NMR, resulting in a DS value of 48%.

### 5.2.2 FTIR Analysis

The FTIR spectra of CS, QCS, Pec, and OxPec are shown in Figure 5.1. For CS and QCS spectra, the peaks at 3200 and 2800  $\text{cm}^{-1}$  showed the stretching vibration of O–H stretching and C–H stretching, respectively. For CS spectrum, a peak at 1641  $\text{cm}^{-1}$  was attributed to C=O stretching in the amide I. In addition, the peaks at 1580 and 1318  $\text{cm}^{-1}$  were assigned to N–H bending in amide II and N–H stretching in amide III, respectively (Pereira et al., 2019; Butt et al., 2019; Buntum et al., 2022). For QCS spectrum, the peak at 1477  $\text{cm}^{-1}$  showed the absorption peak of C-H bending in the methyl group of trimethylammonium group of GTMAC, proving that the CS had been successfully modified to QCS (Mohamed et al., 2015; Akhmetova et al., 2022). The FTIR spectrum of Pec showed the stretching vibrations of the ester carbonyl group at 1737  $\text{cm}^{-1}$ . The peaks at 1606, 1407, and 1010  $\text{cm}^{-1}$  were assigned to asymmetric carboxylate stretching vibrations and symmetric carboxylate stretching vibrations, and

C–O–C glycosidic bond, respectively (Chetouani et al., 2017; Güzel & Akpınar., 2019; Chanmontri et al., 2023). For OxPec, the stretching band of the O–H group of PEC at  $3362\text{ cm}^{-1}$  was weak and shifted to  $3382\text{ cm}^{-1}$  in OxPec due to the reduction of the number of O–H groups in the Pec backbone after the oxidation reaction (Chetouani et al., 2017).

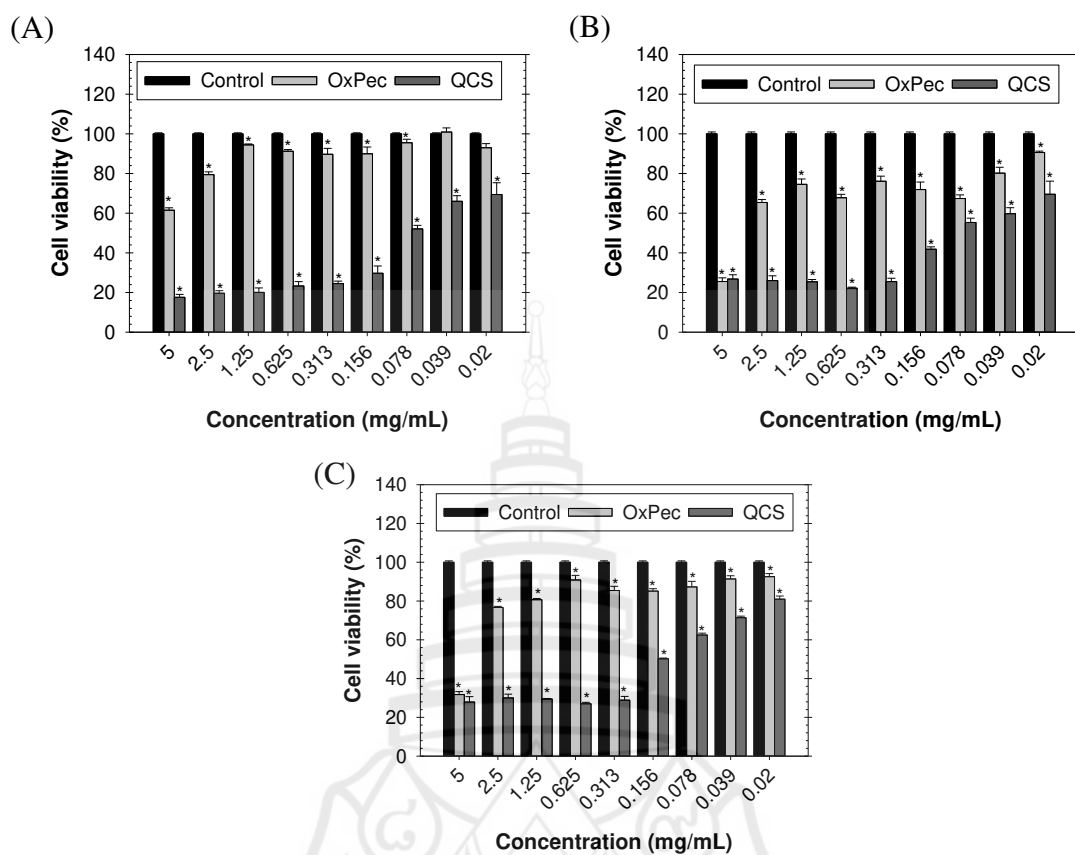


**Figure 5.1** FTIR Spectra of CS, QCS, Pec, and OxPec



### 5.2.3 Indirect Cytotoxicity of QCS and OxPec

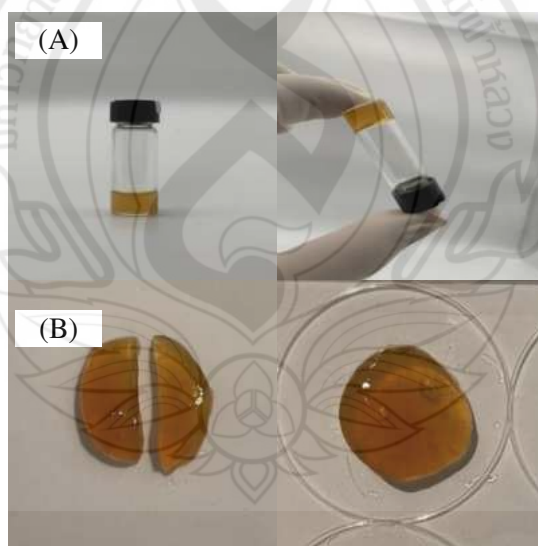
The cytotoxicity of raw materials (QCS and OxPec) was investigated before the injectable self-healing QCS/OxPec hydrogels were fabricated. From Figure 5.2, the viability of cells cultured with QCS was lower than that of OxPec. These results might be the electrostatic interaction between the negatively charged groups of the cell surface and the positively charged groups of the quaternary ammonium salt group in the QCS backbone, resulting in the higher toxicity of QCS to the cells (Lee et al., 2002; Liu et al., 2011). However, the positive charges of QCS might be reduced after interaction with the negatively charged OxPec during the fabrication of the hydrogels, resulting in lower cytotoxicity of the hydrogels. The interaction between QCS and OxPec during hydrogel formation not only contributes to the self-healing properties of the hydrogels but also reduces the overall toxicity, making the hydrogels more biocompatible and safer for potential biomedical applications. These findings suggested that the interaction between QCS and OxPec can be optimized to balance the necessary material properties for hydrogel formation with minimal cytotoxicity.



**Figure 5.2** The Cytotoxicity of OxPec and QCS Cultured with (A) HDFa, (B) MDA-MB-231, and (C) MDA-MB-436 Cells (n = 3). \* $p < 0.05$  Compared with the Control

#### 5.2.4 Gel Formation and Self-Healing Behavior of QCS/OxPec Hydrogels

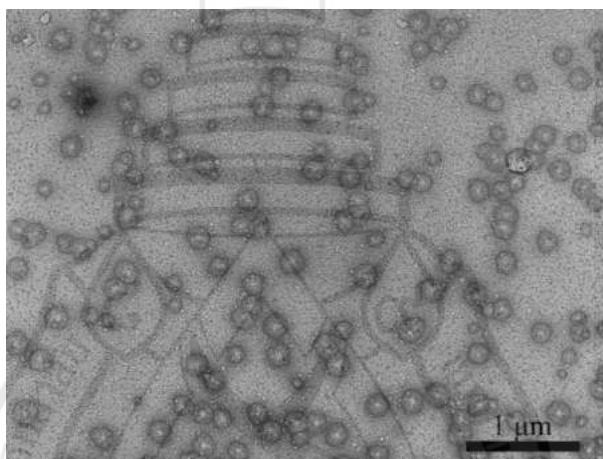
The injectable hydrogel with self-healing properties could protect and deliver drugs to the targeting site without toxicity or leakage of drugs to issues in the surrounding normal tissues. Figure 5.3A shows the selected photographs of gel formation between QCS and OxPec solutions loaded with siRNA nanoparticles at 37 °C after 10 min. Figure 5.3B shows the self-healing properties of the injectable self-healing QCS/OxPec hydrogel loaded with siRNA nanoparticles. The hydrogel was cut into two circular pieces. These two hydrogel pieces were then brought into close contact at 37 °C, and within 4 min, the hydrogel exhibited complete self-healing, forming a single piece. The injectable hydrogel with self-healing properties has two possible interactions between QCS and OxPec. The crosslinking reaction could involve electrostatic interactions between the anionic carboxylate groups in OxPec and the cationic quaternary ammonium groups in QCS. The other reaction involves dynamic covalent bonds, specifically imine bonds formed between the aldehyde groups of OxPec and the amino groups of QCS. (Chanmontri et al., 2023; Devi et al., 2021).



**Figure 5.3** (A) Gel Formation and (B) Self-Healing Behavior of the Hydrogels Loaded with siRNA Nanoparticles at 37 °C

### 5.2.5 Morphology of siRNA Nanoparticles Loaded in Hydrogels

TEM analysis was investigated to confirm the nano-size of the siRNA nanoparticles in the hydrogels. Figure 5.4 shows the morphology of siSVV nanoparticles loaded in the QCS/OxPec hydrogel. The siRNA nanoparticle showed spherical shapes without agglomerated particles. The size of about 50 particles in the images measured by ImageJ153 software was  $199.54 \pm 24.40$  nm. This result confirmed the presence of siRNA nanoparticles in the hydrogel and suggested that the nanoparticles are within an optimal size range for efficient cellular uptake and gene silencing (Wang et al., 2023; Yotsomnuk et al., 2025).



**Figure 5.4** Selected TEM Image of siSVV Nanoparticles Loaded in the Hydrogel, with a Magnification of 10,000× at 80 kV

### 5.2.6 Gelation Time, Self-Healing Time, and Gel Fraction of Hydrogels

The effect of OxPec concentrations and siRNA nanoparticles on the gelation time, self-healing time, and gel fraction of the hydrogels was evaluated, as shown in Table 5.2. The increased OxPec concentration caused the gelation time of the hydrogels to decrease. The increase in OxPec concentration caused the increased number of the possible aldehyde groups and the anionic groups of the carboxylate groups in OxPec to react more with the amino groups of QCS and the cationic groups of quaternary ammonium groups in QCS. Besides, the increased OxPec concentration caused the self-healing time of the hydrogels to increase. The addition of siRNA nanoparticles also increased the gelation time and decreased the self-healing time. These results might be due to siRNA nanoparticles preventing the interaction between QCS and OxPec.

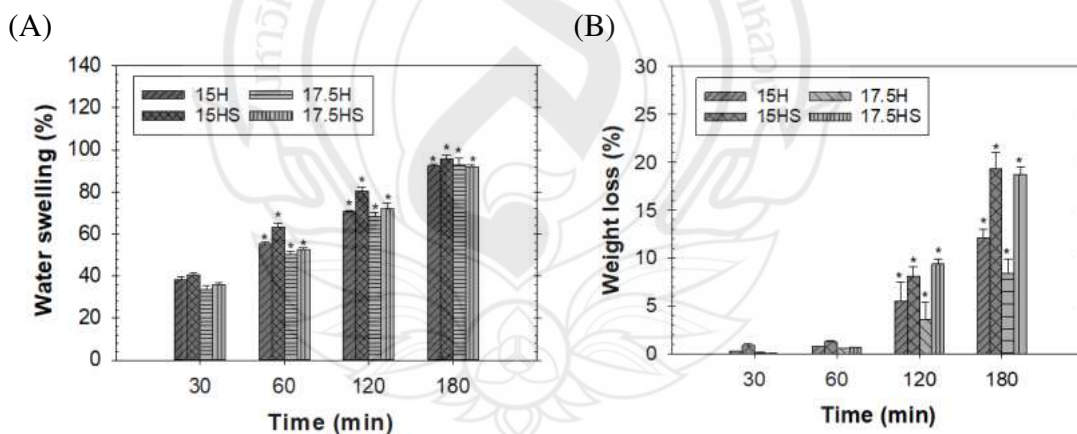
Moreover, the hydrogels loaded with siRNA nanoparticles appeared more flexible and flowable than those without siRNA nanoparticles. The gel fraction study is the qualitative measurement of the degree of hydrogel crosslinking formation. The results showed that the gel fraction of all hydrogels was more than 70%. Chanmontri et al. developed the injectable self-healing hydrogel from QCS and OxPec for wound management. The injectable self-healing hydrogels were prepared through Schiff's base reaction and ionic interactions to achieve the self-healing and gel-forming properties. The injectable self-healing hydrogels can form gel and recover after cutting for 30 min. Moreover, the gel fraction of the hydrogels was 74-76% (Chanmontri et al., 2023).

**Table 5.2** Gelation Time, Self-Healing Time, and Gel Fraction of Injectable Self-Healing Hydrogels (n=3)

Samples	Gelation time (min)	Self-healing time (min)	Gel fraction (%)
15H	14	5	70.04±2.08
15HS	18	3	71.84±2.68
17.5H	10	10	72.10±0.88
17.5HS	13	4	71.28±1.35

### 5.2.7 Water Swelling and Weight Loss Behaviors of Hydrogels

The water swelling and weight loss behaviors of hydrogels are important properties for studying fluid absorption and water retention ability, aiding in controlling the release of siRNA nanoparticles from the hydrogel. Thus, the water swelling and weight loss of the hydrogels were investigated, and the results are shown in Figure 5.5. All hydrogels were completely disintegrated at 240 min. The 17.5H and 17.5HS showed lower swelling than the 15H and 15HS, as shown in Figure 5.5A. These results might reflect the increase in possible interactions between the aldehyde groups in OxPec and the amino groups in QCS, which caused more stability in the hydrogels and decreased swelling. For the weight loss results, the hydrogels could retain their structure for 180 min, but complete disintegration was achieved after submersion for 240 min (Figure 5.5B). The weight loss of 15H, 15HS, 17.5H, and 17.5HS was  $12.16 \pm 0.85$ ,  $19.36 \pm 1.69$ ,  $8.36 \pm 1.54$ , and  $18.72 \pm 0.85$ , respectively, after submersion for 180 min. These results indicated that increasing OxPec concentration tended to decrease the weight loss of the hydrogels. Increasing amounts of OxPec increased the possibility of crosslinking density, resulting in the enhanced stability of the hydrogels (Chanmontri et al.2023).



**Figure 5.5** (A) Water Swelling and (B) Weight Loss of the Hydrogels at 37°C (n =3)

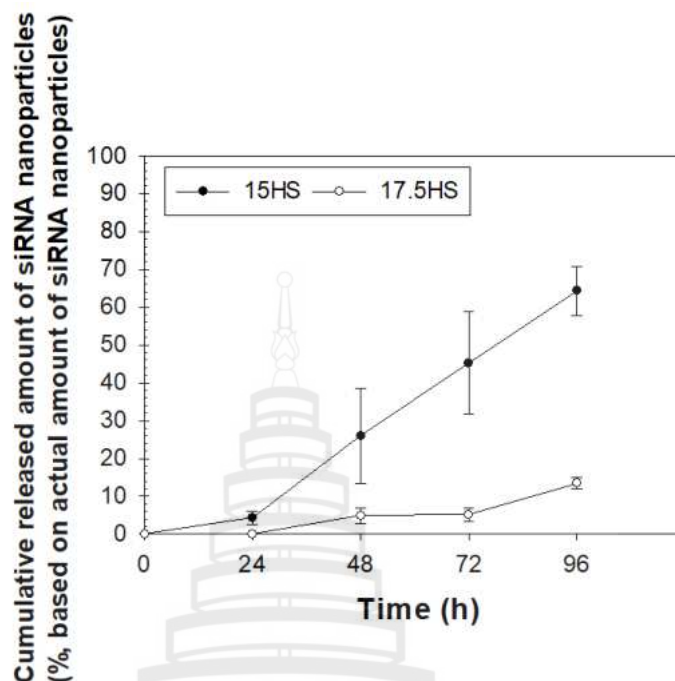
\* $p < 0.05$  Compared with the Values at 30 min at Any Given Material Type

### 5.2.8 Released Profiles

The drug content of 15HS and 17.5HS was  $74.80 \pm 16.26\%$  and  $80.73 \pm 10.90\%$ , respectively, indicating that both formulations were capable of efficiently encapsulating siRNA nanoparticles. High drug content is beneficial as it ensures a greater amount of therapeutic siRNA can be delivered within a limited volume of hydrogel, which is particularly important for localized treatments. It also increases the potential for sustained release over an extended period, supporting prolonged therapeutic effects.

The release profiles of hydrogels are shown in Figure 5.6. The amount of released siRNA nanoparticles gradually increased over time, indicating that the hydrogels enable sustained release. This property is particularly advantageous for breast cancer therapy, as it allows for continuous delivery of therapeutic siRNA to target cells over extended periods. The controlled and prolonged release can help maintain effective siRNA concentrations at the cancer site, supporting consistent gene silencing while minimizing the need for repeated dosing and reducing systemic side effects. The sustained release behavior is due to the hydrogel's self-healing and internally crosslinked network, which regulates the diffusion of siRNA nanoparticles. This prolonged availability near cancer cells may enhance cellular uptake and silencing efficiency, ultimately improving therapeutic outcomes.

Repeat experiments are still required to confirm and validate these findings. Nonetheless, the current results demonstrate the hydrogel's promising potential for sustained siRNA delivery, providing a solid foundation for further research and development.



**Figure 5.6** Released Study of siRNA Nanoparticles-Loaded Self-Healing Hydrogels

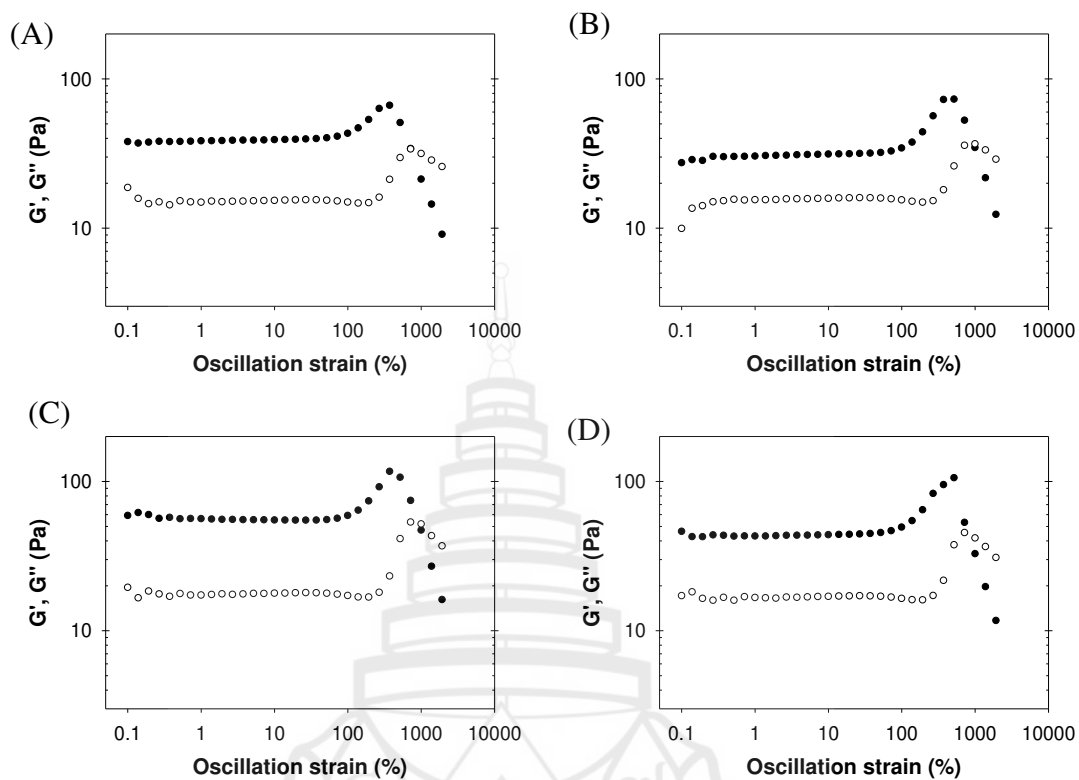
### 5.2.9 Rheological Analysis

The rheological analysis was studied to confirm the formation of 15H, 15HS, 17.5H, and 17.5HS, as shown in Figure 5.7. The sol/gel transition is referred to as the crossover point of storage modulus ( $G'$ ) and loss modulus ( $G''$ ). After the crossover point, the hydrogels lose their gel characteristic and form in the liquid state. The crossover points of  $G'$  and  $G''$  of 15H, 15HS, 17.5H, and 17.5HS were at a strain of 996%. When the  $G'$  became lower than the  $G''$ , it indicated that the hydrogels had a deformed network structure of the hydrogel. The dynamic time sweep rheological test of  $G'$  and  $G''$  was carried out at 37 °C and the results are shown in Figure 5.8. The  $G'$  of 15H, 15HS, 17.5H, and 17.5HS was 29, 25, 42, and 36 Pa, respectively. It was observed that 17.5H and 17.5HS showed a higher  $G'$  than 15H and 15HS. The increased OxPec concentration improved the mechanical properties of the hydrogels. These results might be increased possible interactions between the aldehyde groups in OxPec and the amino groups in QCS, resulting in higher crosslinking density (Basu et al., 2020).

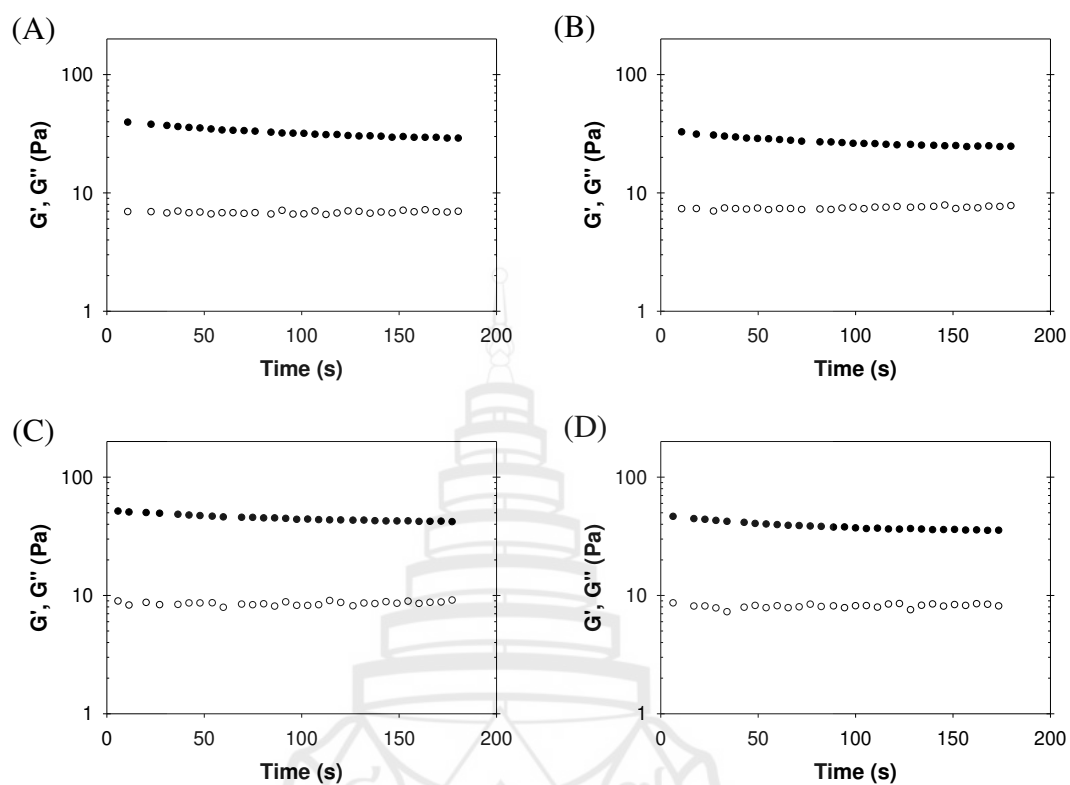
The self-healing properties of 15H, 15HS, 17.5H, and 17.5HS were confirmed by continuous step strain analysis to alternate cycles of high oscillatory shear strain (3000%) and low oscillatory shear strain (1%) (Figure 5.9). When the first 1% strain



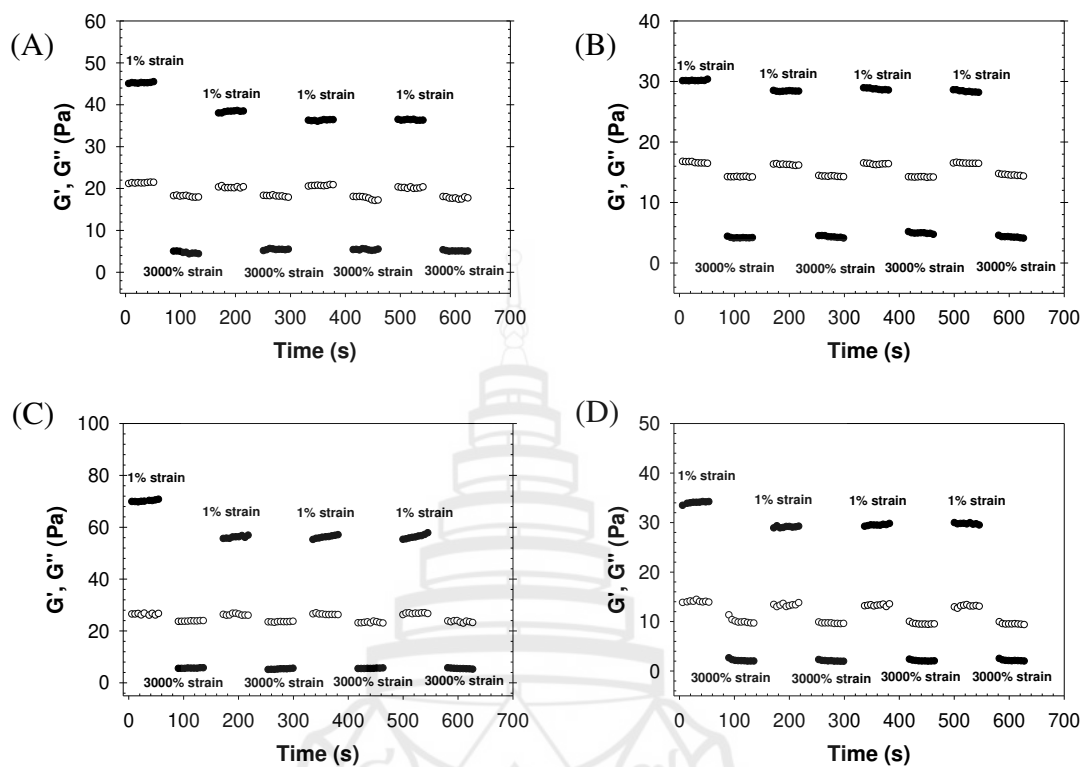
was applied,  $G'$  was higher than  $G''$ , showing the gel state of the hydrogels. When a high oscillatory shear strain at 3000% was applied,  $G''$  was higher than  $G'$ , indicating the hydrogels deformed or collapsed. After 1% strain was applied, the gel recovery ( $G' > G''$ ) was observed over a period of time. However,  $G'$  of all hydrogels after healing was lower than that of the hydrogels before healing, indicating the hydrogels were not fully recovered. From the results, all hydrogels showed self-healing behavior due to the reversible imine bonds. Basu et al. developed the self-healing hydrogels from oxidized alginate as carriers for sustained delivery. The hydrogel formations exhibited self-healing properties due to the covalent imine bonds between the aldehyde groups and the amine groups (Basu et al., 2020). Chanmontri et al. developed injectable self-healing hydrogels from QCS and OxPec as wound dressing materials. The results showed that the hydrogels formed gel in around 5-10 min at 37 °C and displayed the self-healing time for 30 min after cutting. Moreover, the hydrogels recovered like their original  $G'$  after applying high oscillatory shear strain due to the Schiff base reaction occurred between the aldehyde groups of OxPec and the amino groups of QCS and the electrostatic interactions between the negatively charged carboxylate group of OxPeC and the positively charged quaternary ammonium group of QCS (Chanmontri et al., 2023).



**Figure 5.7** Rheological Analysis of (A) 15H, (B) 15HS, (C) 17.5H, and (D) 17.5HS. Storage Modulus  $G'$  (●) and Loss Modulus  $G''$  (○) Strain Sweep at 37 °C and Frequency 10 rad/s



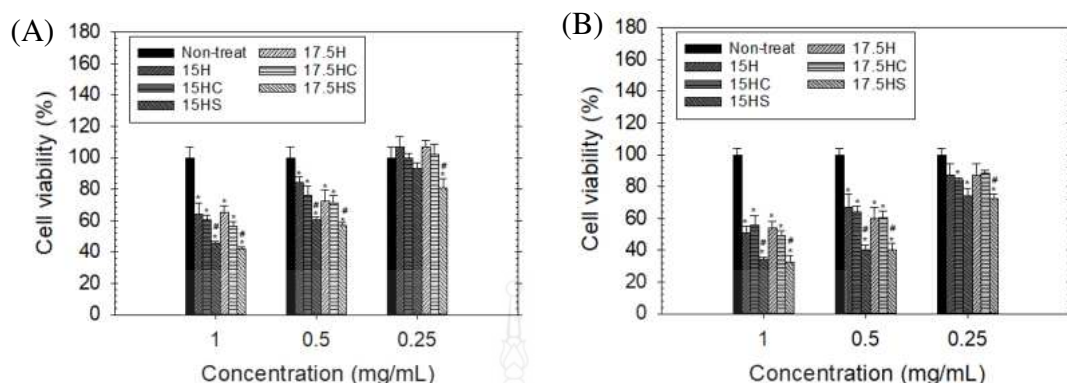
**Figure 5.8** Rheological Analysis (A) 15H, (B) 15HS, (C) 17.5H, and (D) 17.5HS. Storage Modulus  $G'$  (●) and Loss Modulus  $G''$  (○) Time Sweep at 37 °C, Frequency 10 rad/s, and Strain 1%



**Figure 5.9** Continuous Step Strain Analysis of (A) 15H, (B) 15HS, (C) 17.5H, and (D) 17.5HS. Storage Modulus  $G'$  (●) and Loss Modulus  $G''$  (○) at Low Strain of 1% and High Strain of 3000% with 50 s of Intervals

### 5.2.10 *In Vitro* Cytotoxicity Evaluation of Hydrogels

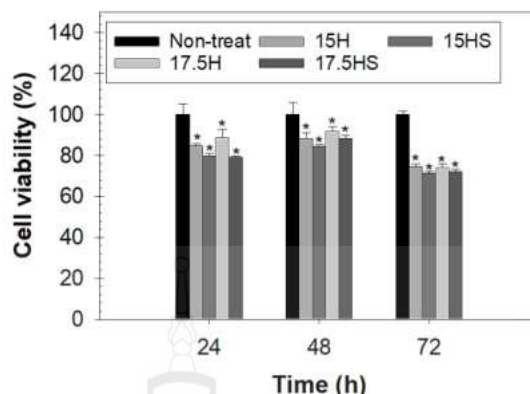
The indirect cytotoxicity of the injectable self-healing hydrogels was tested against MDA-MB-231 and MDA-MB-436 cells using MTT assay for 72 h. Figure 5.10 shows the viability of cells cultured with the extraction media from the hydrogels. At 1 mg/mL of extraction medium, the viability of MDA-MB-231 cells cultured with 15H, 15HC, 15HS, 17.5H, 17.5HC, and 17.5HS was  $63.94 \pm 7.19\%$ ,  $60.59 \pm 2.74\%$ ,  $45.33 \pm 1.55\%$ ,  $65.15 \pm 4.27\%$ ,  $56.56 \pm 2.96\%$ , and  $42.01 \pm 1.44\%$ , respectively. While the viability of MDA-MB-436 cells cultured with 15H, 15HC, 15HS, 17.5H, 17.5HC, and 17.5HS was  $50.77 \pm 4.28\%$ ,  $55.69 \pm 5.96\%$ ,  $34.23 \pm 1.36\%$ ,  $53.90 \pm 4.47\%$ ,  $18.98 \pm 3.36\%$ , and  $32.21 \pm 4.21\%$ , respectively. According to the ISO 10993-5 cytotoxicity standard, cell viability lower than 70% has a cytotoxicity effect on the cells. The pure hydrogels and the hydrogels containing CsiRNA nanoparticles showed a slight cytotoxicity (cell viability < 70%). However, the hydrogels containing siSVV nanoparticles displayed significantly higher level of cytotoxicity compared to the hydrogels containing CsiRNA nanoparticles after 72 h treatment. These results confirmed that the hydrogels containing siSVV nanoparticles had the potential effect on breast cancer inhibition and were used for further study.



**Figure 5.10** Indirect Cytotoxicity of Extraction Media from Hydrogels Cultured with (A) MDA-MB-231 and (B) MDA-MB-436 Cells for 72 h (n = 3). \* $p < 0.05$  Compared with the Non-treat at Any Given Concentration. # $p < 0.05$  Compared Between 15HC and 15HS and Compared between 17.5HC and 17.5HS at Any Given Concentration

### 5.2.11 Biocompatibility of Hydrogels Loaded with siRNA Nanoparticles

For breast cancer treatment, materials must be biocompatible, non-toxic, and promote the growth of normal cells. In this study, the biocompatibility of injectable self-healing hydrogels was evaluated using HDFa cells. From the results (Figure 5.11), it was observed that the hydrogels at a concentration of 0.5 mg/mL did not exhibit any toxicity toward the cells for 72 h. These results confirmed that the hydrogels are biocompatible and do not negatively impact cell viability or growth at this concentration for 72 h. According to the ISO 10993-5 cytotoxicity standard, cell viability below 70% is considered cytotoxic. The cell viability consistently remained above this threshold, suggesting the hydrogels do not cause cellular stress or damage. These findings confirm that the hydrogels are non-toxic to normal cells, indicating good biocompatibility. Importantly, the hydrogels exhibited selective cytotoxicity toward breast cancer cells, highlighting their potential for targeted breast cancer therapy.

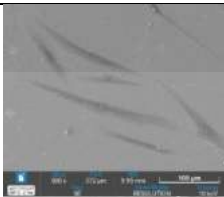
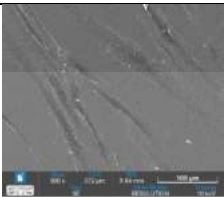
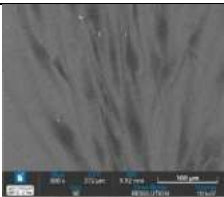








**Figure 5.11** Biocompatibility of Hydrogels (n=3). \* $p < 0.05$  Compared with the Non-Treated Group at Each Time Point

#### 5.2.12 Cell Morphology

FE-SEM was used to examine HDFa cell morphology after treatments. This high-resolution technique enabled detailed observation of surface changes caused by injectable self-healing hydrogels loaded with siRNA nanoparticles compared to non-treated cell. The morphology of HDFa cells cultured with the extraction media from 15HS and 17.5HS was observed using FE-SEM, as shown in Table 5.3. The results showed that the HDFa cells treated with 15HS and 17.5HS were well attached to the cover glass and maintained a spindle-shaped appearance, which is a normal feature of healthy fibroblast cells. These results suggested that 15HS and 17.5HS provide a good environment for cells to stick and spread, supporting their growth without affecting their normal shape. No signs of toxicity or adverse interactions were observed between the hydrogels and HDFa cells. This is crucial for breast cancer therapy, where delivery systems must target cancer cells without harming healthy cells.

**Table 5.3** Morphology of HDFa Cells Cultured with Extraction Media of Injectable Self-Healing Hydrogels Loaded with siRNA Nanoparticles

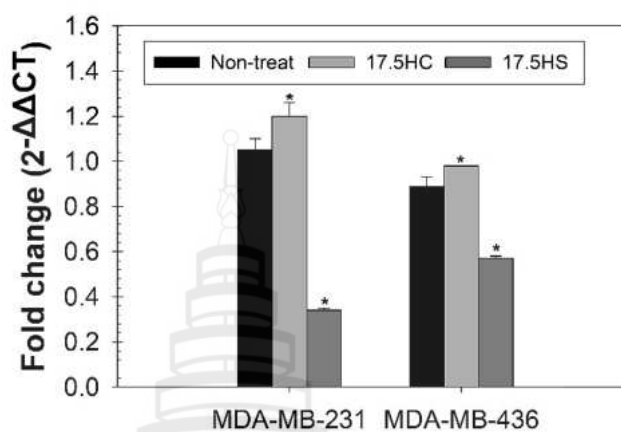
Condition	Time points (h)		
	24	48	72
Non-treated			
15HS			
17.5HS			

### 5.2.13 RT-qPCR for Gene Silencing of siRNA Nanoparticles Loaded in Hydrogel

To evaluate the effect of siRNA nanoparticles-loaded injectable self-healing hydrogels on gene expression, MDA-MB-231 and MDA-MB-436 cells were treated for 72 h, and gene silencing was assessed using RT-qPCR (Figure 5.12). In MDA-MB-231 cells, the non-treated control showed baseline gene expression (1.05-fold), while the 17.5HC exhibited a slight increase (1.20-fold), indicating that the control hydrogel (without siRNA nanoparticles) did not affect gene expression. In contrast, the treatment with 17.5HS significantly reduced gene expression to 0.34-fold, confirming effective gene silencing. In MDA-MB-436 cells, survivin expression remained unchanged in the non-treated group (0.89-fold) and the 17.5HC group (0.98-fold), indicating no off-target effects from the hydrogel. However, the treatment with 17.5HS led to a substantial decrease in survivin expression (0.57-fold), demonstrating effective and specific gene silencing in these cells. The results showed that self-healing hydrogels effectively deliver siRNA nanoparticles to reduce gene expression in cancer cells. Lower gene expression (0.34-fold for MDA-MB-231 and 0.57-fold for MDA-MB-436



of 17.5HS) indicated successful silencing of target genes. This makes the system promising for targeted breast cancer therapies.

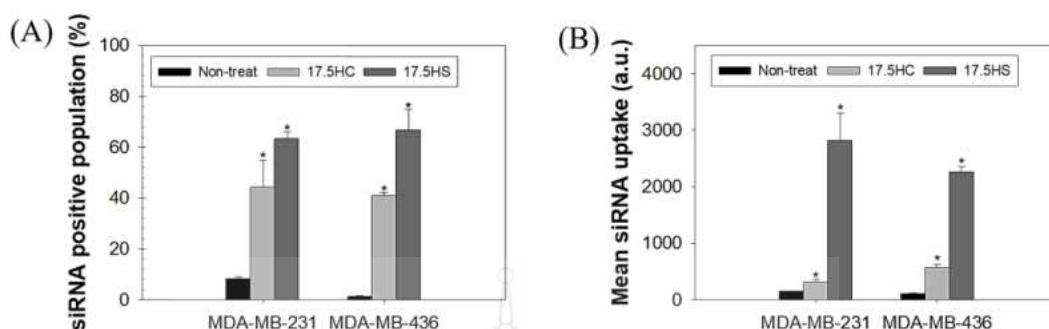


**Figure 5.12** Relative Fold Change of Hydrogels Loaded with siRNA Nanoparticles Cultured with MDA-MB-231 and MDA-MB-436 Cells by RT-qPCR After Transfection for 72 h. \* $p < 0.05$  Compared with the Non-Treated Group

#### 5.2.14 Cellular Uptake Study by Flow Cytometry

Cellular uptake was evaluated using flow cytometry by incubating cells with FAM-siRNA nanoparticles loaded in the hydrogels, followed by fluorescence measurement to quantify internalization. The siRNA positive population in the non-treated, 17.5HC, and 17.5HS groups is shown in Figure 5.13A. In both MDA-MB-231 and MDA-MB-436 cell lines, the non-treated groups showed the lowest siRNA-positive populations (8.27% and 1.10%, respectively), indicating minimal uptake in the absence of treatment. Treatment with 17.5HC increased the siRNA positive population significantly in MDA-MB-231 (44.23%) and MDA-MB-436 (40.97%) cells. This increase may be due to both CsiRNA and the hydrogel being internalized, with overlapping fluorescence potentially leading to higher apparent uptake. When comparing the 17.5HS-treated groups, MDA-MB-231 cells showed 63.20% siRNA positive cells, while MDA-MB-436 cells had an even higher percentage (66.73%). These results confirmed that the hydrogels do not hinder siRNA release and suggested that incorporating siRNA nanoparticles into the self-healing hydrogels improved siRNA internalization and protected the siRNA nanoparticles from degradation.

The analysis of mean siRNA uptake in the non-treated, 17.5HC, and 17.5HS is shown in Figure 5.13B. Non-treated MDA-MB-231 and MDA-MB-436 cells exhibited minimal siRNA uptake, with values of 153 a.u. and 105 a.u., respectively. When treated with 17.5HC, both cell types showed an increase in siRNA nanoparticles uptake, with values of 314.00 a.u. for MDA-MB-231 cells, and 570.67 a.u. for MDA-MB-436 cells. However, this increase might be influenced by fluorescence from the hydrogels interacting with the cells, potentially affecting the accuracy of these results. In contrast, the treatment with 17.5HS resulted in significantly higher siRNA nanoparticle uptake in both breast cancer cell lines. Specifically, MDA-MB-231 cells showed values of 2816.00 a.u., while MDA-MB-436 cells reached 2256.33 a.u. The substantially higher mean siRNA uptake observed in both MDA-MB-231 and MDA-MB-436 cells treated with 17.5HS suggests that these hydrogel formulations improve the internalization of siRNA nanoparticles, possibly due to the hydrogel's protective properties against siRNA degradation.


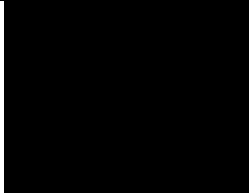


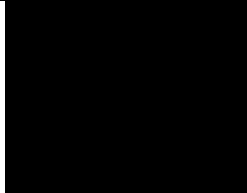


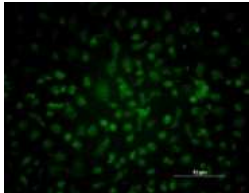


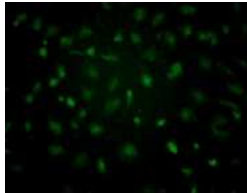
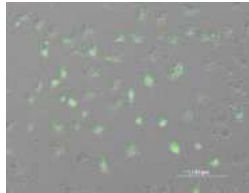
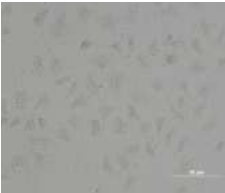
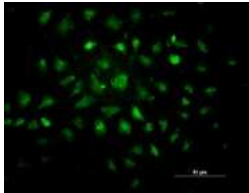

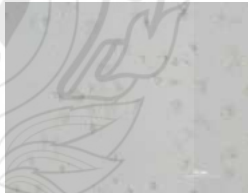
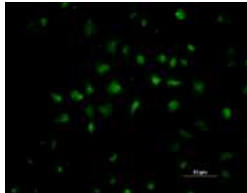
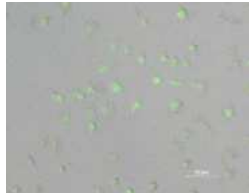


**Figure 5.13** Cell Uptake of siRNA Nanoparticles Loaded in Hydrogels (A) Percentage of FAM-Labeled siRNA Positive Cell Population and (B) Mean Fluorescence Intensity of FAM-Labeled siRNA Nanoparticles After 72 h Treatment. \* $p < 0.05$  Compared with the Non-Treated Group at Each Time Point

#### 5.2.15 Fluorescence Microscopy Analysis

The cellular uptake of FAM-siSVV nanoparticles loaded in the hydrogels was confirmed using fluorescence imaging (Table 5.4). The cellular uptake was investigated in MDA-MB-231 and MDA-MB-436 cells for 72 h. The images obtained showed green fluorescence, indicating the presence of FAM-labeled siRNA nanoparticles inside the cells for both the 15HS and 17.5HS hydrogel formulations after 72 h of transfection. Notably, the 17.5HS exhibited similar cellular uptake compared to the 15HS, suggesting that the hydrogel concentration or composition did not significantly impact siRNA nanoparticles delivery efficiency. These results were consistent across both MDA-MB-231 and MDA-MB-436 cells, demonstrating the self-healing hydrogel system's effectiveness in delivering siRNA nanoparticles to different breast cancer cell types. These findings strongly suggest that injectable self-healing hydrogels loaded with siRNA nanoparticles can effectively protect siRNA from enzymatic degradation and facilitate targeted delivery to cancer cells. Moreover, the self-healing properties of the hydrogel likely enhance the retention and localized release of the therapeutic siRNA nanoparticles, positioning this approach as promising for improving the efficacy of gene silencing in breast cancer treatment.

**Table 5.4** Cellular Uptake of FAM-siSVV Nanoparticles Loaded-Injectable Self-Healing Hydrogels After Transfection of 72 h was Captured by Fluorescence Microscopy (Magnification 20×)

Condition	MDA-MB-231			MDA-MB-436		
	Brightfield	FAM	Merged	Brightfield	FAM	Merged
Non-treat						
15HS						
17.5HS						

## CHAPTER 6

# INJECTABLE THERMOSENSITIVE CHITOSAN/SILK SERICIN HYDROGELS LOADED WITH siRNA NANOPARTICLES FOR BREAST CANCER TREATMENT

## 6.1 Methodology

### 6.1.1 Extraction of SS

SS was extracted using a modified version of the method described by Pankongadisak and Suwantong (Pankongadisak & Suwantong, 2018). First, raw Thai silk cocoons were cut into small pieces and degummed with 500 mL of 0.5% w/v sodium carbonate at 85 °C for 45 min. The aqueous SS solution was collected and filtered to remove insoluble materials using a cheesecloth. The SS solution was dialyzed in deionized water for 3 days using a dialysis bag and the deionized water was replaced every 24 h to remove salts. The lipid and impurities were subsequently removed from the SS solution by centrifugation at 5000 rpm, 25 °C for 10 min. Finally, the SS solution was lyophilized using a freeze-drying method for 48 h.

### 6.1.2 FTIR Analysis

The functional groups of CS, SS,  $\beta$ -GP, and injectable thermosensitive hydrogel containing siRNA nanoparticles were characterized using the ATR mode of the FTIR spectrophotometer (PerkinElmer, USA). The CS, SS, and  $\beta$ -GP powders were mixed with KBr and prepared as a pellet to identify the structure of CS, SS, and  $\beta$ -GP. The thermosensitive hydrogel containing siRNA nanoparticles was lyophilized using a freeze-drying method for 48 h and prepared as a disk before observation. All spectra of the samples were observed in the range of 4000-400  $\text{cm}^{-1}$  at a resolution of 4  $\text{cm}^{-1}$  in a transmittance mode.

### **6.1.3 *In Vitro* Cytotoxicity Evaluation of CS and SS**

The cytotoxicity evaluation of CS and SS was adapted from the ISO 10993-5 standard test method using MDA-MB-231, MDA-MB-436, and HDFa cells. First, 100  $\mu$ L of cells were seeded in a 96-well tissue culture plate at 8,000 cells/well and incubated at 37 °C for 24 h. CS was dissolved in 1%v/v of acetic acid at room temperature overnight to obtain a homogeneous solution. SS solution was prepared by dissolving SS in deionized water under magnetic stirring to obtain a clear homogenous solution. Each raw material was diluted with cell culture medium by a 2-fold dilution method to produce various concentration solutions as 10, 5, 2.5, 1.25, 0.625, 0.313, 0.156, 0.078, 0.039, and 0.02 mg/mL. The cells were then replaced with CS and SS solution and cultured for 24 h. The viability of cultured cells was determined by MTT assay. After the incubation period, the medium was removed, and then 100  $\mu$ L of 1 mg/mL MTT solution was added. The mixture was incubated in 5% CO<sub>2</sub> at 37 °C for 3 h. After that, the medium was removed and the formazan crystals formed were dissolved with DMSO. The absorbance of the solution was measured by a microplate reader (BioTek Synergy H1, USA) at a wavelength of 570 nm. The viability of cells cultured in fresh DMEM was used as a control.

### **6.1.4 Preparation of Injectable Thermosensitive Hydrogels Containing siRNA Nanoparticles**

The optimal conditions for preparing injectable thermosensitive hydrogels were identified. To prepare these hydrogels, a 3% w/v CS solution was created by dissolving CS powder in a 1% v/v acetic acid solution under magnetic stirring at room temperature until a clear, homogeneous solution was obtained. In addition, a 50% w/v of  $\beta$ -GP solution was prepared by dissolving  $\beta$ -GP powder in deionized water under magnetic stirring to obtain a homogeneous solution at room temperature. Then, 7% w/v of SS solution was prepared by dissolving SS in deionized water at room temperature under magnetic stirring to obtain a homogeneous solution. After that, SS solution was centrifuged at 5,000 rpm at 25 °C for 20 min to remove lipids and impurities from the SS solution. Then, SS solution was added dropwise to the CS solution in the volume ratio (mL) of CS:SS as 1:0.5 under magnetic stirring at room temperature for 20 min to obtain a clear homogeneous solution. The mixture and  $\beta$ -GP solutions were cooled using an ice bath for 30 min. Next,  $\beta$ -GP solution was added dropwise to the mixture

solution under stirring in an ice bath for 30 min with various volume ratios of CS to  $\beta$ -GP (i.e., 1:0.2, 1:0.5, 1:0.8, and 1:1 mL). Finally, the mixture solutions were incubated at 37 °C to obtain the injectable thermosensitive hydrogels.

To prepare the injectable thermosensitive hydrogels loaded with siRNA nanoparticles, the mixture solutions of 3% w/v CS solution and 7% w/v of SS solution in the volume ratio (mL) of CS to SS as 1:0.5 and 50% w/v of  $\beta$ -GP solutions were cooled using an ice bath for 30 min. Next,  $\beta$ -GP solution was added dropwise to the mixture solution under stirring in an ice bath for 30 min with various CS to  $\beta$ -GP volume ratios (i.e., 1:0.8 and 1:1 mL). To prepare siRNA nanoparticles for loading in the hydrogels, 10  $\mu$ M of siRNA solution was added to DMEM at siRNA:additive ratio of 1:1 (w/w). Then, 0.14  $\mu$ g/ $\mu$ L of Trans-Booster solution was added to the siRNA solution as an additive. Next, 1  $\mu$ g/ $\mu$ L of Prime-Fect solution as a transfection reagent was added to the mixture solution in the darkroom at room temperature for 30 min to allow an optimal complexation process. The siRNA:Prime-Fect ratio in the complexes was 1:10 (w/w). After the complexation process, 100  $\mu$ L of siRNA nanoparticles was added dropwise to the mixture solution and stirred with a spatula. The final concentration of siRNA nanoparticles was 80 nM. Finally, the mixture solutions were incubated at 37 °C to obtain the injectable thermosensitive hydrogels loaded with siRNA nanoparticles. The compositions of the injectable thermosensitive hydrogels containing siRNA nanoparticles are shown in Table 6.1.

**Table 6.1** Preparation Parameters and Gelation Time of the Injectable Thermosensitive Hydrogels Loaded with siRNA Nanoparticles

Code	CS (%w/v)	SS (%w/v)	CS : SS (mL:mL)	CS : 50% w/v $\beta$ -GP (mL:mL)	siRNA nanoparticles at 80 nM ( $\mu$ L)
0.2H	3	7	1:0.5	1:0.2	0
0.2HS	3	7	1:0.5	1:0.2	100
0.5H	3	7	1:0.5	1:0.5	0
0.5HS	3	7	1:0.5	1:0.5	100
0.8H	3	7	1:0.5	1:0.8	0
0.8HS	3	7	1:0.5	1:0.8	100
1.0H	3	7	1:0.5	1:1	0
1.0HS	3	7	1:0.5	1:1	100

### 6.1.5 Morphology of siRNA Nanoparticles in Hydrogels

The morphology of the siRNA nanoparticles loaded in the hydrogels was examined using an HT7800 transmission electron microscope (Hitachi, Japan). The siRNA nanoparticles in the CS solution were prepared on a carbon-coated grid by adding a 20  $\mu$ L droplet of the nanoparticle suspension into 0.2 mL of 1% (w/v) CS solution for 5 min, followed by blotting with filter paper. The samples were then negatively stained with a UranylLess solution for 3 min. Subsequently, the samples were observed by TEM at an accelerating voltage of 80 kV. The particle size of the siRNA nanoparticles loaded in the hydrogel was analyzed using ImageJ153 software, with measurements conducted on 120 individual particles ( $n = 120$ ).



### 6.1.6 Gelation Time and Gel Fraction of Hydrogels

The gelation time of the injectable thermosensitive hydrogels loaded with siRNA nanoparticles was observed in the vial tubes using the inverting method. For the injectable thermosensitive hydrogels, 50% w/v  $\beta$ -GP solution with various volume ratios of CS to  $\beta$ -GP (i.e., 1:0.2, 1:0.5, 1:0.8, and 1:1 mL) was added dropwise into the mixture solutions of 1 mL of 3% w/v CS solution and 0.5 mL of 7% w/v SS solution under stirring in an ice bath for 30 min to obtain a homogeneous solution. For the injectable thermosensitive hydrogels loaded with siRNA nanoparticles, 50% w/v of  $\beta$ -GP solutions with various volume ratios of CS to  $\beta$ -GP (i.e., 1:0.2, 1:0.5, 1:0.8, and 1:1 mL) were added dropwise into the mixture solutions of 1 mL of 3% w/v CS solution and 0.5 mL of 7% w/v SS solution under stirring in an ice bath for 30 min to obtain a homogeneous solution. After that, 100  $\mu$ L of siRNA nanoparticles was added to the vial and stirred with a spatula for 10 s to obtain a homogeneous solution and incubated at 37 °C. The final concentration of siRNA nanoparticles loaded in the hydrogel was 80 nM. The formation of gel was observed every 1 min. The gelation time was recorded by inverting the vial upside down until the gels did not flow over 30 s.

The gel fraction was performed to determine the gel proportion of the hydrogel. After the gel formation, the hydrogels were stored in the refrigerator at -20 °C overnight. The hydrogels were then lyophilized by the freeze-drying method for 48 h to obtain the initial dry mass ( $m_{d,i}$ ). The dried samples were immersed in deionized water at 37 °C for 24 h. After 24 h, the swollen hydrogels were removed and wiped thoroughly with Kimtech tissue paper (Kimwipes®) and then freeze-dried to obtain the final dry mass ( $m_{d,w}$ ). The measurements of each sample were calculated as shown in equations (6.1):

$$\text{Gel fraction (\%)} = \frac{m_{d,w}}{m_{d,i}} \times 100 \quad (6.1)$$

### 6.1.7 Water Swelling and Weight Loss

The water swelling and weight loss behavior of the injectable thermosensitive hydrogels was examined by an immersion method. 250  $\mu\text{L}$  of each injectable thermosensitive hydrogel was formed in a plastic bottle plug and incubation at 37 °C for 6 h. Each hydrogel was weighed ( $M_{w,i}$ ) and immersed in 2 mL of phosphate buffer solution (pH 7.4) at 37 °C for 24, 72, 120, and 168 h. At predetermined time intervals, the hydrogels were removed from the phosphate buffer solution and weighed as swollen mass ( $M_{w,t}$ ). Then, the swollen hydrogels were dried using freeze-dryer and weighed as  $M_d$ . To evaluate the weight loss of hydrogels, the actual macromer fraction (AMF) was calculated using equation (6.2). The initial weight of the hydrogels in dry state ( $M_{d,i}$ ) was calculated using equation (6.3). The water swelling and weight loss of the hydrogels were calculated using equations (6.4) and (6.5), respectively.

Weight loss in PBS and lysozyme of the injectable thermosensitive hydrogels was investigated by an immersion method. First, the hydrogels were immersed in 2 mL of phosphate buffer solution (pH 7.4) containing 10,000 units/mL lysozyme enzyme at 37 °C for 24, 72, 120, and 168 h, respectively. After interval time, the swollen hydrogels were dried using freeze-dryer and weighed as  $M_d$ . To evaluate the *in vitro* degradation of the injectable thermosensitive hydrogels, the actual macromer fraction (AMF) was calculated using equation (6.2). The  $M_{d,i}$  was calculated using equation (6.3). The weight loss of each hydrogel was calculated according to the following equations (6.5):

$$\text{Actual macromer fraction (AMF)} = \frac{M_{d,i}}{M_{w,i}} \quad (6.2)$$

$$M_{d,i} = M_{i,w} \times \text{AMF} \quad (6.3)$$

$$\text{Water swelling (\%)} = \frac{M_{w,t} - M_{w,i}}{M_{w,i}} \times 100 \quad (6.4)$$

$$\text{Weight loss (\%)} = \frac{M_{d,i} - M_d}{M_{d,i}} \times 100 \quad (6.5)$$

### 6.1.8 Released Profiles

Before assessing the release behavior, the actual amount of siRNA nanoparticles loaded in each hydrogel sample was quantified. In this study, 100 mg of siRNA nanoparticle-loaded hydrogel was used per sample. Each hydrogel sample was fully dissolved in 1.0 mL of PBS (pH 7.4) at 37 °C. Then, 0.1 mL of the resulting solution was measured using a fluorescence microplate reader (Thermo Ascent;  $\lambda_{\text{ex}}$  485 nm,  $\lambda_{\text{em}}$  527 nm) to determine the siRNA nanoparticle content.

To evaluate the release profile, 100 mg of each hydrogel was placed into a 24-well transwell insert (Corning Incorporated Costar®, USA). These inserts were transferred into individual wells of a 24-well plate containing 1.0 mL of PBS (pH 7.4) and incubated at 37 °C for 24, 48, 72, and 96 h. After incubation, 0.1 mL of the release medium was collected and analyzed using the fluorescence microplate reader at the same excitation and emission wavelengths.

### 6.1.9 Rheological Properties and Viscosity Measurements

The rheological properties of injectable thermosensitive hydrogels were measured using a Bohlin Gemini 200HR nano-rotational rheometer (Malvern, UK) equipped with a parallel geometry with a diameter of 40 mm, and the gap was set to 1 mm. 1 mL of injectable thermosensitive hydrogel solution was placed on top of the rheometer and equilibrated at 20 °C. During the gelation process, the rheological properties of samples were measured within the temperature range of 20 °C to 50 °C. The changes in the elastic (storage) modulus ( $G'$ ) and the viscous (loss) modulus ( $G''$ ) were recorded as a function of temperature. The rheology properties of the injectable thermosensitive hydrogels were determined at 37 °C for 1000 s, and changes in elastic modulus and the viscous modulus were recorded as functions of time to assess the gelation time of the samples. The sol–gel transition behavior of the injectable thermosensitive hydrogels was investigated in terms of the viscosity of the hydrogels within the temperature range of 20–50 °C.

#### **6.1.10 *In Vitro* Evaluation of Cell Growth Inhibition by Injectable Thermosensitive Hydrogels**

The ability of the injectable thermosensitive hydrogels to inhibit cell growth was conducted indirectly by immersion of the hydrogels in 10% DMEM (containing 10% fetal bovine serum and 1% antibiotic agent). First, MDA-MB-231 (passage 14<sup>th</sup>) and MDA-MB-436 (passage 14<sup>th</sup>) cells were cultured in 10% DMEM at 12,000 cells/well in a 96-well cell culture plate and incubated at 37 °C for 24 h. The hydrogels were immersed in the cell culture media for 24 h to produce the extraction media at different concentrations of 1, 0.5, and 0.25 mg/mL. Then, the cell culture media were removed from the cells, and the cells were cultured with the extraction media for 72 h. Finally, the viability of cultured cells was determined by MTT assay using a microplate reader (Molecular Devices, Spectramac 250) at a wavelength of 570 nm. The viability of cells cultured in fresh DMEM was used as a control. The CsiRNA nanoparticles-loaded hydrogels were used as a negative control compared with the siSVV nanoparticles loaded-hydrogels and the non-treatment group. The compositions of the injectable thermosensitive hydrogels used for this experiment are shown in Table 6.2.

**Table 6.2** Compositions of the Injectable Thermosensitive Hydrogels Loaded with CsiRNA Nanoparticles and siRNA Nanoparticles

Code	CS (%w/v)	SS (%w/v)	CS : SS (mL:mL)	CS : 50% w/v $\beta$ -GP (mL:mL)	siRNA nanoparticles at 80 nM ( $\mu$ L)	
					CsiRNA	siSVV
0.8H	3	7	1:0.5	1:0.8	0	0
0.8HC	3	7	1:0.5	1:0.8	100	0
0.8HS	3	7	1:0.5	1:0.8	0	100
1.0H	3	7	1:0.5	1:1	0	0
1.0HC	3	7	1:0.5	1:1	100	0
1.0HS	3	7	1:0.5	1:1	0	100

### **6.1.11 Biocompatibility Evaluation of Injectable Thermosensitive Hydrogels**

The biocompatibility of 0.8HS and 1.0HS hydrogels was evaluated using HDFa cells. Cells were seeded at 8,000 cells/well in the 96-well tissue culture plates and incubated for 24 h. Before testing, the hydrogels were sterilized under UV light for 30 min and immersed in the culture media to prepare the extraction media solutions. After replacing the culture media with 100  $\mu$ L of each extraction media solution, cells were cultured for 24, 48, and 72 h. Cell viability was assessed at 24, 48, and 72 h using the MTT assay to determine the effect of the extraction media from hydrogels on the cell growth.

### **6.1.12 Cell Morphology**

Cell morphology after treatment with 0.8HS and 1.0HS was examined using FE-SEM. HDFa cells were seeded at 25,000 cells/well on cover glasses in the 24-well plates and cultured for 24 h to allow attachment. The hydrogels were sterilized under UV light for 30 min and immersed in culture media at a concentration of 0.5 mg/mL for 24 h. Each extraction medium was added to the wells and incubated for 24, 48, and 72 h. At each time point, the medium was removed, and cells were rinsed with 500  $\mu$ L of PBS (pH 7.4). Cells were then fixed with 250  $\mu$ L of 3% glutaraldehyde for 30 min, followed by dehydration through an ethanol series dilution (30%, 50%, 70%, 90%, and 100% v/v) for 2 min each. Afterward, samples were treated with 500  $\mu$ L of 100% hexamethyldisilazane for 5 min and air-dried in a desiccator at room temperature for 24 h. Finally, the samples were gold-coated and imaged under FE-SEM.

### **6.1.13 Cellular Uptake Study by Flow Cytometry**

To quantify siRNA nanoparticle uptake, MDA-MB-231 and MDA-MB-436 cells were seeded at a density of  $8 \times 10^5$  cells/well in 24-well plates 24 h before treatment with 0.8HS and 1.0HS for 72 h. The cells were washed and soaked in 500  $\mu$ L of HBSS for 20 min, with this step repeated three times to remove the dissolved hydrogel coating from the cells. Next, the cells were trypsinized with 200  $\mu$ L of 1X Trypsin-EDTA (0.5%), without phenol red, and then incubated in a hot air oven at 37 °C for 15 min. After incubation, the cells were collected and transferred into 1.5 mL centrifuge tubes. Subsequently, the tubes were centrifuged at 3,000 rpm for 10 min. The supernatant was then removed, and the cell pellet was fixed by adding 200  $\mu$ L of 3.7%

formaldehyde. The fixed cell suspension was then transferred to a flow cytometer tube and supplemented with 200  $\mu$ L of HBSS. The high-parameter flow cytometer LSRFortessa™ (BD Biosciences, Franklin Lakes, New Jersey) was used to quantify the mean fluorescence in cells and the FAM-positive cell population. To ensure accurate analysis of fluorescence signals by excluding background interference, the mean fluorescence intensity and the percentage of FAM-fluorescent cells in the recovered population were determined. This was achieved by gating a representative portion of nontreated cells to account for autofluorescence, typically set at 1% of the total population.

#### **6.1.14 RT-qPCR for Gene Silencing**

First, either 500  $\mu$ L of MDA-MB-231 or MDA-MB-436 cells, at a density of  $3.2 \times 10^5$  cells/well, was seeded in 12-well cell culture plates and incubated at 37 °C in 5% CO<sub>2</sub> for 24 h. The hydrogels were sterilized by UV light for 30 min and then immersed in cell culture media to prepare 10 mg/mL extraction media solutions for each sample. Following the incubation period, 500  $\mu$ L of each sample solution was applied to the cultured cells. Gene expression was evaluated 72 h post-transfection using RT-qPCR. Prior to cell lysis, the cells were rinsed twice with 500  $\mu$ L of HBSS to remove residual media and non-adherent substances. Subsequently, 200  $\mu$ L of TRIzol™ reagent was directly added to each well for total RNA extraction. The resulting lysates were incubated at room temperature for 15 min, then transferred to 1.5 mL microcentrifuge tubes and mixed with 300  $\mu$ L of chloroform. The tubes were centrifuged at 6,500 rpm for 10 min to separate the phases. The upper aqueous layer (clear phase) was carefully collected and transferred to a new 1.5 mL tube. Then, 500  $\mu$ L of 2-propanol was added to precipitate the RNA. This mixture was centrifuged at 12,200 rcf at 4 °C for 10 min, and the supernatant was discarded. The resulting RNA pellet was air-dried for 45 min. Subsequently, the pellet was washed with 500  $\mu$ L of 75% ethanol, and the tubes were stored at -20 °C overnight. The following day, the samples were centrifuged again at 12,200 rcf at 4 °C for 5 min. After discarding the supernatant, the RNA pellet was air-dried for an additional 60 min and then dissolved in 15  $\mu$ L of RNase-free water. The solution was gently vortexed at medium speed for 10 s at room temperature and then incubated in a 60 °C water bath for 10 min to ensure complete dissolution. For cDNA synthesis, 1  $\mu$ g of total RNA was used in a reaction

mixture containing 15  $\mu\text{L}$  of RNA, 4  $\mu\text{L}$  of TransAmp buffer, and 1  $\mu\text{L}$  of reverse transcriptase, following the manufacturer's protocol (SensiFAST™ cDNA Synthesis Kit, Meridian Bioscience, USA). SVV was selected as internal reference (housekeeping) genes for RT-qPCR.

#### **6.1.15 Fluorescence Microscopy Analysis**

Fluorescence microscopy was used to evaluate the cellular uptake of FAM-siSVV nanoparticles-injectable thermosensitive hydrogels. 300  $\mu\text{L}$  of MDA-MB-231 or MDA-MB-436 cells were seeded into the 24-well plates at a density of  $3 \times 10^5$  cells/well and incubated for 24 h. After incubation, the culture medium was replaced with 300  $\mu\text{L}$  of extraction medium at a concentration of 0.5 mg/mL and further cultured for 72 h. After 72 h, the cells were washed with 500  $\mu\text{L}$  of phosphate-buffered saline and fixed with 250  $\mu\text{L}$  of 4% (w/v) paraformaldehyde at 37 °C for 10 min. Cellular uptake was then observed using an ECLIPSE Ti<sub>2</sub> inverted microscope (Nikon Instruments Inc., Japan).

#### **6.1.16 Statistical Analysis**

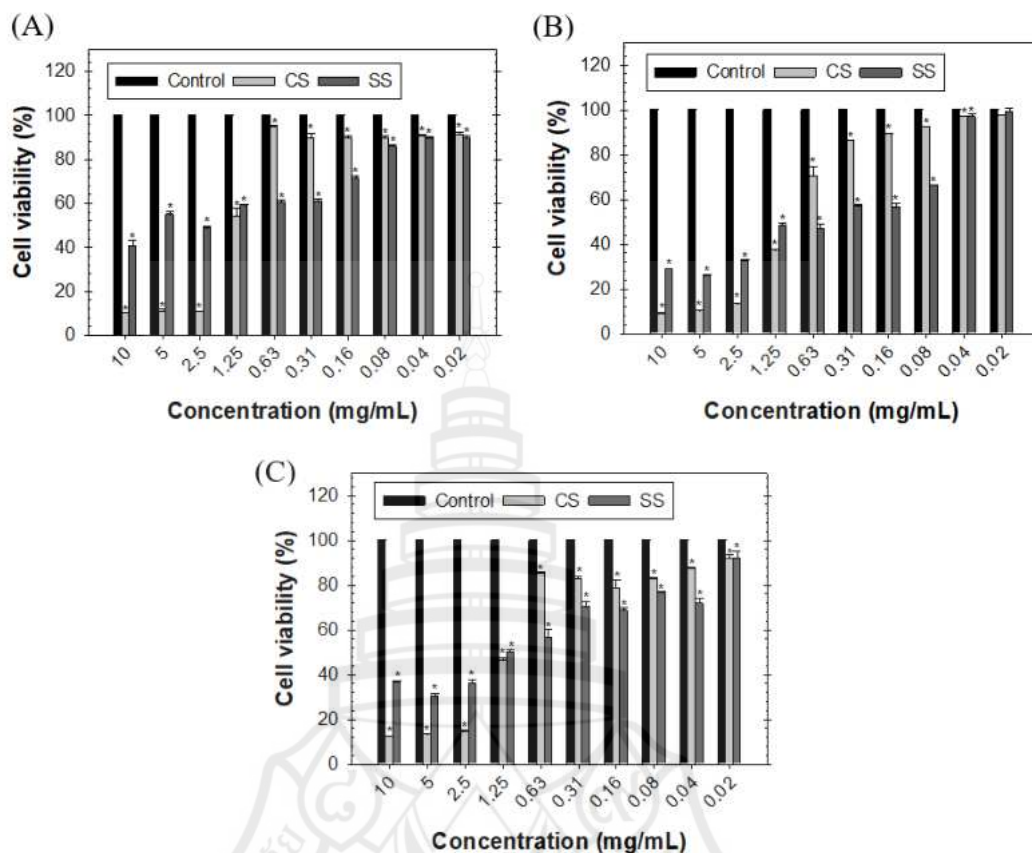
Experimental data from all studies are presented as mean  $\pm$  standard deviation (SD). Multiple group comparisons were performed using one-way ANOVA with Tukey's post hoc test (SPSS, IBM SPSS Statistics 26, USA). Two independent groups were compared using Student's t-test. Statistical significance was defined as  $p < 0.05$ .



## 6.2 Results and Discussion

### 6.2.1 *In Vitro* Cytotoxicity Evaluation of CS and SS

Prior to fabricating the injectable thermosensitive SS/CS hydrogels, the cytotoxicity of the raw materials, CS and SS, was evaluated. This assessment was necessary to ensure that these materials were safe for biomedical applications, with no toxic effects on cells. From Figure 6.1, the viability of cells cultured with CS was lower than that of SS at 10 mg/mL, presumably due to the electrostatic interactions between the negatively charged cell surface and the positively charged groups in the CS structure. These interactions may disrupt the cell membrane, leading to cell death. Specifically, the cell membrane, which possesses negatively charged molecules and phosphate groups on phospholipids, interacts with the positively charged amino groups in CS. This interaction can result in membrane de-stabilization, structural damage, and increased permeability (Lee et al., 2002; Liu et al., 2011). However, SS demonstrated higher toxicity than CS at lower concentrations. This difference can be attributed to several factors related to its chemical structure and behavior in biological systems. SS, a protein-based substance, can sometimes induce more significant interactions with cell membranes, potentially leading to membrane disruption, inflammation, or immune responses, particularly at low concentrations. Therefore, SS at lower concentrations may also exhibit a higher chance of binding to cell surface receptors or proteins, leading to adverse effects (Kunz et al., 2016; Tamulytė et al., 2024; Jiang et al., 2022). In contrast, CS, a polysaccharide, generally exhibits a more favorable biocompatibility profile due to its biopolymeric nature. It is often less likely to trigger immune responses or cytotoxic effects at lower concentration than proteins like SS. However, it is important to note that the specific properties of each material, including its molecular weight, degree of deacetylation, and surface charge, can significantly influence the observed cytotoxicity (Jiao et al., 2017; Chollakup et al., 2020; Desai et al., 2023).

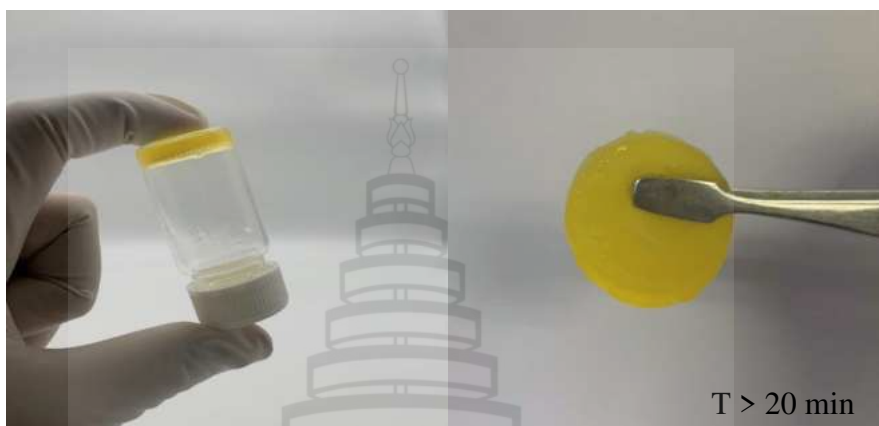


**Figure 6.1** The Indirect Cytotoxicity of Raw Materials Cultured with (A) HDFa, (B) MDA-MB-231, and (C) MDA-MB-436 Cells for 24 h

### 6.2.2 Gel Formation of Injectable Thermosensitive Hydrogels

Injectable thermosensitive hydrogels are extensively used in controlled drug delivery systems. The ability to inject them as liquids should allow them to gel at the target site after ensuring they do not premature gelling in the delivery device or body. Figure 6.2 shows the selected photographs of the gel derived from the injectable thermosensitive hydrogel formulation loaded with siRNA nanoparticles at 37 °C after 20 min. The combination of CS, SS, and  $\beta$ -GP can form a thermosensitive hydrogel through synergistic hydrophobic interaction and chemical crosslinking between the components. The amino groups on CS are protonated at low pH (acidic conditions), which makes them positively charged and able to react with negatively charged molecules of  $\beta$ -GP through electrostatic interactions. This leads to the formation of ionic crosslinking between CS, promoting gelation. Moreover, the chemical

crosslinking between  $\beta$ -GP can also act as a crosslinking agent, reacting with hydroxyl or amino groups on CS to form covalent bonds that enhance the mechanical stability of the hydrogels (Pankongadisak & Suwantong, 2018; Chenite et al., 2000; Cho et al., 2005).



**Figure 6.2** Photographs of Injectable Thermosensitive Hydrogel Loaded with siRNA Nanoparticles at 37 °C

### 6.2.3 Gelation Time and Gel Fraction

The injectable thermosensitive SS/CS hydrogels were formed through gelation mechanisms involving electrostatic and hydrophobic interactions between CS and  $\beta$ -GP. The gelation time of the thermosensitive hydrogels prepared using different volume ratios between CS and  $\beta$ -GP is shown in Table 6.3. The gelation time for 0.2H, 0.2HS, 0.5H, and 0.5HS was 960 min. In contrast, the gelation time for 0.8H and 1.0H was 25 min and 20 min, respectively. Furthermore, the addition of siRNA nanoparticles into the thermosensitive hydrogels increased the gelation time of the hydrogels, particularly for 0.8HS and 1.0HS. The results indicated that an increased volume ratio of  $\beta$ -GP solution decreased the gelation time. This is because a higher  $\beta$ -GP amount increases the release of phosphate ions ( $\text{PO}_4^{3-}$ ) during hydrolysis. Consequently, this leads to an increased ionic crosslinking density between the amino groups of CS molecules, resulting in stronger ionic interactions and a faster gelation time for the hydrogel. Furthermore, the interaction between SS and CS leads to stronger and more extensive crosslinking within the hydrogel matrix, enhancing its stability. Pankongadisak and Suwantong reported that incorporating SS molecules into the CS solution increased the

attractive forces between neighboring macromolecular chains, thereby reducing the gelation time (Pankongadisak & Suwantong, 2018).

The gel fraction is directly related to the degree of crosslinking within the hydrogel. A higher gel fraction signifies a more extensively crosslinked network, which enhances the mechanical stability and resistance to degradation of the hydrogels. The 0.2H, 0.2HS, 0.5H, and 0.5HS formed the hydrogels after 960 min. This delayed that the hydrogel formation may be attributed to an improper ratio of CS, SS, and  $\beta$ -GP, which likely resulted in slower gelation. An imbalance in these components may hinder the optimal crosslinking process, leading to the extended time required for hydrogel formation. Consequently, these 0.2H, 0.2HS, 0.5H, and 0.5HS hydrogels were not selected for the gel fraction study. From Table 6.3, the gel fractions of 0.8H, 0.8HS, 1.0H, and 1.0HS were  $80.35 \pm 2.73$ ,  $82.55 \pm 0.44$ ,  $81.60 \pm 0.86$ , and  $79.70 \pm 0.80$ , respectively. The values were relatively consistent across all samples, showing only slight variations between hydrogels with and without siRNA nanoparticles. The gel fraction, representing the proportion of polymer crosslinked into the network, was consistently high (around 80%). This indicates efficient crosslinking and successful network formation, resulting in stable hydrogels with minimal sol content. These high gel fractions are desirable for injectable hydrogel systems, signifying robust structural integrity, reduced leaching of unreacted components, and enhanced retention of encapsulated agents such as siRNA nanoparticles.

**Table 6.3** Preparation Parameters and Gelation Time of the Injectable Thermosensitive Hydrogels Loaded with siRNA Nanoparticles

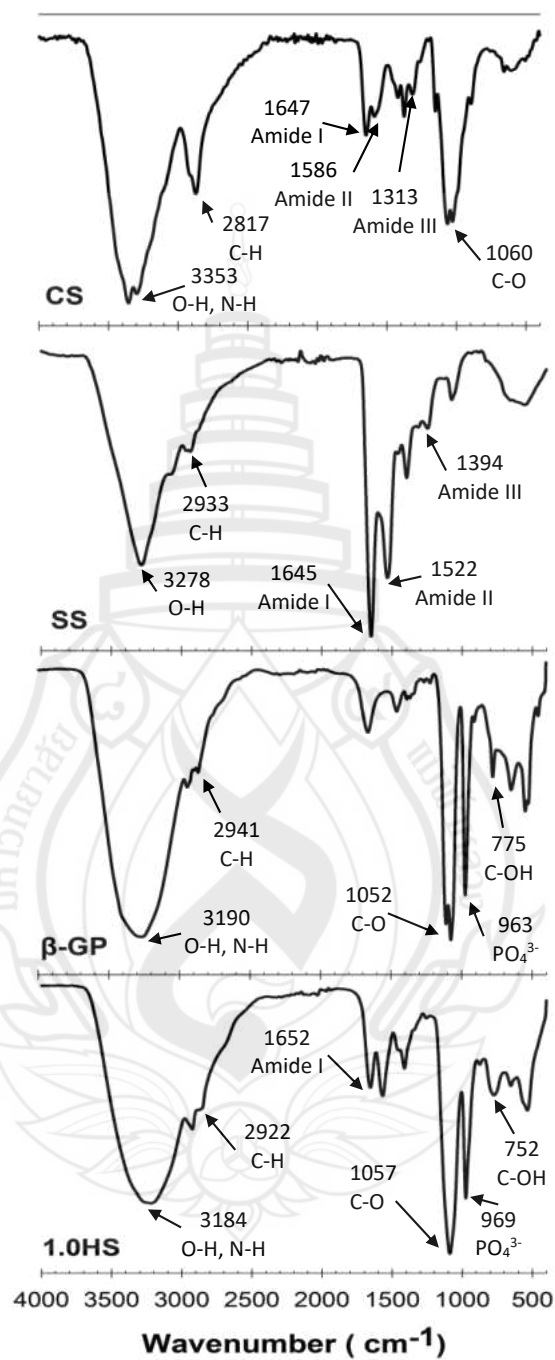
Code	CS (%w/v)	SS (%w/v)	CS : SS (mL:mL)	CS : 50% w/v β-GP (mL:mL)	siRNA nanoparticles at 80 nM (μL)	Gelation time at 37 °C (min)	Gel fraction (%)
0.2H	3	7	1:0.5	1:0.2	0	960	-
0.2HS	3	7	1:0.5	1:0.2	100	960	-
0.5H	3	7	1:0.5	1:0.5	0	960	-
0.5HS	3	7	1:0.5	1:0.5	100	960	-
0.8H	3	7	1:0.5	1:0.8	0	25	80.35±2.73
0.8HS	3	7	1:0.5	1:0.8	100	29	82.55±0.44
1.0H	3	7	1:0.5	1:1	0	20	81.60±0.86
1.0HS	3	7	1:0.5	1:1	100	23	79.70±0.80

#### 6.2.4 FTIR Analysis

FTIR was used to identify the chemical structure and functional groups of CS, SS,  $\beta$ -GP, and 1.0HS, as shown in Figure 6.3. The FTIR spectrum of CS typically showed several significant peaks, representing different functional groups in the structure. A broad peak around  $3353\text{ cm}^{-1}$  indicates N-H stretching of primary amines and O-H stretching. The peak at  $2817\text{ cm}^{-1}$  represents C-H stretching, which arises from the methyl and methylene groups in the CS backbone. The C=O stretching vibration at  $1647\text{ cm}^{-1}$  is linked to amide I, while a peak at  $1586\text{ cm}^{-1}$  corresponds to N-H stretching due to amide II. The peak at  $1313\text{ cm}^{-1}$  is assigned to C-N stretching vibrations in amide III (Drabczyk et al., 2020). For the FTIR spectrum of SS, the broad peak at  $3278\text{ cm}^{-1}$  represents the N-H stretching vibrations of amide groups and the O-H stretching vibrations of hydroxyl groups in SS. A peak at  $2933\text{ cm}^{-1}$  represents the stretching of C-H bonds in the side chains of amino acids, especially those with methyl or methylene groups. The C=O stretching (amide I) at  $1645\text{ cm}^{-1}$  is related to the carbonyl group in the protein backbone. The N-H bending vibration (amide II) appears at  $1522\text{ cm}^{-1}$ , resulting from the bending of the N-H bond in proteins. A peak at  $1394\text{ cm}^{-1}$  represents the C-N stretching vibration (amide III), which is associated with N-H vibrations in the protein backbone. These peaks identify the functional groups and structure of SS, mainly when it contains proteins or amino acids (Baptista-Silva et al., 2021; Al Masud et al., 2021; Radu et al., 2021). The FTIR spectrum of  $\beta$ -GP showed the O-H stretching peak at  $3190\text{ cm}^{-1}$ , indicating the presence of hydroxyl groups. The C-H stretching peak at  $2941\text{ cm}^{-1}$  corresponds to the aliphatic backbone of  $\beta$ -GP. The C-O stretching peak at  $1052\text{ cm}^{-1}$  reflects the ether and alcohol functional groups in  $\beta$ -GP. The peaks at  $963$  and  $775\text{ cm}^{-1}$  indicate bonding within the phosphate group, specifically the asymmetric and symmetric stretching vibrations of  $\text{PO}_4^{3-}$  (Yao et al., 2025; Ke et al., 2020). The FTIR spectrum of 1.0HS exhibited peaks in the range of  $3600\text{--}3000\text{ cm}^{-1}$ , corresponding to O-H stretching. The peaks at  $752\text{ cm}^{-1}$  and  $969\text{ cm}^{-1}$  were observed, attributing to the inorganic phase of  $\text{PO}_4^{3-}$  groups. After gel formation, the peaks associated with N-H and O-H stretching in CS were shifted, suggesting interactions between the N-H groups in CS and the O-H groups in  $\beta$ -GP, or potentially hydrogen bonding between the

C=O groups in CS and the O–H groups in  $\beta$ -GP. Moreover, the amide I, II, and III peaks in CS and SS decreased, indicating the formation of hydrogen bonds and chemical complexes between the amino groups in CS or SS and the OH and  $\text{PO}_4^{3-}$  groups in  $\beta$ -GP. A decrease in the C-CH<sub>3</sub> symmetric deformation peak further supported the formation of hydrogen bonds. These findings suggest that hydrogen bonding and electrostatic interactions play a significant role in the interaction between CS and  $\beta$ -GP (Srihanam et al., 2009; Pankongadisak & Suwantong, 2018).



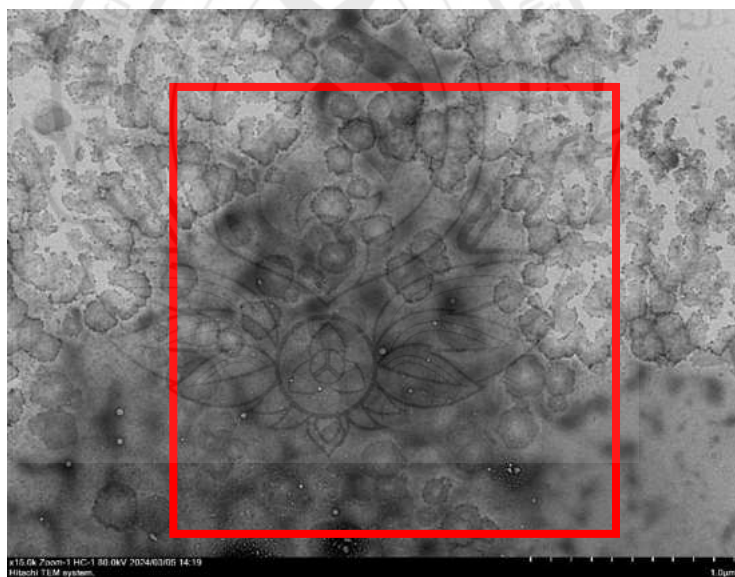


**Figure 6.3** ATR-FTIR Spectra of CS, SS,  $\beta$ -GP, and 1.0HS



### 6.2.5 Morphology of siRNA Nanoparticles Loaded in Hydrogel

The formation of siRNA nanoparticles loaded in the hydrogel was characterized by TEM measurement to confirm the ability of the Prime-Fect and Trans-Booster to complex with siRNA. The siRNA nanoparticles were prepared using siRNA:Trans-Booster:Prime-Fect ratio of 1:1:10. The results showed that the shape of siRNA nanoparticles loaded in the hydrogel was spherical with an average particle size of  $182 \pm 24$  nm, as shown in Figure 6.4. This analysis provides valuable insight into the characteristics of the nanoparticles, which are crucial for understanding their behavior and performance in the hydrogel system. The results confirmed that siRNA nanoparticles were successfully formed and loaded into the hydrogel. According to Santadkha et al., siRNA nanoparticles were prepared using Prime-Fect:siRNA ratios of 1:5 and 1:10, both with and without the additive, and the resulting particles were similar. The complexes without additives had more heterogeneous structures, featuring smaller individual particles and some aggregation. However, in the presence of the Trans-Booster, the particles became more uniform in size and shape, showing individual spherical particles without agglomeration (Santadkha et al., 2022).

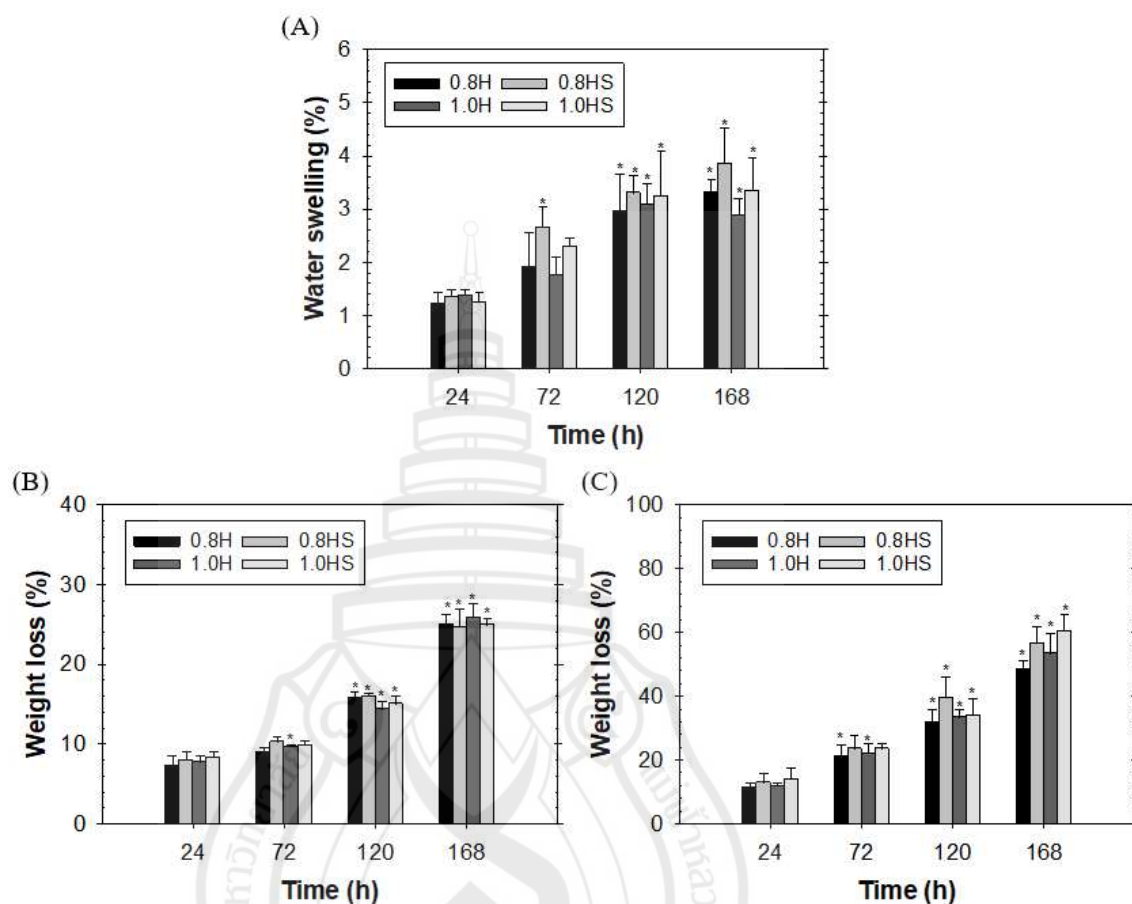


**Figure 6.4** TEM Images of siRNA Nanoparticles Loaded in the Hydrogel at 15.0k Magnification 15.0k and at 80.0 kV

### 6.2.6 Water Swelling and Weight Loss

The water swelling of a hydrogel describes its capacity to absorb and retain water when placed in a moist or aqueous environment, such as exudate. This is a crucial property of hydrogels, contributing to their utility in various applications within medicine and pharmacy, including controlled drug delivery, wound care, and tissue repair. Consequently, water swelling was investigated, and the results are presented in Figure 6.5A. The results showed that the hydrogels exhibited water absorption and swelling throughout the 24 to 168 h testing period. Notably, the water swelling of the hydrogels prepared under all conditions remained below 5%. The results suggested that the incorporation of  $\beta$ -GP increased the phosphate groups and facilitated the formation of ionic crosslinks within the amino groups of the CS network. This stability enhancement in the hydrogels consequently reduced their water absorption and swelling capacity.

Weight loss typically indicates the breakdown or degradation of a material, often over time. This measurement is used to evaluate the material's stability, integrity, and performance under specific conditions. From Figures 6.5B and 6.5C, the weight loss of all hydrogels increased with submersion time over 7 days, both in medium with and without lysozyme. Notably, the hydrogels immersed in the absence of lysozyme exhibited lower weight loss values than those immersed in lysozyme. The *in vitro* degradation test employs lysozyme to hydrolyze  $\beta$ -1,4-glycosidic bonds in materials such as CS, thereby mimicking natural enzymatic degradation within the body and resulting in accelerated and more specific material breakdown. In contrast to enzymatic tests, a control using PBS maintains pH stability without inducing enzymatic action, leading to slower, primarily physical changes and minimal chemical breakdown of the material (Kean & Thanou, 2010; Loncarevic et al., 2017; Maiz-Fernández et al., 2020).

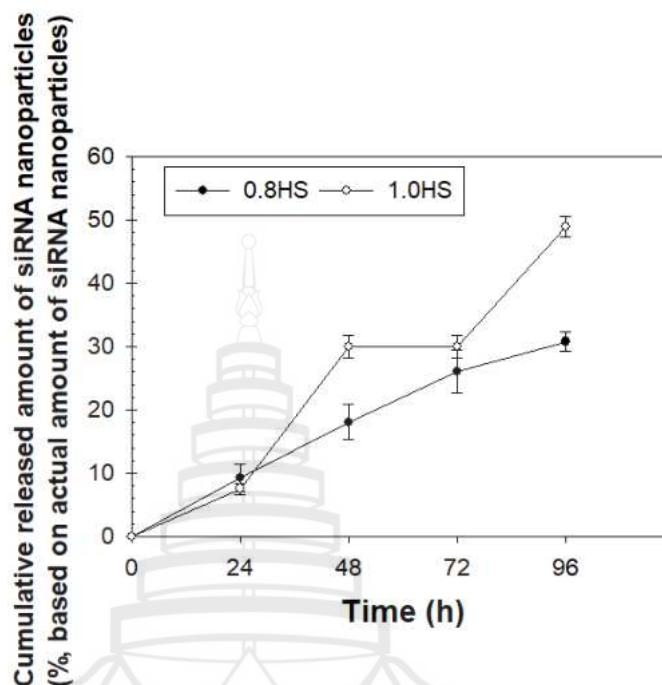


**Figure 6.5** (A) Water Swelling, (B) Weight Loss in PBS, and (C) Weight Loss in PBS containing Lysozyme of the Injectable Thermosensitive Hydrogels. \* $p < 0.05$  Compared with The Values at 24 h. # $p < 0.05$  Compared 0.8H with 0.8HS and 1.0H with 1.0HS at Each Time Point

### 6.2.7 Released Profiles

The drug content of the 0.8HS and 1.0HS formulations was  $62.01 \pm 1.53\%$  and  $77.21 \pm 1.04\%$ , respectively, indicating efficient siRNA nanoparticles encapsulation in both formulations. The high drug content is advantageous for maintaining therapeutic siRNA levels at the target site, thereby promoting sustained release and prolonged gene silencing effects. These results support the suitability of these hydrogels for controlled siRNA delivery in cancer treatment, where consistent and prolonged siRNA exposure is essential for therapeutic efficacy.

The release profiles of injectable thermosensitive hydrogels are shown in Figure 6.6. The released amount of siRNA nanoparticles increased steadily over time, demonstrating controlled and sustained release. This gradual release is important for prolonged therapeutic effects, enabling extended gene silencing or targeted delivery. The sustained release results from the hydrogel's temperature-responsive properties, which form a network controlling siRNA diffusion. This thermosensitive behavior allows easy injection as a liquid, followed by in situ gelation that localizes and retains siRNA at the target site. Such controlled release benefits cancer therapies like breast cancer by maintaining effective siRNA levels at the tumor, ensuring ongoing suppression of oncogenes or cancer pathways. This reduces dosing frequency, minimizes side effects, and improves precision. Moreover, this type of release reduces the need for frequent repeated dosing, lowers potential side effects caused by sudden large doses, and enhances treatment accuracy by targeting the delivery directly to the desired site. Prolonged siRNA availability near cancer cells may also enhance uptake and gene silencing, resulting in improved outcomes.



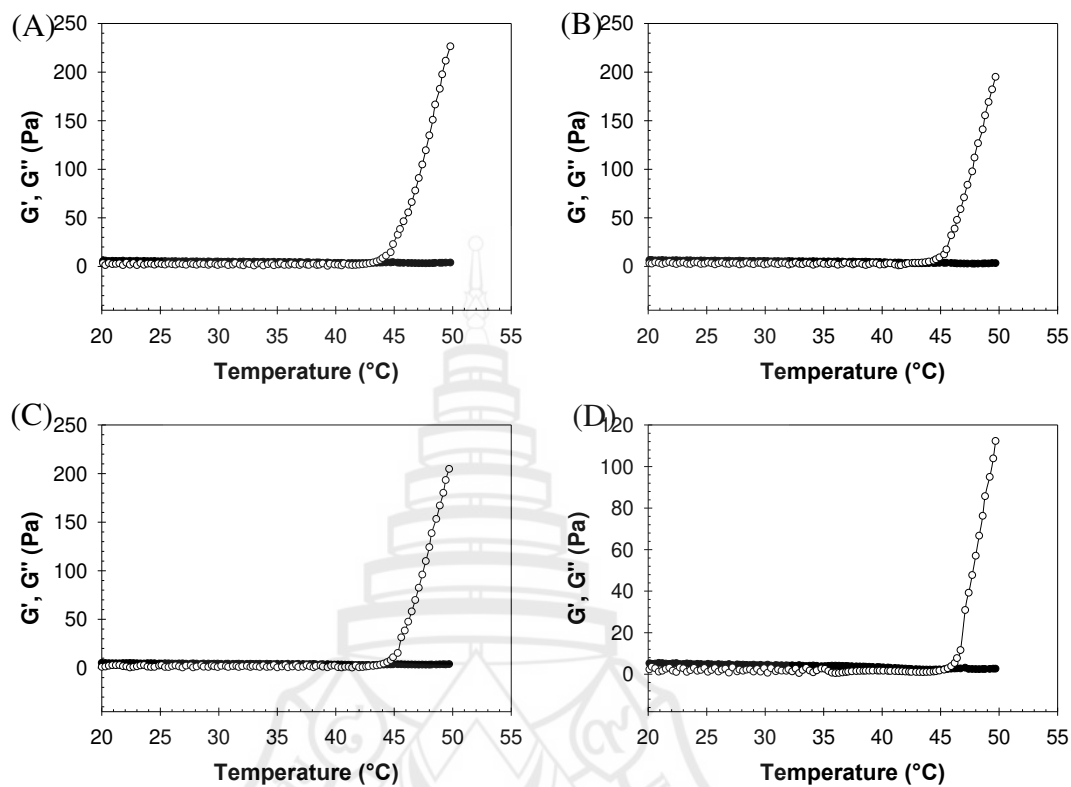
**Figure 6.6** Released Study of siRNA Nanoparticles-Loaded Thermosensitive Hydrogels

### 6.2.8 Rheological Properties

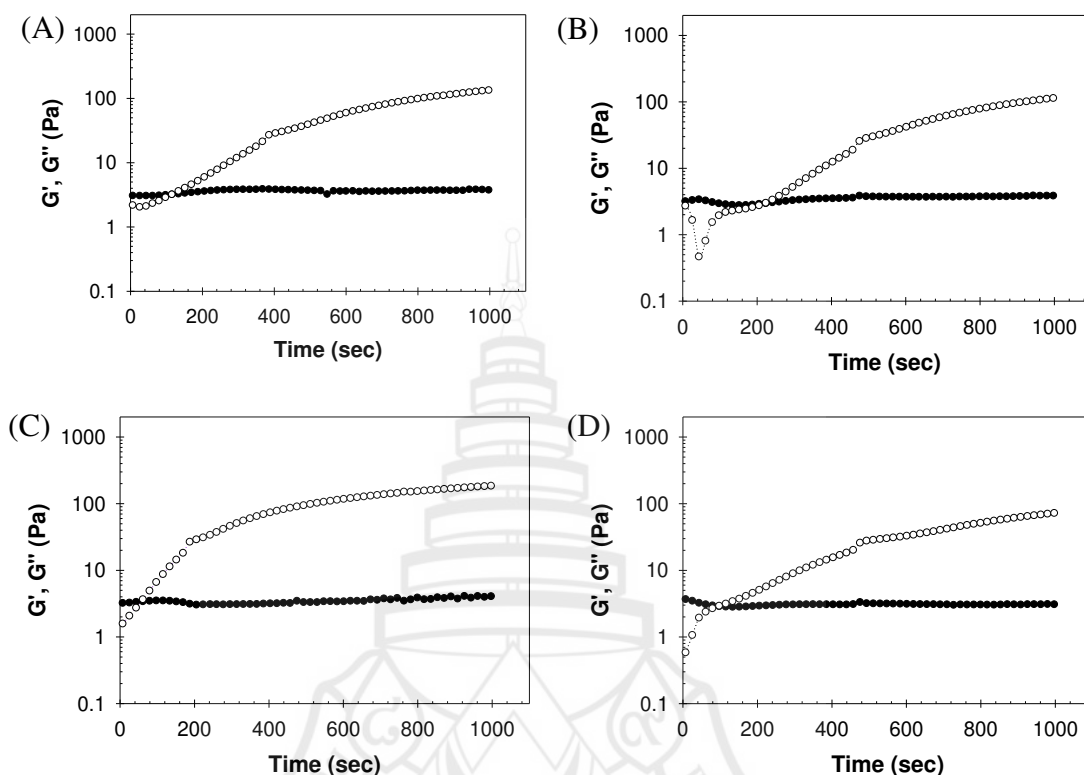
The rheological properties are essential for understanding the flow and deformation behaviors of materials, which is crucial for designing hydrogels that can perform optimally in drug delivery systems. Initially, the hydrogel solution exhibited  $G'$  lower than  $G''$ , indicating solution-like behavior. However, as the temperature increased above the critical gelation temperature, a greater portion of the solution transitioned into a gel. The critical gelation temperature of a hydrogel is the temperature at which it transforms into a gel state. For thermosensitive hydrogels, this temperature is a key factor in determining the timing of the sol-gel transition. The effect of hydrogel gelation temperature on  $G'$  and  $G''$  was determined using a rotational rheometer, as shown in Figure 6.7. The critical gelation temperatures for 0.8H, 0.8HS, 1.0H, and 1.0HS were 43, 43, 44, and 46 °C, respectively. The increase in  $G'$  relative to  $G''$  after the gelling point clearly indicated the formation and strengthening of the gel network, leading to increased elasticity and gel strength (Chenite et al., 2000). At 50 °C, beyond the gelling point,  $G'$  values for 0.8H, 0.8HS, 1.0H, and

1.0HS were 226, 195, 204, and 112 Pa, respectively. Notably, 0.8H and 1.0H exhibited higher  $G'$  than 0.8HS and 1.0HS. The incorporation of siRNA nanoparticles into the hydrogels resulted in a decrease in their mechanical strength. This change in mechanical properties can be attributed to electrostatic interactions between the negatively charged siRNA nanoparticles and the positively charged CS chains. These interactions may interfere with the crosslinking network of the hydrogels, thereby reducing structural integrity and altering mechanical behavior. In addition, increasing the  $\beta$ -GP ratio from 0.8 to 1.0 resulted in a slight decrease in  $G'$  value. This result suggested that at a  $\beta$ -GP ratio of 0.8, the hydrogel network had already achieved an optimal level of crosslinking, yielding maximum elastic moduli. While increasing the  $\beta$ -GP ratio to 1.0 made the network slightly denser, this additional crosslinking did not significantly affect the elastic moduli of the hydrogels. Therefore, the network is sufficiently crosslinked, and further addition of  $\beta$ -GP does not lead to improvements in the mechanical properties of the hydrogels.

The gelation time of a hydrogel is the time required for it to transition from a liquid to a gel. This transition results in the formation of a gel network structure, occurring when  $G'$  of the hydrogel exceeds its  $G''$ , as illustrated in Figure 6.8. The gelation times of 0.8H, 0.8HS, 1.0H, and 1.0HS at 37 °C were 133, 223, 61, and 97 s, respectively. A higher concentration of  $\beta$ -GP resulted in a shorter gelation time. This is because the addition of  $\beta$ -GP to the hydrogels increased the availability of phosphate ions for crosslinking with the amino groups in CS, leading to stronger ionic interactions that facilitated hydrogel network formation. Furthermore, the results showed that hydrogels containing siRNA nanoparticles exhibited longer gelation times compared to those without them. This suggests that siRNA nanoparticles may have interfered with crosslinking by altering the interaction between the CS chains and phosphate ions from  $\beta$ -GP. Consequently, the hydrogel network formation was delayed, possibly due to the disruption of the expected ionic interactions.



**Figure 6.7** Typical Temperature Dependence of ( $\circ$ )  $G'$  and ( $\bullet$ )  $G''$  Values of (A) 0.8H, (B) 0.8HS, (C) 1.0H, and (D) 1.0HS



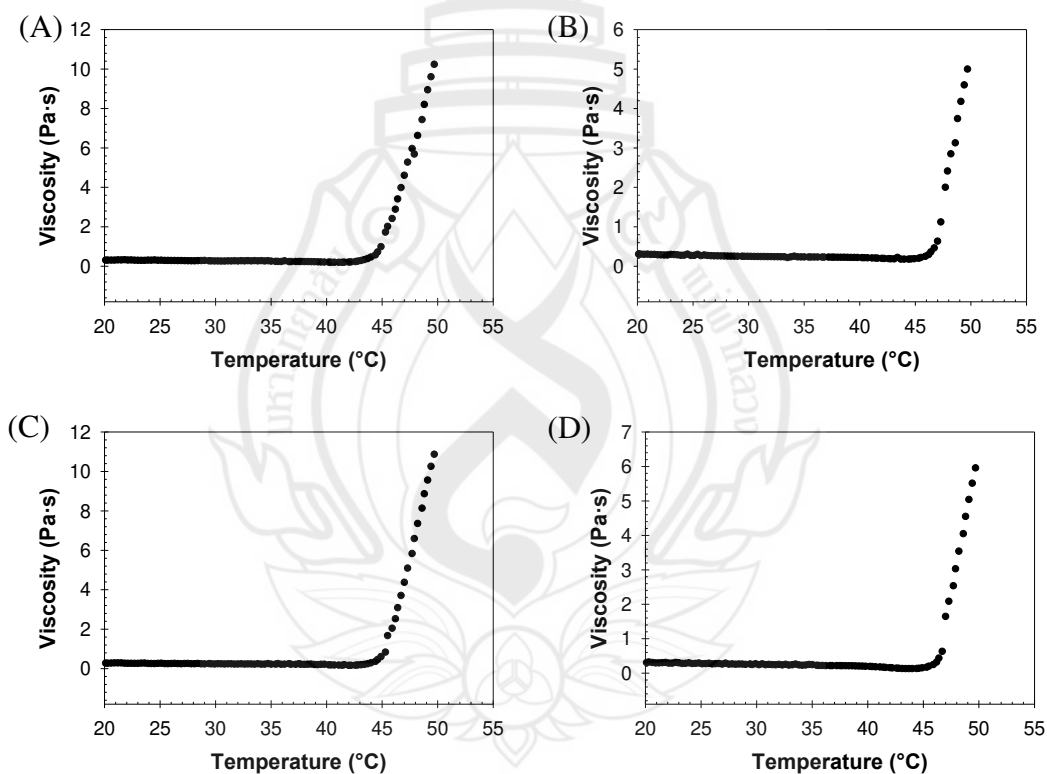
**Figure 6.8** Rheology Curves of ( $\circ$ )  $G'$  and ( $\bullet$ )  $G''$  Values of (A) 0.8H, (B) 0.8HS, (C) 1.0H, and (D) 1.0HS

### 6.2.9 Viscosity Measurements

Injectable thermosensitive hydrogels hold significant potential for drug delivery applications. However, these hydrogels must possess sufficient strength to form stable gels for their intended uses. To assess the sol-gel transition behavior, the viscous modulus of the thermosensitive hydrogels was measured at various temperatures, as shown in Figure 6.9. The maximum viscosity values for 0.8H, 0.8HS, 1.0H, and 1.0HS were 10.24, 5.00, 10.87, and 5.96 Pa·s, respectively. Increasing the CS to  $\beta$ -GP ratio from 1:0.8 to 1:1 did not result in a significant change in viscosity. This suggests that the added  $\beta$ -GP did not substantially alter the crosslinking density or structural integrity of the hydrogels. At the higher  $\beta$ -GP ratio, the crosslinking effect may have reached a saturation point, where further increases in  $\beta$ -GP content do not produce a noticeable improvement in the



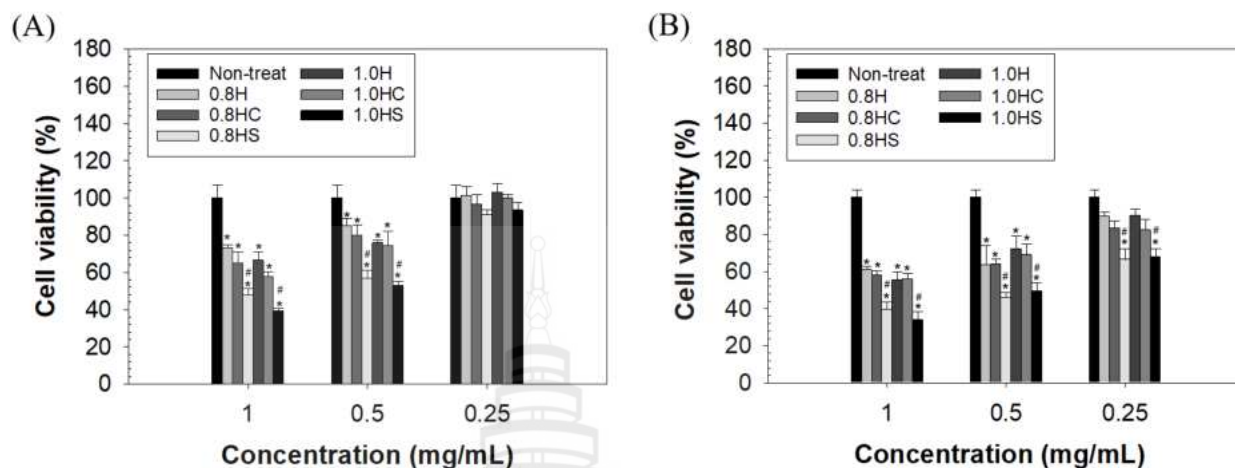
mechanical properties of the hydrogels. Furthermore, the addition of siRNA nanoparticles to the hydrogels led to a decrease in viscosity. This could be attributed to electrostatic interactions between the negatively charged siRNA nanoparticles and the positively charged CS chains. These interactions may have disrupted the network structure that typically supports gel formation, thus preventing the expected enhancement of the mechanical properties of the hydrogels. The interaction between siRNA and CS chains may have resulted in a less stable or more disordered hydrogel network, rather than enhancing the gel structure or facilitating crosslinking. Consequently, the viscosity of 0.8HS and 1.0HS was diminished compared to that of 0.8H and 1.0H.



**Figure 6.9** Solution Viscosity of (A) 0.8H, (B) 0.8HS, (C) 1.0H, and (D) 1.0HS as a Function of Temperature

### 6.2.10 *In Vitro* Evaluation of Cell Growth Inhibition by Injectable Thermosensitive Hydrogels

The siRNA nanoparticles were used to reduce the growth of breast cancer cells by silencing targeted genes involved in cell survival. The inhibitory effects of the injectable thermosensitive hydrogels on breast cancer cell growth were evaluated using MTT assays against MDA-MB-231 and MDA-MB-436 cells over 72 h. Figure 6.10 shows the cell viability of cells cultured with the extraction media from the thermosensitive hydrogels. At an extraction medium concentration of 1 mg/mL, the viability of MDA-MB-231 cells cultured with 0.8H, 0.8HC, 0.8HS, 1.0H, 1.0HC, and 1.0HS was  $73.1 \pm 1.9\%$ ,  $64.9 \pm 6.2\%$ ,  $47.8 \pm 3.6\%$ ,  $66.5 \pm 4.3\%$ ,  $57.6 \pm 2.6\%$ , and  $39.1 \pm 1.5\%$ , respectively. While the viability of MDA-MB-436 cells cultured with 0.8H, 0.8HC, 0.8HS, 1.0H, 1.0HC, and 1.0HS was  $60.9 \pm 2.1\%$ ,  $58.0 \pm 2.4\%$ ,  $39.4 \pm 4.1\%$ ,  $55.5 \pm 4.4\%$ ,  $55.8 \pm 3.3\%$ , and  $33.8 \pm 4.5\%$ , respectively. According to the ISO 10993-5 standard, cell viability below 70% indicates a cytotoxic effect on cells. The hydrogels containing siRNA nanoparticles exhibited significantly higher cytotoxicity levels than those containing CsiRNA and the non-treatment groups after 72 h of treatment. Santadkha et al. investigated the influence of siRNA nanoparticles on cell viability in the treatment of breast cancer cells. After treatment with siRNA nanoparticles at a siRNA:Trans-Booster:Prime-Fect weight ratio of 1:1:10, the cell viability of the survivin nanoparticles was reduced to less than 50% (Santadkha et al., 2022). It was found that siRNA nanoparticles effectively killed breast cancer cells by targeting and silencing specific genes involved in their survival. The hydrogel without siRNA nanoparticles also showed a reduction in the growth of breast cancer cells. When these siRNA nanoparticles are loaded into a hydrogel, the hydrogel provides stability and controlled release, improving the delivery and effectiveness of the treatment for localized cancer therapy.

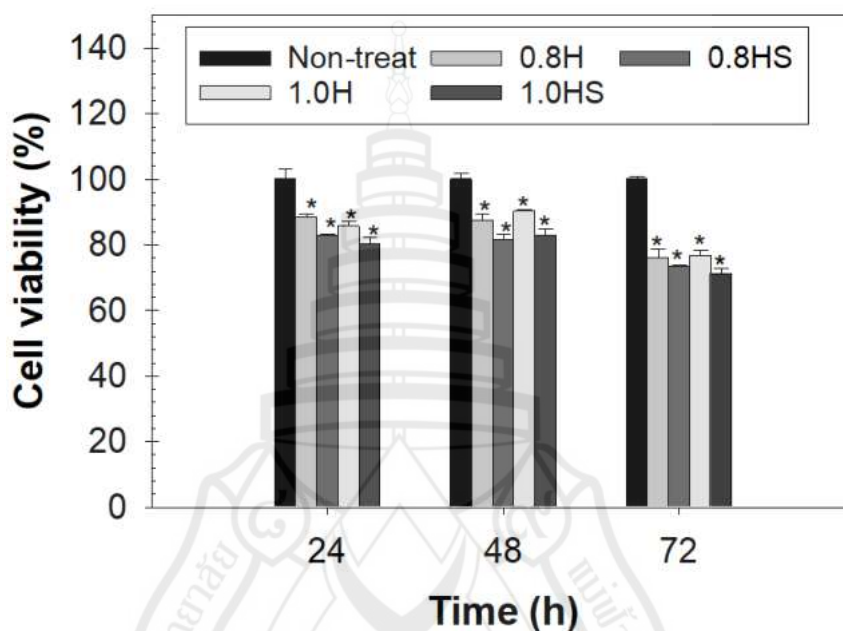


**Figure 6.10** Indirect Cytotoxicity of Extraction Media from Hydrogels Cultured with (A) MDA-MB-231 and (B) MDA-MB-436 Cells for 72 h (n = 3). \* $p < 0.05$  Compared with the Non-Treatment at Each Concentration. # $p < 0.05$  Compared 0.8HC with 0.8HS and 1.0HC with 1.0HS at Each Concentration

### 6.2.11 Biocompatibility of Injectable Thermosensitive Hydrogels

For breast cancer treatment, materials must be biocompatible, non-toxic, and supportive of normal cell growth. In this study, injectable thermosensitive hydrogels were evaluated for their compatibility with HDFa cells. Cell viability assay was used to determine any adverse effects of the hydrogels on cell survival. These results help confirm that the hydrogels are not only effective in delivering treatment but also safe for healthy cells, thus making them suitable for therapeutic use. As shown in Figure 6.11, the hydrogel samples at a concentration of 0.5 mg/mL exhibited no cytotoxic effects on HDFa cells after 24, 48, and 72 h. Cell viability remained consistently high throughout the testing period, indicating that the hydrogels are biocompatible and do not interfere with normal cell growth or function. According to ISO 10993-5 standards, materials are considered non-cytotoxic if cell viability remains above 70%. In this study, all values exceeded this threshold, further supporting the safety of the hydrogels. These findings are significant for breast cancer treatment, where delivery systems must be safe for healthy cells while

effectively targeting cancer cells. Therefore, at this concentration, the hydrogels are suitable for therapeutic applications, providing a safe platform that can be integrated into treatment strategies without harming surrounding normal tissue.



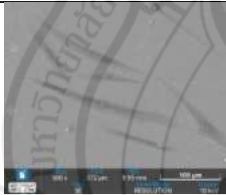
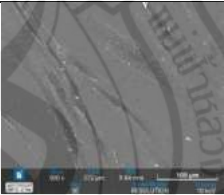
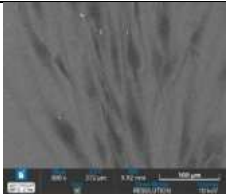




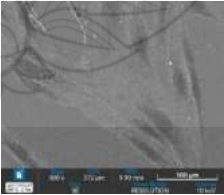
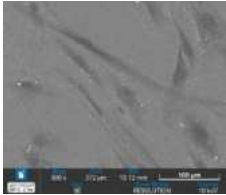
**Figure 6.11** Biocompatibility of Thermosensitive Hydrogels (n=3). \* $p < 0.05$  Compared with the Non-Treated Group at Each Time Point

### 6.2.12 Cell Morphology of Injectable Thermosensitive Hydrogels

The morphological effects of siRNA nanoparticle-loaded injectable thermosensitive hydrogels on HDFa cells were investigated using FE-SEM. This advanced imaging method allowed for detailed observation of cell surface modifications, enabling a direct comparison between treated and untreated cells to identify any resulting morphological changes. The morphology of HDFa cells cultured with 0.8HS and 1.0HS was observed using FE-SEM, as shown in Table 6.4. The morphological analysis of HDFa cells using FE-SEM revealed that cells treated with 0.8HS and 1.0HS maintained a normal spindle-shaped structure and adhered well to the cover glass, comparable to the untreated control group. Both hydrogel formulations supported normal cell morphology and

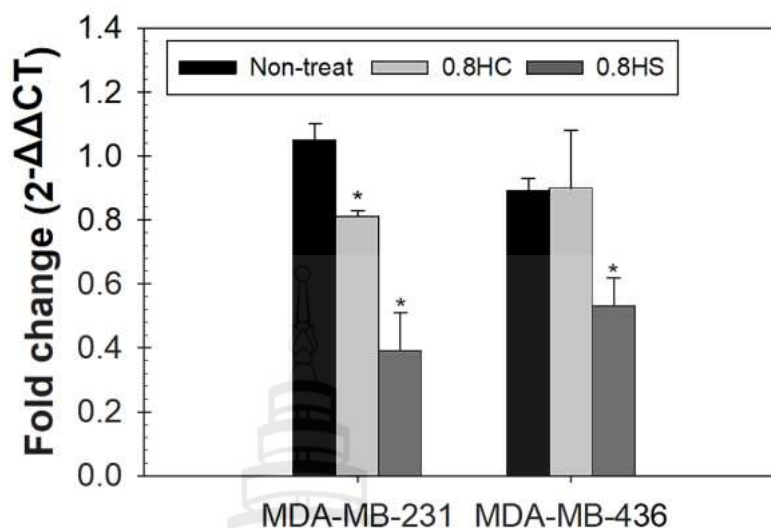
attachment, key indicators of biocompatibility. The absence of observable cytotoxicity or morphological abnormalities suggests that the hydrogels do not compromise cellular integrity or function. This observation corroborates the MTT assay results, further substantiating the non-toxic nature of the hydrogels at the tested concentration. Preserving normal fibroblast morphology is particularly significant in therapeutic applications, as it demonstrates the material's capacity to maintain healthy tissue structure during treatment. In breast cancer therapy, where delivery systems must selectively target malignant cells while preserving healthy ones, such biocompatibility is paramount. The capacity of these thermosensitive hydrogels to support healthy cell behavior underscores their potential as safe and effective vehicles for siRNA nanoparticle-based therapies.

**Table 6.4** Morphology of HDFa Cells Cultured with Extraction Media of Hydrogels Loaded with siRNA Nanoparticles

Condition	Time points (h)		
	24	48	72
Non-treated			
0.8HS			
1.0HS			

### **6.2.13 RT-qPCR for Gene Silencing of siRNA Nanoparticles Loaded in Hydrogel**

To investigate the impact of siRNA nanoparticles loaded in a thermoresponsive hydrogel on gene expression, MDA-MB-231 and MDA-MB-436 cells were incubated for 72 h. Gene expression efficiency was analyzed using RT-qPCR (Figure 6.12). The RT-qPCR analysis of gene silencing in MDA-MB-231 cells revealed significant differences in gene expression across treatments. The non-treated group exhibited a baseline expression level of 1.05, indicating no treatment effect. The 1.0HC group, which contained control siRNA nanoparticles, showed a moderate reduction in expression to 0.81, suggesting a slight silencing effect. In contrast, the 1.0HS group, which contained siRNA nanoparticles, demonstrated a more significant reduction in gene expression to 0.39, indicating higher silencing efficiency. These results suggest a greater efficacy of the 1.0HS in delivering siRNA nanoparticles and silencing gene expression compared to the 1.0HC. This trend was consistent in MDA-MB-436 cells. Specifically, the non-treated group in these cells showed a survivin expression level of 0.89, confirming the absence of gene silencing. Similarly, the 1.0HC group displayed a survivin expression level of 0.90, also indicating no silencing effect. In contrast, the 1.0HS group exhibited a reduction in survivin expression to 0.53, demonstrating the thermosensitive hydrogel's effectiveness in silencing the survivin gene within MDA-MB-436 cells. These results highlight the significant role thermosensitive hydrogels could play in improving the delivery and silencing effectiveness of siRNA nanoparticles, hinting at their potential utility in treating cancer.



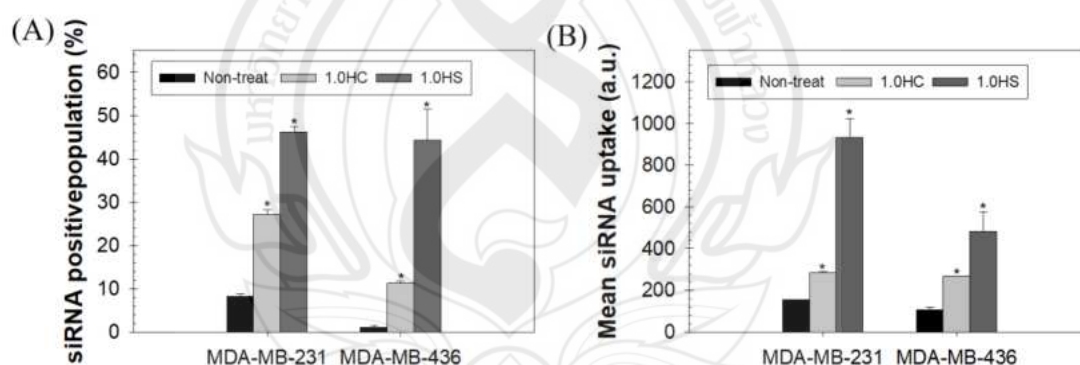
**Figure 6.12** Relative Fold Change of CsiRNA and siSVV Nanoparticles Loaded in Hydrogel Cultured with MDA-MB-231 and MDA-MB-436 Cells by RT-qPCR After Transfection for 72 h

#### 6.2.14 Cellular Uptake Study by Flow Cytometry

Cell uptake was assessed by flow cytometry after incubating cells with FAM-siRNA nanoparticles loaded in hydrogels. Fluorescence intensity was then measured to quantify the uptake (Peng et al., 2019). The siRNA positive population (%) represents the percentage of cells that internalized FAM-siRNA nanoparticles, determined by fluorescence signals within the cells. This indicates the proportion of cells that took up siRNA relative to the total population. Meanwhile, mean siRNA uptake (a.u.) reflects the average amount of siRNA internalized by the cells, based on fluorescence intensity. The analysis of the siRNA-positive population in the non-treated, 1.0HC, and 1.0HS groups is shown in Figure 6.13A. In MDA-MB-231 and MDA-MB-436 cells, the untreated control groups exhibited the lowest percentages of siRNA-positive cells, at 8.27% and 1.10%, respectively. This indicates minimal spontaneous siRNA uptake. However, treatment with 1.0HC increased the siRNA-positive cell population to 27.13% in MDA-MB-231 cells and 11.27% in MDA-MB-436 cells. This observed increase could be partially attributed to the hydrogel's own internalization, which might generate fluorescence signals that overlap with those from FAM-siRNA. Such overlap could potentially lead to an overestimation of siRNA uptake. In contrast, treatment with



1.0% HS resulted in 46.10% siRNA-positive cells in MDA-MB-231 and 44.27% in MDA-MB-436 cells. These findings confirm that the hydrogels do not impede the release of siRNA nanoparticles, suggesting that incorporating siRNA nanoparticles into thermosensitive hydrogels enhances siRNA internalization and protects the nanoparticles from degradation. Figure 6.13B illustrates the mean siRNA uptake in the non-treated, 1.0HC, and 1.0HS groups. Minimal siRNA uptake was observed in non-treated MDA-MB-231 and MDA-MB-436 cells, with values of 153 a.u. and 105 a.u., respectively. Treatment with 1.0HC led to an increase in uptake to 283.16 a.u. in MDA-MB-231 cells and 266.33 a.u. in MDA-MB-436 cells. However, it's important to note that this increase could be attributed to fluorescence originating from the hydrogel's interaction with the cells. In contrast, treatment with 1.0HS resulted in a significant increase in siRNA uptake, reaching 932.33 a.u. in MDA-MB-231 cells and 481.67 a.u. in MDA-MB-436 cells. These results demonstrate enhanced siRNA delivery by the hydrogel formulations. The higher uptake observed in both cell types treated with 1.0HS suggests improved siRNA internalization, likely due to the hydrogel's protective properties against nanoparticle degradation.



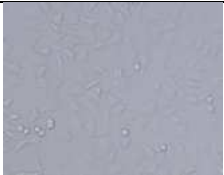

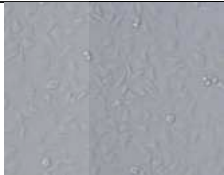
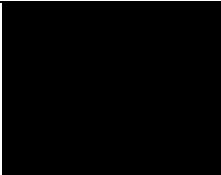

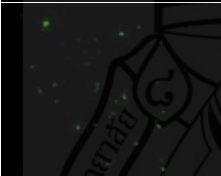

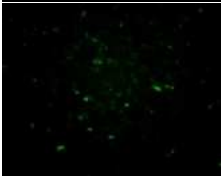



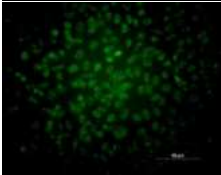

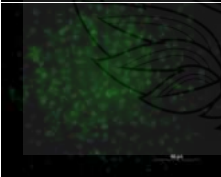

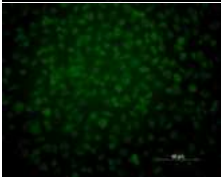
**Figure 6.13** Cell Uptake of siRNA Nanoparticles Loaded in Hydrogel. (A) Percentage of FAM-Labeled siRNA Positive Cell Population and (B) Mean Fluorescence Intensity of FAM-Labeled siRNA Nanoparticles After 72 h Treatment



### 6.2.15 Fluorescence Microscopy Analysis

Fluorescence microscopy was used to visualize and track the distribution and delivery of siRNA nanoparticles loaded in thermosensitive hydrogels to breast cancer cells. The cellular uptake of FAM-siRNA nanoparticles and FAM-siRNA nanoparticles loaded in the thermosensitive hydrogels was confirmed using fluorescence cell imaging, as shown in Table 6.5. To confirm cell uptake, MDA-MB-231 and MDA-MB-436 cells transfected with FAM-siRNA nanoparticles were examined using a fluorescence microscope after 72 h. The results showed a clear green signal from the FAM-siRNA nanoparticles, indicating successful cellular uptake. Images of cells treated with 0.8HS and 1.0HS demonstrated FAM-labeled siRNA fluorescence within the cells after 72 h of transfection. These findings suggest that the injectable thermosensitive hydrogels loaded with FAM-siRNA nanoparticles can protect siRNA from enzymatic degradation and deliver it to target sites, which is an essential requirement for siRNA delivery in breast cancer treatment. The loading of siRNA nanoparticles in the thermosensitive hydrogels enhances stability and enables targeted delivery to the desired site, which is crucial for improving gene silencing efficacy and minimizing side effects. Therefore, the injectable thermosensitive hydrogels loaded with siRNA nanoparticles can protect siRNA from enzymatic degradation during transit to target sites, demonstrating potential for breast cancer treatments.

**Table 6.5** Cellular Uptake of FAM-siRNA Nanoparticles and FAM-siRNA Nanoparticles Loaded in the Hydrogels After Transfection of 72 h was Captured by Fluorescence Microscope. (Magnification 20×)

Condition	MDA-MB-231		MDA-MB-436	
	Brightfield	FAM	Brightfield	FAM
Non-treatment				
FAM siSVV nanoparticles				
0.8HS				
1.0HS				

## CHAPTER 7

### CONCLUSION

This study successfully developed and evaluated injectable self-healing hydrogels and injectable thermosensitive hydrogels, both loaded with siRNA nanoparticles, as promising platforms for breast cancer therapy. The siRNA nanoparticles were engineered through electrostatic interactions of siRNA, Prime-Fect, and Trans-Booster, which protected against enzymatic degradation and boosted cellular uptake. The optimal nanoparticle formulation (siRNA:Trans-Booster:Prime-Fect ratio of 1:1:10) exhibited a small, uniform size (230 nm, PDI < 0.2) and a stable zeta potential (-6.8 to -10.2 mV), confirming good stability and potential for efficient delivery. TEM image revealed that the siRNA nanoparticles were spherical and well-dispersed. Fluorescence microscopy demonstrated that the siRNA nanoparticles were effectively internalized into breast cancer cells. Flow cytometry analysis showed over 98% cellular uptake in both MDA-MB-231 and MDA-MB-436 cells. Importantly, siSVV nanoparticles effectively silenced the survivin gene and inhibited breast cancer cell viability, whereas CsiRNA nanoparticles showed negligible cytotoxic effects. These findings confirmed that siSVV nanoparticles possess desirable gene-silencing efficacy, making them a promising strategy for targeted siRNA delivery in breast cancer therapy. Therefore, the siRNA nanoparticles prepared at a siRNA:Trans-Booster:Prime-Fect weight ratio of 1:1:10 were selected for incorporation into injectable self-healing hydrogels and injectable thermosensitive hydrogels to investigate their potential application in breast cancer therapy.

Injectable self-healing QCS/OxPec hydrogels and injectable thermosensitive CS/SS hydrogels, both loaded with siRNA nanoparticles, were successfully developed as promising platforms for targeted breast cancer therapy. A comparative evaluation of injectable self-healing QCS/OxPec hydrogels and injectable thermosensitive CS/SS hydrogels for siRNA nanoparticles delivery revealed distinct differences in their physical and biological performance. The injectable self-healing hydrogels demonstrated a shorter gelation time (10-18 min), allowing for quicker formulation,

whereas the injectable thermosensitive hydrogel required a longer gelation time (20-29 min) but formed more stable networks, as indicated by a higher gel fraction (80% for thermosensitive hydrogels vs. 70% for self-healing hydrogels). Morphological analysis confirmed the presence of spherical siRNA nanoparticles in both hydrogels, with an average size of 199 nm in the self-healing hydrogels and 182 nm in the thermosensitive hydrogels. The injectable thermosensitive hydrogel showed superior structural integrity, with no observable weight loss over 7 days, unlike the self-healing hydrogel, which began degrading after 180 min. Biological assessments further supported their distinct functionalities. Both hydrogels achieved significant gene knockdown in MDA-MB-231 and MDA-MB-436 cell lines, although the injectable thermosensitive hydrogels resulted in a slightly higher proportion of siRNA-positive cells. However, the injectable self-healing hydrogels enabled substantially greater intracellular siRNA uptake, with values of 2816.00 a.u. and 2256.33 a.u. for MDA-MB-231 and MDA-MB-436, respectively, compared to 932.33 a.u. and 481.67 a.u. for the injectable thermosensitive hydrogels. Furthermore, the cellular uptake of siRNA nanoparticles was found to be influenced by the delivery system. The siRNA nanoparticles exhibited the highest cellular internalization in both MDA-MB-231 and MDA-MB-436 cell lines. In comparison, siRNA nanoparticles delivered via self-healing hydrogels demonstrated moderate uptake levels, while thermosensitive hydrogel-based delivery resulted in the lowest uptake efficiency. These differences can be attributed to the nature of the delivery systems. The siRNA nanoparticles are readily available for cellular internalization, leading to efficient and rapid uptake. In contrast, hydrogel matrices act as controlled-release platforms, slowing down the release of nanoparticles and limiting their immediate availability to cells. The self-healing hydrogel may possess a more dynamic and porous structure, allowing better nanoparticle diffusion compared to the more rigid thermosensitive hydrogel, which could explain the observed difference in uptake between the two hydrogel types. Thus, while hydrogel-based systems offer the advantage of localized and sustained delivery, they may compromise short-term uptake efficiency relative to siRNA nanoparticles.

In summary, the injectable thermosensitive hydrogels were more stable and formed a stronger gel, which may be useful for long-term delivery. The choice between them depends on whether long-lasting stability or strong siRNA nanoparticles delivery

is more important for the specific treatment. According to experimental results, both types of hydrogels demonstrated effective performance in delivering siRNA nanoparticles. However, the developed siRNA nanoparticles-loaded hydrogels still face challenges related to siRNA stability, modified PEI cytotoxicity, and limited *in vivo* retention. Future studies will focus on optimizing the formulation and storage conditions, exploring alternative biocompatible polymers, and enhancing *in vivo* retention. Additionally, further investigations will be conducted to evaluate the release profile, cell migration, cell adhesion, and wound closure capabilities of the hydrogels to support their clinical application potential.



## REFERENCES

- Agrawal, N., Dasaradhi, P. V. N., Mohammed, A., Malhotra, P., Bhatnagar, R. K., & Mukherjee, S. K. (2003). RNA interference: biology, mechanism, and applications. *Microbiology and Molecular Biology Reviews*, 67(4), 657-685.
- Ahmadi, R., & de Bruijn, J. D. (2008). Biocompatibility and gelation of chitosan–glycerol phosphate hydrogels. *Journal of Biomedical Materials Research Part A*, 86(3), 824-832.
- Ahsan, A., Farooq, M. A., & Parveen, A. (2020). Thermosensitive chitosan-based injectable hydrogel as an efficient anticancer drug carrier. *ACS Omega*, 5(32), 20450-20460.
- Al Masud, M. A., Shaikh, H., Alam, M. S., Karim, M. M., Momin, M. A., Islam, M. A., & Khan, G. A. (2021). Green synthesis of silk sericin-embedded silver nanoparticles and their antibacterial application against multidrug-resistant pathogens. *Journal of Genetic Engineering and Biotechnology*, 19, 74.
- Almurshidi medical agency. (2020). *Breast cancer treatment in Thailand*. <http://almurshidimed.com/breast-cancer-treatment-in-thailand/s/syc-20352470>.
- American cancer society. (2023). *Breast cancer treatment: Treatment options for breast cancer*. <https://www.cancer.org/cancer/breast-cancer/treatment.html>.
- Bahmanpour, A., Ghaffari, M., Milan, P. B., Moztarzadeh, F., & Mozafari, M. (2021). Synthesis and characterization of thermosensitive hydrogel based on quaternized chitosan for intranasal delivery of insulin. *Biotechnology and Applied Biochemistry*, 68(2), 247-256.
- Bajpai, A. K., Shukla, S. K., Bhanu, S., & Kankane, S. (2008). Responsive polymers in controlled drug delivery. *Progress in Polymer Science*, 33(11), 1088-1118.
- Baldrick, P. (2010). The safety of chitosan as a pharmaceutical excipient. *Regulatory Toxicology and Pharmacology*, 56(3), 290-299.
- Baptista-Silva, S., Borges, S., Costa-Pinto, A. R., Costa, R., Amorim, M., . . . Oliveira, A. L. (2021). *In situ* forming silk sericin-based hydrogel: A novel wound healing biomaterial. *ACS Biomaterials Science & Engineering*, 7(4), 1573–1586.

- Basu, S., Pacelli, S., & Paul, A. (2020). Self-healing DNA-based injectable hydrogels with reversible covalent linkages for controlled drug delivery. *Acta Biomaterialia*, 105, 159-169.
- Bertsch, P., Diba, M., Mooney, D. J., & Leeuwenburgh, S. C. (2022). Self-healing injectable hydrogels for tissue regeneration. *Chemical Reviews*, 123(2), 834-873.
- Bordat, A., Boissenot, T., Nicolas, J., & Tsapis, N. (2019). Thermoresponsive polymer nanocarriers for biomedical applications. *Advanced Drug Delivery Reviews*, 138, 167-192.
- Breast cancer: american cancer society. (2023). *Breast cancer: Risk and prevention*. <https://www.cancer.org/cancer/breast-cancer/risk-and-prevention.html>
- American Cancer Society. (2023). *Cancer facts & figures 2023*. <https://www.cancer.org/research/cancer-facts-statistics/all-cancer-facts-figures/2023-cancer-facts-figures.html>.
- Cao, C., Yan, C., Hu, Z., & Zhou, S. (2015). Potential application of injectable chitosan hydrogel treated with siRNA in chronic rhinosinusitis therapy. *Molecular Medicine Reports*, 12(5), 6688-6694.
- Chan, C. Y., Carmack, C. S., Long, D. D., Maliyekkel, A., Shao, Y., Roninson, I. B., & Ding, Y. (2009). A structural interpretation of the effect of GC-content on efficiency of RNA interference. *BMC Bioinformatics*, 10, 1-7.
- Chandra, P. K., Kundu, A. K., Hazari, S., Chandra, S., Bao, L., Ooms, T., . . . Dash, S. (2012). Inhibition of hepatitis C virus replication by intracellular delivery of multiple siRNAs by nanosomes. *Molecular Therapy*, 20(9), 1724-1736.
- Chanmontri, M., Swilem, A. E., Mutch, A. L., Grøndahl, L., & Suwantong, O. (2023). Physicochemical and in vitro biological evaluation of an injectable self-healing quaternized chitosan/oxidized pectin hydrogel for potential use as a wound dressing material. *International Journal of Biological Macromolecules*, 242, 124984.
- Chen, H., Cheng, J., Ran, L., Yu, K., Lu, B., Lan, G., & Lu, F. (2018). An injectable self-healing hydrogel with adhesive and antibacterial properties effectively promotes wound healing. *Carbohydrate Polymers*, 201, 522-531.

- Chen, J., Liu, W., Liu, C. M., Li, T., Liang, R. H., & Luo, S. J. (2015). Pectin modifications: a review. *Critical Reviews in Food Science and Nutrition*, 55(12), 1684-1698.
- Chenite, A., Chaput, C., Wang, D., Combes, C., Buschmann, M. D., Hoemann, C. D., . . . Selmani, A. (2000). Novel injectable neutral solutions of chitosan form biodegradable gels in situ. *Biomaterials*, 21(21), 2155–2161.
- Chiou, G. Y., Cherng, J. Y., Hsu, H. S., Wang, M. L., Tsai, C. M., Lu, K. H., . . . Chiou, S. H. (2012). Cationic polyurethanes-short branch PEI-mediated delivery of Mir145 inhibited epithelial–mesenchymal transdifferentiation and cancer stem-like properties and in lung adenocarcinoma. *Journal of Controlled Release*, 159(2), 240-250.
- Cho, J., Heuzey, M. C., Bégin, A., & Carreau, P. J. (2005). Physical gelation of chitosan in the presence of  $\beta$ -glycerophosphate: The effect of temperature. *Biomacromolecules*, 6(6), 3267–3275.
- Chollakup, R., Uttayarat, P., Chworos, A., & Smitthipong, W. (2020). Noncovalent sericin-chitosan scaffold: Physical properties and low cytotoxicity effect. *International Journal of Molecular Sciences*, 21(3), 775.
- Collins, K. K., Liu, Y., Schootman, M., Aft, R., Yan, Y., Dean, G., . . . Jeffe, D. B. (2011). Effects of breast cancer surgery and surgical side effects on body image over time. *Breast Cancer Research and Treatment*, 126, 167-176.
- Croisier, F., & Jérôme, C. (2013). Chitosan-based biomaterials for tissue engineering. *European Polymer Journal*, 49(4), 780-792.
- Dalmoro, A., Abrami, M., Galzerano, B., Bochicchio, S., Angela Barba, A., Grassi, M., & Larobina, D. (2017). Injectable chitosan/ $\beta$ -glycerophosphate system for sustained release: Gelation study, structural investigation, and erosion tests. *Current Drug Delivery*, 14(2), 216-223.
- Danaei, M., Dehghankhold, M., Ataei, S., Hasanzadeh Davarani, F., Javanmard, R., Dokhani, A., . . . Mozafari, M. R. (2018). Impact of particle size and polydispersity index on the clinical applications of lipidic nanocarrier systems. *Pharmaceutics*, 10(2), 57.



- Dastjerd, N. T., Valibeik, A., Rahimi Monfared, S., Goodarzi, G., Moradi Sarabi, M., Hajabdollahi, F., . . . Samavarchi Tehrani, S. (2022). Gene therapy: A promising approach for breast cancer treatment. *Cell Biochemistry and Function*, 40(1), 28-48.
- Desai, N., Rana, D., Salave, S., Gupta, R., Patel, P., Karunakaran, B., . . . Kommineni, N. (2023). Chitosan: A potential biopolymer in drug delivery and biomedical applications. *Pharmaceutics*, 15(4), 1313.
- Devi VK, A., Shyam, R., Palaniappan, A., Jaiswal, A. K., Oh, T. H., & Nathanael, A. J. (2021). Self-healing hydrogels: Preparation, mechanism and advancement in biomedical applications. *Polymers*, 13(21), 3782.
- Ding, Z., Jiang, Y., & Liu, X. (2018). Nanoemulsions-based drug delivery for brain tumors. In *Nanotechnology-Based Targeted Drug Delivery Systems for Brain Tumors*, 327–358.
- Drabczyk, A., Kudłacik-Kramarczyk, S., Głąb, M., Kędzierska, M., Jaromin, A., Mierzwinski, D., & Tyliczszak, B. (2020). Physicochemical investigations of chitosan-based hydrogels containing aloe vera designed for biomedical use. *Materials*, 13(14), 3073.
- Drosopoulos, K., & Linardopoulos, S. (2019). Integration of RNAi and small molecule screens to identify targets for drug development. *Target Identification and Validation in Drug Discovery: Methods and Protocols*, 33-42.
- Fan, L., Sun, Y., Xie, W., Zheng, H., & Liu, S. (2012). Oxidized pectin cross-linked carboxymethyl chitosan: a new class of hydrogels. *Journal of Biomaterials Science, Polymer Edition*, 23(16), 2119-2132.
- Fares, J., Fares, M. Y., Khachfe, H. H., Salhab, H. A., & Fares, Y. (2020). Molecular principles of metastasis: a hallmark of cancer revisited. *Signal Transduction and Targeted Therapy*, 5(1), 28.
- Freitas, C. M. P., Coimbra, J. S. R., Souza, V. G. L., & Sousa, R. C. S. (2021). Structure and applications of pectin in food, biomedical, and pharmaceutical industry: A review. *Coatings*, 11(8), 922.

- Gandhi, A., Paul, A., Sen, S. O., & Sen, K. K. (2015). Studies on thermoresponsive polymers: Phase behaviour, drug delivery and biomedical applications. *Asian journal of Pharmaceutical Sciences*, 10(2), 99-107.
- Golara, A., Kozłowski, M., Lubikowski, J., & Cymbaluk-Płoska, A. (2024). Types of breast cancer surgery and breast reconstruction. *Cancers*, 16(18), 3212.
- Gumustas, M., Sengel-Turk, C. T., Gumustas, A., Ozkan, S. A., & Uslu, B. (2017). Effect of polymer-based nanoparticles on the assay of antimicrobial drug delivery systems. *Multifunctional Systems for Combined Delivery, Biosensing and Diagnostics*, 67-108.
- Gupta, B., Tummalapalli, M., Deopura, B. L., & Alam, M. S. (2013). Functionalization of pectin by periodate oxidation. *Carbohydrate Polymers*, 98(1), 1160-1165.
- Han, H. D., Mora, E. M., Roh, J. W., Nishimura, M., Lee, S. J., Stone, R. L., . . . Sood, A. K. (2011). Chitosan hydrogel for localized gene silencing. *Cancer Biology & Therapy*, 11(9), 839-845.
- Hanzlíková, M., Ruponen, M., Galli, E., Raasmaja, A., Aseyev, V., Tenhu, H., . . . Yliperttula, M. (2011). Mechanisms of polyethylenimine-mediated DNA delivery: free carrier helps to overcome the barrier of cell-surface glycosaminoglycans. *The Journal of Gene Medicine*, 13(7-8), 402-409.
- Harholt, J., Suttangkakul, A., & Vibe Scheller, H. (2010). Biosynthesis of pectin. *Plant physiology*, 153(2), 384-395.
- Hasnain, M. S., Ahmad, S. A., Hoda, M. N., Rishishwar, S., Rishishwar, P., & Nayak, A. K. (2019). Stimuli-responsive carbon nanotubes for targeted drug delivery. In *Stimuli Responsive Polymeric Nanocarriers for Drug Delivery Applications* (pp. 321-344). Woodhead Publishing
- Hennequin, C., Belkacémi, Y., Bourgier, C., Cowen, D., Cutuli, B., Fourquet, A., . . . Rivera, S. (2022). Radiotherapy of breast cancer. *Cancer/Radiotherapie*, 26(1-2), 221-230.
- Höbel, S., & Aigner, A. (2013). Polyethylenimines for siRNA and miRNA delivery *in vivo*. *Wiley Interdisciplinary Reviews: Nanomedicine and Nanobiotechnology*, 5(5), 484-501.

- Huang, C. L., Chen, Y. B., Lo, Y. L., & Lin, Y. H. (2016). Development of chitosan/ $\beta$ -glycerophosphate/glycerol hydrogel as a thermosensitive coupling agent. *Carbohydrate Polymers*, 147, 409-414.
- Huang, H., Qi, X., Chen, Y., & Wu, Z. (2019). Thermo-sensitive hydrogels for delivering biotherapeutic molecules: A review. *Saudi Pharmaceutical Journal*, 27(7), 990-999.
- Hulka, B. S., & Stark, A. T. (1995). Breast cancer: Cause and prevention. *The Lancet*, 346(8979), 883-887.
- Jayakumar, R., Prabakaran, M., Kumar, P. S., Nair, S. V., & Tamura, H. (2011). Biomaterials based on chitin and chitosan in wound dressing applications. *Biotechnology Advances*, 29(3), 322-337.
- Jiang, Y., Thienpont, B., Sapuru, V., Hite, R. K., Dittman, J. S., Sturgis, J. N., & Scheuring, S. (2022). Membrane-mediated protein interactions drive membrane protein organization. *Nature Communications*, 13, 7373.
- Jiao, Z., Song, Y., Jin, Y., Zhang, C., Peng, D., Chen, Z., . . . Wang, L. (2017). *In vivo* characterizations of the immune properties of sericin: An ancient material with emerging value in biomedical applications. *Macromolecular Bioscience*, 17(10), 1700229.
- Karimi, Z., Taymouri, S., Minaian, M., & Miran, M. (2022). Evaluation of thermosensitive chitosan hydrogel containing gefitinib loaded cellulose acetate butyrate nanoparticles in a subcutaneous breast cancer model. *International Journal of Pharmaceutics*, 624, 122036.
- Ke, X., Li, M., Wang, X., Liang, J., Wang, X., Wu, S., . . . Hu, C. (2020). An injectable chitosan/dextran/ $\beta$ -glycerophosphate hydrogel as cell delivery carrier for therapy of myocardial infarction. *Carbohydrate Polymers*, 229, 115516.
- Kean, T., & Thanou, M. (2010). Biodegradation, biodistribution and toxicity of chitosan. *Advanced Drug Delivery Reviews*, 62(1), 3-11.
- Khan, A. A., Alanazi, A. M., Jabeen, M., Chauhan, A., & Ansari, M. A. (2019). Therapeutic potential of functionalized siRNA nanoparticles on regression of liver cancer in experimental mice. *Scientific Reports*, 9(1), 15825.

- Kichler, A., Leborgne, C., Coeytaux, E., & Danos, O. (2001). Polyethylenimine-mediated gene delivery: a mechanistic study. *The Journal of Gene Medicine*, 3(2), 135-144.
- Kim, Y. M., Park, M. R., & Song, S. C. (2012). Injectable polyplex hydrogel for localized and long-term delivery of siRNA. *ACS Nano*, 6(7), 5757-5766.
- Koh, L. D., Cheng, Y., Teng, C. P., Khin, Y. W., Loh, X. J., Tee, S. Y., . . . Han, M. Y. (2015). Structures, mechanical properties and applications of silk fibroin materials. *Progress in Polymer Science*, 46, 86-110.
- Kori, S. (2018). An overview: Several causes of breast cancer. *Epidemiology International Journal*, 2(1), 01-17.
- Kumar, M. V., Ram, S. A., Nageswari, C. S., Raveena, C., & Rajan, S. (2021). Early-stage detection of cancer in breast using artificial intelligence. *Revista Gestão Inovação e Tecnologias*, 11(2), 2016-2028.
- Kunz, R. I., Brancalhão, R. M. C., Ribeiro, L. D. F. C., & Natali, M. R. M. (2016). Silkworm sericin: Properties and biomedical application. *BioMed Research International*, 2016, 8175701.
- Kurreck, J. (2006). siRNA efficiency: structure or sequence-that is the question. *BioMed Research International*, 2006(1), 083757.
- Labi, V., & Erlacher, M. (2015). How cell death shapes cancer. *Cell Death & Disease*, 6(3), e1675-e1675.
- Lam, J. K., Chow, M. Y., Zhang, Y., & Leung, S. W. (2015). siRNA versus miRNA as therapeutics for gene silencing. *Molecular Therapy-Nucleic Acids*, 4, e252.
- Le, M., Huang, W., Chen, K. F., Lin, C., Cai, L., Zhang, H., & Jia, Y. G. (2022). Upper critical solution temperature polymeric drug carriers. *Chemical Engineering Journal*, 432, 134354.
- Lee, J. K., Lim, H. S., & Kim, J. H. (2002). Cytotoxic activity of aminoderivatized cationic chitosan derivatives. *Bioorganic & Medicinal Chemistry Letters*, 12(20), 2949-2951.
- Li, D. Q., Li, J., Dong, H. L., Li, X., Zhang, J. Q., Ramaswamy, S., & Xu, F. (2021). Pectin in biomedical and drug delivery applications: A review. *International Journal of Biological Macromolecules*, 185, 49-65.

- Li, H., Cheng, F., Wei, X., Yi, X., Tang, S., Wang, Z., . . . Huang, Y. (2020). Injectable, self-healing, antibacterial and hemostatic N, O-Carboxymethyl chitosan/oxidized chondroitin sulfate composite hydrogel for wound dressing. *Materials Science and Engineering: C*, 118, 111324.
- Li, J. M., Zhang, W., Su, H., Wang, Y. Y., Tan, C. P., Ji, L. N., & Mao, Z. W. (2015). Reversal of multidrug resistance in MCF-7/Adr cells by codelivery of doxorubicin and BCL2 siRNA using a folic acid-conjugated polyethylenimine hydroxypropyl- $\beta$ -cyclodextrin nanocarrier. *International Journal of Nanomedicine*, 10, 3147.
- Li, Y., Liu, F., Cai, Q., Deng, L., Ouyang, Q., Zhang, X. H. F., & Zheng, J. (2025). Invasion and metastasis in cancer: molecular insights and therapeutic targets. *Signal Transduction and Targeted Therapy*, 10(1), 57.
- Liang, Y., Zhao, X., Ma, P. X., Guo, B., Du, Y., & Han, X. (2019). pH-responsive injectable hydrogels with mucosal adhesiveness based on chitosan-grafted-dihydrocaffeic acid and oxidized pullulan for localized drug delivery. *Journal of Colloid and Interface Science*, 536, 224-234.
- Liu, X., Zeng, A., Li, L., Yang, F., Wang, Q., Sun, Z., & Shen, J. (2011). Synthesis of a novel amphiphilic quaternized chitosan and its distribution in rats. *Journal of Biomaterials Science, Polymer Edition*, 22(9), 1115–1130.
- Liu, Y., & Hsu, S. H. (2018). Synthesis and biomedical applications of self-healing hydrogels. *Frontiers in Chemistry*, 6, 449.
- Loncarevic, A., Ivankovic, M., & Rogina, A. (2017). Lysozyme-induced degradation of chitosan: The characterisation of degraded chitosan scaffolds. *Journal of Tissue Repair and Regeneration*, 1(1), 23–27.
- Ma, Z., Yang, C., Song, W., Wang, Q., Kjemis, J., & Gao, S. (2014). Chitosan hydrogel as siRNA vector for prolonged gene silencing. *Journal of Nanobiotechnology*, 12, 1-9.
- MacMahon, B., Cole, P., & Brown, J. (1973). Etiology of human breast cancer: A review. *Journal of the National Cancer Institute*, 50(1), 21–42.
- Mahanta, A. K., & Maiti, P. (2019). Injectable hydrogel through hydrophobic grafting on chitosan for controlled drug delivery. *ACS Applied Bio Materials*, 2(12), 5415-5426.

- Maiz-Fernández, S., Guaresti, O., Pérez-Álvarez, L., Ruiz-Rubio, L., Gabilondo, N., Vilas-Vilela, J. L., & Lanceros-Mendez, S. (2020).  $\beta$ -Glycerol phosphate/genipin chitosan hydrogels: A comparative study of their properties and diclofenac delivery. *Carbohydrate Polymers*, 248, 116811.
- Mandal, B. B., & Kundu, S. C. (2009). Cell proliferation and migration in silk fibroin 3D scaffolds. *Biomaterials*, 30(15), 2956-2965.
- Marsili, L., Dal Bo, M., Berti, F., & Toffoli, G. (2021). Chitosan-based biocompatible copolymers for thermoresponsive drug delivery systems: on the development of a standardization system. *Pharmaceutics*, 13(11), 1876.
- Mathew, A. P., Uthaman, S., Cho, K. H., Cho, C. S., & Park, I. K. (2018). Injectable hydrogels for delivering biotherapeutic molecules. *International Journal of Biological Macromolecules*, 110, 17-29.
- McManus, M. T., & Sharp, P. A. (2002). Gene silencing in mammals by small interfering RNAs. *Nature Reviews Genetics*, 3(10), 737-747.
- Mirza, Z., & Karim, S. (2021, February). Nanoparticles-based drug delivery and gene therapy for breast cancer: Recent advancements and future challenges. In *Seminars in Cancer Biology*, 69, 226-237.
- Mirzaei, S., Paskeh, M. D. A., Entezari, M., Bidooki, S. H., Ghaleh, V. J., Rezaei, S., . . . Samarghandian, S. (2023). siRNA and targeted delivery systems in breast cancer therapy. *Clinical and Translational Oncology*, 25(5), 1167-1188.
- Mo, C., Xiang, L., & Chen, Y. (2021). Advances in injectable and self-healing polysaccharide hydrogel vased on the schiff base reaction. *Macromolecular Rapid Communications*, 42(10), 2100025.
- Mobahat, M., Narendran, A., & Riabowol, K. (2014). Survivin as a preferential target for cancer therapy. *International Journal of Molecular Sciences*, 15(2), 2494-2516.
- Mohammed, A. M., Osman, S. K., Saleh, K. I., & Samy, A. M. (2020). In vitro release of 5-fluorouracil and methotrexate from different thermosensitive chitosan hydrogel systems. *Aaps Pharmscitech*, 21, 1-11.
- Musarurwa, H., & Tavengwa, N. T. (2022). Stimuli-responsive polymers and their applications in separation science. *Reactive and Functional Polymers*, 175, 105282.

- Neuberg, P., & Kichler, A. (2014). Recent developments in nucleic acid delivery with polyethylenimines. *Advances in Genetics*, 88, 263-288.
- Nguyen, K., Dang, P. N., & Alsberg, E. (2013). Functionalized, biodegradable hydrogels for control over sustained and localized siRNA delivery to incorporated and surrounding cells. *Acta Biomaterialia*, 9(1), 4487-4495.
- Nguyen, M. K., & Lee, D. S. (2010). Injectable biodegradable hydrogels. *Macromolecular Bioscience*, 10(6), 563-579.
- Nguyen, T. P., Nguyen, Q. V., Nguyen, V. H., Le, T. H., Huynh, V. Q. N., Vo, D. V. N., . . . Le, Q. V. (2019). Silk fibroin-based biomaterials for biomedical applications: A review. *Polymers*, 11(12), 1933.
- NHS: Breast cancer in women.(2019). [https://www.nhs.uk/conditions/breast-cancer/?fbclid=IwAR3CxzjSTI81L86sR3oV2RU1w\\_-6CeSlssTrkvapHC9-JD8cbX7ErdNzPUU](https://www.nhs.uk/conditions/breast-cancer/?fbclid=IwAR3CxzjSTI81L86sR3oV2RU1w_-6CeSlssTrkvapHC9-JD8cbX7ErdNzPUU).
- Niculescu, C., Schilb, A., Kim, J., Sun, D., Hall, R., Gao, S., . . . Lu, Z. R. (2023). Evaluating dual-targeted ECO/siRNA nanoparticles against an oncogenic lncRNA for triple negative breast cancer therapy with magnetic resonance molecular imaging. *Chemical & Biomedical Imaging*, 1(5), 461-470.
- Niskanen, J., & Tenhu, H. (2017). How to manipulate the upper critical solution temperature (UCST). *Polymer Chemistry*, 8(1), 220-232.
- Oprîș, O., Mormile, C., Lung, I., Stegarescu, A., Soran, M. L., & Soran, A. (2024). An overview of biopolymers for drug delivery applications. *Applied Sciences*, 14(4), 1383.
- Otrock, Z. K., Mahfouz, R. A., Makarem, J. A., & Shamseddine, A. I. (2007). Understanding the biology of angiogenesis: review of the most important molecular mechanisms. *Blood Cells, Molecules, and Diseases*, 39(2), 212-220.
- Owens, D. E., & Peppas, N. A. (2006). Opsonization, biodistribution, and pharmacokinetics of polymeric nanoparticles. *International Journal of Pharmaceutics*, 307(1), 93-102.
- Pankongadisak, P., & Suwantong, O. (2018). The potential use of thermosensitive chitosan/silk sericin hydrogels loaded with longan seed extract for bone tissue engineering. *RSC Advances*, 8(70), 40219-40231.

- Pankongadisak, P., & Suwantong, O. (2019). Enhanced properties of injectable chitosan-based thermogelling hydrogels by silk fibroin and longan seed extract for bone tissue engineering. *International Journal of Biological Macromolecules*, 138, 412-424.
- Park, S. B., Lih, E., Park, K. S., Joung, Y. K., & Han, D. K. (2017). Biopolymer-based functional composites for medical applications. *Progress in Polymer Science*, 68, 77-105.
- Parmar, M. B., KC, R. B., & Lobenberg, R. (2018). Additive polyplexes to undertake siRNA therapy against CDC20 and survivin in breast cancer cells. *Biomacromolecules*, 19(11), 4193–4206.
- Pecot, C. V., Calin, G. A., Coleman, R. L., Lopez-Berestein, G., & Sood, A. K. (2011). RNA interference in the clinic: challenges and future directions. *Nature Reviews Cancer*, 11(1), 59-67.
- Perwitasari, O., Bakre, A., Tompkins, S. M., & Tripp, R. A. (2013). siRNA genome screening approaches to therapeutic drug repositioning. *Pharmaceuticals*, 6(2), 124-160.
- Qin, H., Wang, J., Wang, T., Gao, X., Wan, Q., & Pei, X. (2018). Preparation and characterization of chitosan/ $\beta$ -glycerophosphate thermal-sensitive hydrogel reinforced by graphene oxide. *Frontiers in Chemistry*, 6, 565.
- Radu, I. C., Zaharia, C., Hudiță, A., Tanasă, E., Ginghină, O., Marin, M., . . . Costache, M. (2021). In vitro interaction of doxorubicin-loaded silk sericin nanocarriers with MCF-7 breast cancer cells leads to DNA damage. *Polymers*, 13(13), 2047.
- Rahmanian-Devin, P., Baradaran Rahimi, V., & Askari, V. R. (2021). Thermosensitive chitosan- $\beta$ -glycerophosphate hydrogels as targeted drug delivery systems: an overview on preparation and their applications. *Advances in Pharmacological and Pharmaceutical Sciences*, 2021(1), 6640893.
- Reynolds, A., Leake, D., Boese, Q., Scaringe, S., Marshall, W. S., & Khvorova, A. (2004). Rational siRNA design for RNA interference. *Nature Biotechnology*, 22(3), 326-330.

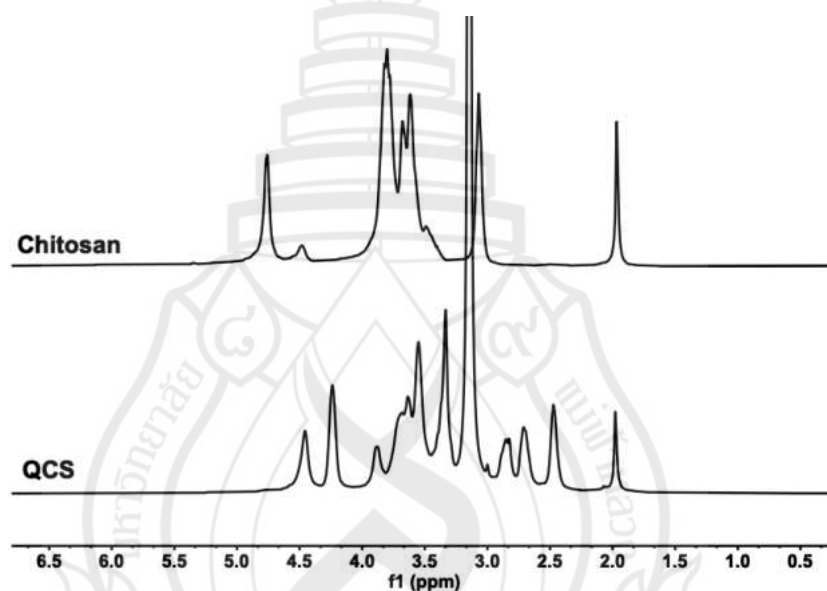


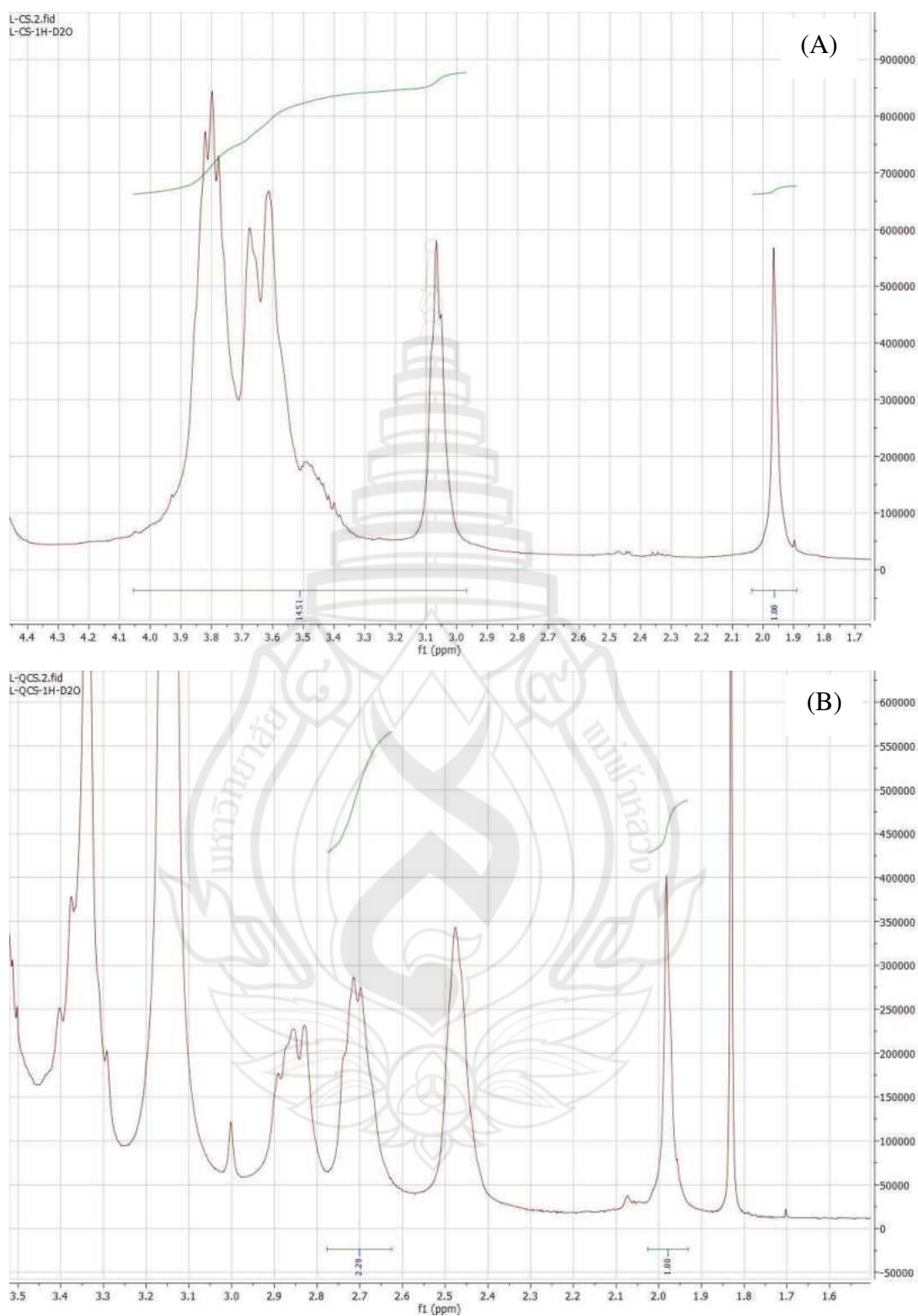
- Rezakhani, L., Alizadeh, M., & Alizadeh, A. (2021). A three dimensional *in vivo* model of breast cancer using a thermosensitive chitosan-based hydrogel and 4 T1 cell line in Balb/c. *Journal of Biomedical Materials Research Part A*, 109(7), 1275-1285.
- Ruihua, H., Bingchao, Y., Zheng, D., & Wang, B. (2012). Preparation and characterization of a quaternized chitosan. *Journal of Materials Science*, 47, 845-851.
- Rutqvist, L. E., Rose, C., & Cavallin-Ståhl, E. (2003). A systematic overview of radiation therapy effects in breast cancer. *Acta oncologica*, 42(5-6), 532-545.
- Safari, F., Barouji, S. R., & Tamaddon, A. M. (2017). Strategies for improving siRNA-induced gene silencing efficiency. *Advanced Pharmaceutical Bulletin*, 7(4), 603.
- Sajjan, A. M., Premakshi, H. G., & Kariduraganavar, M. Y. (2015). Synthesis and characterization of GTMAC grafted chitosan membranes for the dehydration of low water content isopropanol by pervaporation. *Journal of Industrial and Engineering Chemistry*, 25, 151-161.
- Santadkha, T., Skolpap, W., KC, R., Ansari, A., Kucharski, C., Atz Dick, T., & Uludağ, H. (2022). Improved delivery of Mcl-1 and survivin siRNA combination in breast cancer cells with additive siRNA complexes. *Investigational New Drugs*, 40(5), 962-976.
- Santadkha, T., Skolpap, W., KC, R., Ansari, A., Kucharski, C., Atz Dick, T., & Uludağ, H. (2022). Improved delivery of Mcl-1 and survivin siRNA combination in breast cancer cells with additive siRNA complexes. *Investigational New Drugs*, 40, 962–976.
- Shaker, D. S., Shaker, M. A., Klingner, A., & Hanafy, M. S. (2016). In situ thermosensitive Tamoxifen citrate loaded hydrogels: An effective tool in breast cancer loco-regional therapy. *Journal of Drug Delivery Science and Technology*, 35, 155-164.
- Sharma, G. N., Dave, R., Sanadya, J., Sharma, P., & Sharma, K. (2010). Various types and management of breast cancer: an overview. *Journal of Advanced Pharmaceutical Technology & Research*, 1(2), 109-126.

- Siegel, R. L., Miller, K. D., Wagle, N. S., & Jemal, A. (2023). Cancer statistics. *CA: A Cancer Journal for Clinicians*, 73(1), 17–48.
- Singh, A., Trivedi, P., & Jain, N. K. (2018). Advances in siRNA delivery in cancer therapy. *Artificial Cells, Nanomedicine, and Biotechnology*, 46(2), 274–283.
- Srihanam, P., Simcheur, W., & Srisuwan, Y. (2009). Study on silk sericin and chitosan blend film: Morphology and secondary structure characterizations. *Pakistan Journal of Biological Sciences*, 12(21), 1487–1490.
- Subhan, M. A., & Torchilin, V. P. (2023). Biopolymer-based nanosystems for siRNA drug delivery to solid tumors including breast cancer. *Pharmaceutics*, 15(1), 153.
- Sun, C., Jia, H., Lei, K., Zhu, D., Gao, Y., Zheng, Z., & Wang, X. (2019). Self-healing hydrogels with stimuli responsiveness based on acylhydrazone bonds. *Polymer*, 160, 246–253.
- Sun, Y., Nan, D., Jin, H., & Qu, X. (2020). Recent advances of injectable hydrogels for drug delivery and tissue engineering applications. *Polymer Testing*, 81, 106283.
- Tabernero, J., Shapiro, G. I., LoRusso, P. M., Cervantes, A., Schwartz, G. K., Weiss, G. J., . . . Burris III, H. A. (2013). First-in-humans trial of an RNA interference therapeutic targeting VEGF and KSP in cancer patients with liver involvement. *Cancer Discovery*, 3(4), 406–417.
- Tafer, H., Ameres, S. L., Obernosterer, G., Gebeshuber, C. A., Schroeder, R., Martinez, J., & Hofacker, I. L. (2008). The impact of target site accessibility on the design of effective siRNAs. *Nature Biotechnology*, 26(5), 578–583.
- Tamulytė, R., Baronaitė, I., Šulskis, D., Smirnovas, V., & Jankunec, M. (2024). Pro-inflammatory S100A8 protein exhibits a detergent-like effect on anionic lipid bilayers, as imaged by high-speed AFM. *ACS Applied Materials & Interfaces*, 17(3), 2635–2647.
- Tosello, G., Torloni, M. R., Mota, B. S., Neeman, T., & Riera, R. (2018). Breast surgery for metastatic breast cancer. *Cochrane Database of Systematic Reviews*, (3).

- Ui-Tei, K., Naito, Y., Takahashi, F., Haraguchi, T., Ohki-Hamazaki, H., Juni, A., . . . Saigo, K. (2004). Guidelines for the selection of highly effective siRNA sequences for mammalian and chick RNA interference. *Nucleic Acids Research*, 32(3), 936-948.
- Urban-Klein, B., Werth, S., Abuharbeid, S., Czubayko, F., & Aigner, A. (2005). RNAi-mediated gene-targeting through systemic application of polyethylenimine (PEI)-complexed siRNA *in vivo*. *Gene Therapy*, 12(5), 461-466.
- Vaidya, S., Mohod, A., Eedara, A. C., Andugulapati, S. B., & Pabbaraja, S. (2023). Synthesis and characterization of a new cationic lipid: Efficient siRNA delivery and anticancer activity of survivin-siRNA lipoplexes for the treatment of lung and breast cancers. *ChemMedChem*, 18(16), e202300097.
- Van Vlierberghe, S., Dubruel, P., & Schacht, E. (2011). Biopolymer-based hydrogels as scaffolds for tissue engineering applications: a review. *Biomacromolecules*, 12(5), 1387-1408.
- Wang, L. L., & Burdick, J. A. (2017). Engineered Hydrogels for Local and Sustained Delivery of RNA-Interference Therapies. *Advanced Healthcare Materials*, 6(1), 1601041.
- Wang, L. L., Chung, J. J., Li, E. C., Uman, S., Atluri, P., & Burdick, J. A. (2018). Injectable and protease-degradable hydrogel for siRNA sequestration and triggered delivery to the heart. *Journal of Controlled Release*, 285, 152-161.
- Wang, X., Wang, X., Varma, R. K., Beauchamp, L., Magdaleno, S., & Sendera, T. J. (2009). Selection of hyperfunctional siRNAs with improved potency and specificity. *Nucleic Acids Research*, 37(22), e152-e152.
- Wenk, E., Merkle, H. P., & Meinel, L. (2011). Silk fibroin as a vehicle for drug delivery applications. *Journal of controlled release*, 150(2), 128-141.
- Wilson, R. C., & Doudna, J. A. (2013). Molecular mechanisms of RNA interference. *Annual Review of Biophysics*, 42, 217-239.
- World Health Organization. (2021). *Breast cancer*. <https://www.who.int/newsroom/fact-sheets/detail/breast-cancer>

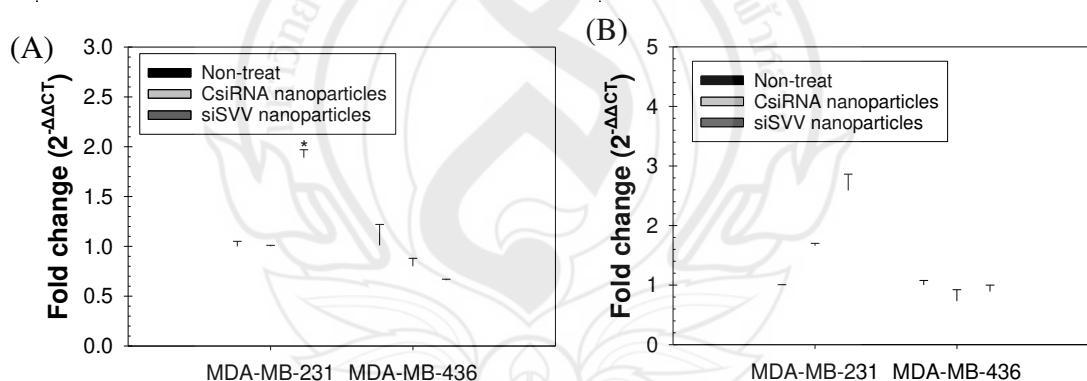
- Wu, L., Xie, J., Li, T., Mai, Z., Wang, L., Wang, X., & Chen, T. (2017). Gene delivery ability of polyethylenimine and polyethylene glycol dual-functionalized nanographene oxide in 11 different cell lines. *Royal Society Open Science*, 4(10), 170822.
- Yang, M., He, S., Su, Z., Yang, Z., Liang, X., & Wu, Y. (2020). Thermosensitive injectable chitosan/collagen/ $\beta$ -glycerophosphate composite hydrogels for enhancing wound healing by encapsulating mesenchymal stem cell spheroids. *ACS Omega*, 5(33), 21015-21023.
- Yao, Y., Li, G., Liu, Z., Wang, B., Yang, X., & Wang, J. (2025). Long-term delivery of salvianolic acid B via injectable chitosan thermosensitive hydrogel for the treatment of steroid-induced osteoporosis. *Journal of Drug Delivery Science and Technology*, 106649.
- Yin, H., Kanasty, R. L., Eltoukhy, A. A., Vegas, A. J., Dorkin, J. R., & Anderson, D. G. (2014). Non-viral vectors for gene-based therapy. *Nature Reviews Genetics*, 15(8), 541-555.
- Yu, Z., Li, Q., He, X., Wang, X., Wen, Y., Zeng, L., . . . Chen, H. (2023). A multifunctional hydrogel based on nature polysaccharide fabricated by Schiff base reaction. *European Polymer Journal*, 197, 112330.
- Zhang, P., Aso, Y., Yamamoto, K., Banno, Y., Wang, Y., Tsuchida, K., . . . Fujii, H. (2006). Proteome analysis of silk gland proteins from the silkworm, *Bombyx mori*. *Proteomics*, 6(8), 2586-2599.
- Zhang, Z., Bu, J., Li, B., Xuan, H., Jin, Y., & Yuan, H. (2022). Dynamic double cross-linked self-healing polysaccharide hydrogel wound dressing based on schiff base and thiol-alkynone reactions. *International Journal of Molecular Sciences*, 23(22), 13817.
- Zhao, X., Li, P., Guo, B., & Ma, P. X. (2015). Antibacterial and conductive injectable hydrogels based on quaternized chitosan-graft-polyaniline/oxidized dextran for tissue engineering. *Acta Biomaterialia*, 26, 236-248.
- Zhong, R., Talebian, S., Mendes, B. B., Wallace, G., Langer, R., Conde, J., & Shi, J. (2023). Hydrogels for RNA delivery. *Nature materials*, 22(7), 818-831.

**APPENDIX****INJECTABLE SELF-HEALING QUATERNIZED CHITOSAN/  
OXIDIZED PECTIN HYDROGELS LOADED  
WITH SMALL INTERFERING RNA  
NANOPARTICLES****Figure 1** 1D DOSY NMR Spectra of CS and QCS



**Figure 2**  $^1\text{H}$  NMR Spectra of (A) CS and (B) QCS

Preliminary experiments to evaluate the efficacy of siRNA nanoparticles in reducing survivin gene expression in MDA-MB-231 and MDA-MB-436 breast cancer cell lines showed results that were inconsistent with theoretical expectations or unclear, as illustrated in Figure 3. In both the first (A) and second (B) experiments, changes in survivin mRNA levels were minimal or in unexpected directions, indicating that the initial experimental conditions were not optimal. Specifically, the fold change of survivin expression was expected to decrease significantly after treatment with siSVV nanoparticles, reflecting effective gene silencing. However, the observed fold change either showed little reduction or even an increase in some cases, suggesting insufficient knockdown efficiency. These unexpected results may arise from suboptimal experimental parameters affecting siRNA delivery or measurement accuracy. Therefore, multiple experimental parameters were adjusted, including cell density, siRNA concentration, incubation time, as well as sample extraction methods, cell lysis procedures, and the analytical instruments used to improve the accuracy and efficiency of the overall process. Following these optimizations, clear and theoretically consistent results were obtained, which are presented in Chapters 5 and 6.



**Figure 3** Relative Fold Change of CsiRNA and siSVV Nanoparticles Loaded in Hydrogel Cultured with MDA-MB-231 and MDA-MB-436 Cells by RT-qPCR After Transfection for 72 h, Showing Initial Inconclusive Gene Silencing Results

## CURRICULUM VITAE

**NAME** Tanawat Buntum

### EDUCATIONAL BACKGROUND

2021 Master of Science  
Applied Chemistry  
Mae Fah Luang University, Thailand

2018 Bachelor of Science  
Applied Chemistry  
Mae Fah Luang University, Thailand

### WORK EXPERIENCE

2018-2021 Teaching Assistant in General Chemistry,  
Principles of Organic Chemistry, and  
Principles of Chemistry  
Mae Fah Luang University

### SCHOLARSHIP

2021 Post-Graduate Tuition Scholarship (MFU-  
2021)/Thesis support grant

### PUBLICATIONS

- Choipang, C., Buntum, T., Chuysinuan, P., Techasakul, S., Supaphol, P., & Suwantong, O. (2021). Gelatin scaffolds loaded with asiaticoside/2-hydroxypropyl- $\beta$ -cyclodextrin complex for use as wound dressings. *Polymers for Advanced Technologies*, 32(3), 1187-1193.
- Buntum, T., Kakumyan, P., Surassmo, S., Thanomsilp, C., & Suwantong, O. (2022). Potential of longan seed extract-loaded alginate-chitosan beads as drug delivery system. *Frontiers in Materials*, 9, 818595.
- Buntum, T., Kiti, K., Surassmo, S., Thanomsilp, C., & Suwantong, O. (2024). Enhancing wound dressing performance with hydrogel-embedded longan seed extract-loaded alginate/chitosan beads. *Polymer*, 300, 127002.



## PRESENTATIONS

Buntum, T., Duangphet, S., & Machan, T. (2018, February 7-9). Synthesis of peanut bean oil-based polymer [Poster presentation]. The 2018 Pure and Applied Chemistry International Conference, PO-P-029, Hat Yai, Thailand.  
[www.paccon2018.com](http://www.paccon2018.com)

Buntum, T., Kakumyan, P., Surassmo, S., & Suwantong, O. (2020, August 6-7). Encapsulation of longan seed extract in alginate/chitosan beads [Oral presentation]. The International Polymer Conference of Thailand (PCT-10), Bangkok, Thailand.  
<https://www.thaipolymersociety.org/pct/theme/index.html>

Buntum, T., Kakumyan, P., Surassmo, S., & Suwantong, O. (2020, December 1-4). Longan seed extract-loaded alginate/chitosan beads embedded in hydrogels and their release characteristics [Poster presentation]. The 5<sup>th</sup> International Conference on Smart Materials and Nanotechnology (SmartMat@2020), Pattaya, Thailand. <https://www.smartmat-2020.com>